

天津大学博士学位论文

球面四杆机构网格的可动性分析与刚性折
纸运动学的研究

**Analysis of Mobile Network of Spherical 4R
Linkages and Kinematics of Rigid Origami**

学科专业： 机械工程

研 究 生： 彭睿

指导教师： 陈焱 教授

天津大学机械工程学院

2018 年 4 月

摘要

本文探讨了构建可动球面四杆机构网络的可行性，分析了折纸图案的刚性可折叠性，提出了一种构建厚板折纸的新型运动学模型。

首先对单个球面四杆机构的运动学特性进行了分析。我们利用对称特性将四个相同的球面四杆机构组成了三种可动装配体，分别为旋转对称、面对称和双面对称。结合球面四杆机构运动学，归纳出这些装配体的协调条件。当机构的几何参数改变时，运动学的输入输出特性也会相应地改变。我们选择其中的 16 种特殊的传递关系来更改调整之前装配体的协调条件。基于新的协调条件，可以构建出由四个不同的球面四杆机构组成的可动装配体，这些装配体的运动一直保持协调。

刚性折纸是折纸艺术的一个分支。刚性折纸图案在折叠过程中，纸片仅沿着折痕旋转，不发生弯曲和拉伸。将纸片比作杆件，折痕比作旋转铰链，刚性折纸图案可以等效为一类特殊的球面机构网络。基于刚性折纸和球面机构网络这种关联性，可以参照可动球面机构网络来设计新的刚性折纸图案，但是需要添加更多的几何条件来保证折纸图案中的纸片为平面。将这些可动球面机构装配体进行几何拓展后得到的机构网络可以用来设计更大尺寸的折纸图案。本文不仅提出了构建可动球面四杆机构装配体的方式，还利用球面四杆机构装配体的运动协调性来设计刚性折纸图案。

通过将球面四杆机构装配体映射到平面上来获得刚性折纸图案后，对于每条折痕有山折法和谷折法两类折叠方式。除了几何设计参数，山谷折痕的排布方式也会影响折纸图案的刚性可折叠性。本文提出了一种运动学方法来分析刚性可折叠性和探讨 *double-corrugated* 图案的刚性几何拓展形式。通过将这些刚性折纸图案多层叠加，可以获得相应的 3D 超材料。一个基本单元的刚性折展运动能够引起整个超材料的刚性运动。由于基本单元的运动特性，所获得的超材料能够在两个方向上具有负泊松比，并且折纸图案的折叠运动特性会影响超材料的结构力学特性。仅仅通过更改山谷线的排布就可以调整负泊松比材料的折展特性。为了体现本文方法的普遍性，本文对 *square-twist* 图案及其对应的超材料也进行了讨论。

折纸图案通常被用于构造零厚度的薄板结构。但是在实际的工程应用中，材

料厚度是不能被忽略的。目前已有多种方法被提出，主要通过调整折痕及折痕周边区域来解决这类问题，所用的运动学模型仍然为球面机构。本文提出了一类全新且具有普遍适用性的机构综合方法来解决厚板折纸问题。使用本文方法构造的厚板折纸模型与零厚度折纸具有相同的运动路径。该方法能够有效地将四折痕、五折痕、六折痕的单顶点和多顶点折纸图案构造为厚板模型，便于折纸技术在实际工程应用中使用。

关键词：球面四杆机构，刚性折纸，山谷线排布，负泊松比，超材料，过约束机构，厚板折纸

ABSTRACT

In this thesis, we explore the possibilities of constructing mobile networks of spherical $4R$ linkages, present the analysis of rigid origami patterns, and propose a kinematic synthesis for rigid origami of thick panels.

This thesis is to analyse the kinematic properties of spherical $4R$ linkage firstly. According to the symmetrical characters, we build three types of mobile assemblies of four identical spherical $4R$ linkages, i.e., the rotational symmetric type, the plane symmetric type and the two-fold symmetric type. Combined with the kinematic of spherical $4R$ linkage, the compatible conditions of these mobile assemblies are proposed. As the geometric parameters of the linkage are changed, the input-output relationships between the kinematic variables changes accordingly, we choose sixteen special alternative relationships to modify the compatible conditions of the assemblies. According to the new compatible conditions, the mobile assemblies of four different spherical $4R$ linkages are derived while the kinematic compatibility is always kept.

Furthermore, rigid origami is a subset of origami and there is no exception for rigid origami where the sheet can neither be bent nor stretched except rotation about creases. With the paper treated as links and the creases as joints, thus the rigid origami pattern is a kind of network of spherical linkages. In order to get new rigid origami patterns by referring to mobile assemblies of spherical linkages, the further geometric condition should be added to make sure that the paper facets are flat. The tessellation of these assemblies gives larger scale origami patterns. This thesis not only provides the solutions for the mobile assemblies of spherical $4R$ linkages, but also shows the feasibility to design rigid origami patterns by studying the kinematic compatibility condition of spherical $4R$ linkage assemblies.

When projecting the mobile assembly of four spherical $4R$ linkages on the flat plane to get rigid origami patterns, there are two possibilities for the folding creases, the mountain fold and the valley fold. Besides geometric design parameters, the mountain-valley fold assignments also affect the rigidity of flat foldable origami patterns. This thesis proposes a kinematic method to analyze rigidity and explores different rigid tessellations of the double corrugated patterns. By stacking a number of those tessellation patterns layer by layer, as a result, some types of 3D metamaterial are generated. When the single unit in the metamaterial folds and extends following the

rigid motion, there will be a large deformation on the metamaterial. And due to the kinematic property of the single unit, the whole metamaterial exhibits negative Poisson's ratios in two directions. And the kinematics of the pattern's folding dominates the metamaterial's structural mechanics. Metamaterials with negative Poisson's ratios are invented whose deformation during the folding can be greatly changed by different mountain-valley assignments. The square-twist pattern and its metamaterials are also discussed to show the generalization of this method.

Origami patterns are commonly created for a zero-thickness sheet. To apply them for real engineering applications where thickness cannot be disregarded, various methods were suggested, almost all of which involve tampering with idealised fold lines and their surrounds whereas the fundamental kinematic model where folding is treated as spherical linkages remains unchanged. This thesis establishes a novel and comprehensive kinematic synthesis for rigid origami of thick panels that is capable of reproducing motions kinematically equivalent to that of zero-thickness origami. The approach, proven to be effective for single and multiple vertex origami consisting of four, five and six creases, can be readily applied to engineering practices involving folding of thick panels.

KEY WORDS: Spherical 4R linkage, Rigid origami, Mountain-valley assignment, Metamaterial, Overconstrained linkage, Thick origami

Content

摘要.....	I
ABSTRACT	III
Content	V
List of Figures	VII
List of Tables.....	XI
List of Notations.....	XIII
Chapter 1 Introduction	1
1.1 Background and Significance	1
1.2 Review of Previous Work	2
1.2.1 Linkages and Kinematic Notations	2
1.2.2 Deployable Structure Constituting by Revolute Hinges	4
1.2.3 Origami	11
1.3 Aim and Scope	18
1.4 Outline of Thesis	19
Chapter 2 Network of Spherical 4R Linkages	21
2.1 Introduction	21
2.2 The Kinematics of Spherical 4R Linkage	21
2.3 One-DOF Mobile Assemblies of Four Identical Spherical 4R Linkages.....	27
2.4 The One-DOF Mobile Assemblies of Four Different Spherical 4R Linkages	33
2.5 The Corresponding Rigid Origami Patterns.....	37
2.6 Conclusion.....	40
Chapter 3 Rigid Foldability Origami Pattern and Metamaterials	41
3.1 Introduction	41
3.2 Double corrugated pattern.....	41
3.2.1 Kinematics of Origami Vertex for Double Corrugated Pattern	44
3.2.2 Rigidity of Unit P and Q.....	51
3.2.3 Tessellation of Double Corrugated Pattern and Its Metamaterials	57
3.3 Square-twist Pattern	66
3.3.1 Rigidity of Square-twist Pattern	67
3.3.2 Tessellations of Square-twist Pattern and Its Metamaterials	69
3.4 Conclusion.....	73

Chapter 4	Origami of Thick Panels	75
4.1	Introduction.....	75
4.2	Four-crease Origami Pattern and Its Thick Model	75
4.3	Five-crease Origami Pattern and Its Thick Model.....	81
4.4	Six-crease Origami Pattern and Its Thick Model	87
4.4.1	Diamond Pattern	87
4.4.2	Waterbomb Pattern	93
4.5	Conclusion	98
Chapter 5	Conclusion and Future Works	101
5.1	Conclusion	101
5.2	Future Works	102
Reference	105
Appendix	111
中文大摘要	123
Publications and Research Projects	129
Acknowledgements	131

List of Figures

Figure 1-1	Coordinate systems, parameters and variables for two adjacent links connected by revolute joints.	3
Figure 1-2	Plate foldable structure, (a) basic component of scissor hinge with a constant angle of embrace, (b) a model of retractable structure.	5
Figure 1-3	Three-dimension shape structure based on scissor joints, (a) two configurations of a two-dimensional foldable structure, projected onto a curved surface, (b) expandable spherical structure.	6
Figure 1-4	A spherical 4R linkage.	7
Figure 1-5	Bennett linkage.	8
Figure 1-6	Original Myard linkage and extended Myard linkage, (a) Myard linkage, (b) extended Myard linkage.	9
Figure 1-7	Model of a network of three-fold Bricard linkages.	11
Figure 1-8	Origami cylinder structure, (a) folding of triangulated cylinders, (b) origami cylinder actuator.	13
Figure 1-9	Origami tent, (a) design of the cylinder, (b) self-deployment of the tent.	13
Figure 1-10	Rigid-foldable cylindrical structures.	14
Figure 1-11	Current methods for thick panel origami based on zero-thickness model, (a) hinge shift method, (b) panel offset method, (c) volume trimming method.	15
Figure 1-12	Thick panel model, (a) thick panel model of miura-ori pattern, (b) thick panel model of diamond pattern.	16
Figure 1-13	Miura-ori solar panel arrays.	17
Figure 1-14	Origami robot, (a) electric drive robot, (b) magnetic drive robot.	17
Figure 2-1	Relationship among the revolute variables of spherical 4R linkages. ...	26
Figure 2-2	Assembly of two spherical 4R linkages.	27
Figure 2-3	Assemblies of four spherical 4R linkages.	28
Figure 2-4	Graph representation of the assemblies.	29
Figure 2-5	Twofold-symmetric case of four identical spherical 4R linkages' assembly.	30
Figure 2-6	Symmetric case of four identical spherical 4R linkages' assembly.	31
Figure 2-7	Rotation case of four identical spherical 4R linkages' assembly.	32
Figure 2-8	A kind of variant two-fold symmetric case.	34
Figure 2-9	A kind of variant symmetric case.	35
Figure 2-10	A kind of variant rotation case.	36
Figure 2-11	Crease pattern inspired by rotation case.	38
Figure 2-12	An origami pattern inspired by rotation case.	38
Figure 2-13	Rigid origami pattern from a kind of variant rotation case.	39

Figure 3-1	Double corrugated pattern and its basic unit patterns, (a) double corrugated pattern (b) mountain-valley assignments of unit P, (c) mountain-valley assignments of unit Q.....	43
Figure 3-2	Spherical 4R linkage and its kinematics curves, (a) Type I of spherical 4R linkage and its kinematics, (b) Type II of spherical 4R linkage and its kinematics.	47
Figure 3-3	Combing curves from Fig. 3-2.	50
Figure 3-4	Network of spherical 4R linkages for P pattern.	51
Figure 3-5	The rotation transmission of rigid types of unit P.	52
Figure 3-6	The rotation transmission of nonrigid types of unit P.	53
Figure 3-7	Network of spherical 4R linkages for Q pattern.....	55
Figure 3-8	(a)-(f) are the transmission loops of the six Q pattern。	56
Figure 3-9	Various tessellations of units P and Q.	58
Figure 3-10	Tessellations and their corresponding metamaterials, (a) Metamaterial 1, (b) Metamaterial 2, (c) Metamaterial 3, (d) Metamaterial 4.	59
Figure 3-11	Geometrical calculation models and physical folding processes of the three basic element, (a) Element 1, (b) Element 2, (c) Element 3.	63
Figure 3-12	Dimensions and Poisson's ratio, (a) Metamaterial 1, (b) Metamaterial 2, (c) Metamaterial 3, (d) Metamaterial 4.	65
Figure 3-13	Square-twist pattern.	66
Figure 3-14	Different mountain-valley fold assignments for square-twist pattern..	67
Figure 3-15	Kinematics of spherical 4R linkage in square-twist pattern ($\alpha = \frac{5\pi}{6}$).68	
Figure 3-16	The kinematic curves of square twist pattern. (a) T1, (b) T2, (c) T3, (d) T4.	68
Figure 3-17	Tessellations of square twist pattern. (a) T1, (b) T2, (c) T3, (d) T4.....	69
Figure 3-18	Tessellation of T1.	70
Figure 3-19	Poisson's ration, (a) in-plane Poisson's ratio, (b) out-of-plane Poisson's ratio.	72
Figure 3-20	Metamaterial and its construction method, (a) construction method of metamaterial for T1 tessellation, (b) metamaterial based on T1.....	73
Figure 4-1	A single vertex of four-crease rigid origami pattern.	75
Figure 4-2	Thick origami model for four-crease origami vertex.	78
Figure 4-3	Kinematics of origami vertex and its thick panel model, (a) relationships between dihedral angles for four-crease single vertex origami, (b) zero-thickness model and its corresponding thick panel model.....	79
Figure 4-4	Thick panel models of square twist pattern, (a) Solidworks model for the square-twist pattern with thick panels, (b) zero-thickness model of square twist pattern and its corresponding thick panel model.	80
Figure 4-5	A specific symmetric single vertex five-crease origami pattern.	81

Figure 4-6	Thick origami model for four-crease origami vertex.	85
Figure 4-7	Dihedral angles φ_1 vs. φ_2 (or φ_1^{My} vs. φ_2^{My}) with different α_{12}	86
Figure 4-8	Multiple five-crease vertex origami zero-thickness model and its corresponding thick panel model.....	86
Figure 4-9	A specific symmetric single vertex six-crease origami pattern.	88
Figure 4-10	Thick origami model for six-crease origami vertex.	91
Figure 4-11	Relationships between dihedral angles for six-crease single vertex origami.	92
Figure 4-12	Zero-thickness model of Diamond pattern and its corresponding thick panel model.....	92
Figure 4-13	Waterbomb pattern.....	93
Figure 4-14	Vertex W of the waterbomb pattern.....	93
Figure 4-15	Thick origami model for origami vertex W.....	96
Figure 4-16	Zero-thickness model of Waterbomb pattern and its corresponding thick panel model.....	97
Figure 4-17	Relationships between dihedral angles for vertex W in the waterbomb origami pattern.....	98
Figure 4-18	A thick panel origami based on a pattern with both four- and six-crease vertices.....	99

List of Tables

Table 2-1.	Relationships between θ_i and θ_{i+1}	23
Table 2-2.	Variant relations for two-fold symmetric case.....	34
Table 2-3.	Variant relations for symmetric case.	35
Table 2-4.	Variant relations for rotation case.	37
Table A1.	The variations of kinematic relationships and the corresponding geometric parameters.....	111
Table A2.	Geometrical conditions of two-fold symmetric assemblies for Kokotsakis meshes	113
Table A3.	Geometrical conditions of symmetric assemblies for Kokotsakis meshes	114
Table A4.	Geometrical conditions of rotation assemblies for Kokotsakis meshes	115

List of Notations

English letter

$\mathbf{I}_3, \mathbf{I}_4$	3 by 3 and 4 by 4 unit matrix, respectively
i, j	number for the axis, $i, j = 1, 2, \dots, n$
$\mathbf{Q}_{i(i+1)}$	3 by 3 transformation matrix between the coordinate system of link $(i-1)i$ and that of link $i(i+1)$ for spherical linkages
$\mathbf{Q}_L^{S4R}, \mathbf{Q}_R^{S4R}$	Left and right part of the 3 by 3 transformation matrix equation for spherical 4R linkages
$\mathbf{Q}_L^{S5R}, \mathbf{Q}_R^{S5R}$	Left and right part of the 3 by 3 transformation matrix equation for spherical 5R linkages
$\mathbf{Q}_L^{S6R}, \mathbf{Q}_R^{S6R}$	Left and right part of the 3 by 3 transformation matrix equation for spherical 6R linkages
$\mathbf{T}_{i(i+1)}$	4 by 4 transformation matrix between the coordinate system of link $(i-1)i$ and that of link $i(i+1)$
$\mathbf{T}_L^{Br}, \mathbf{T}_R^{Br}$	Left and right part of the 4 by 4 transformation matrix equation for Bricard linkages
x_i	Coordinate axis perpendicular to z_i along which the Distance between creases or revolute joints are measured
z_i	axis of creases or revolute joints
a_{ij}	Distance between axes z_i and z_j , positive along x_i
a_{ij}^k	Distance between axes z_i and z_j , positive along x_i in linkage k ($k = a, b, c, d$)
R_i	Distance from link $(i-1)i$ to link $i(i+1)$ positively about z_i
R_i	Relationship types between θ_i and θ_{i+1}
t_i^{2R}	Transmission loop with two alternative relationship R_i
t_i^{3R}	Transmission loop with three alternative relationship R_i
$f_{i(i+1)}$	Function between θ_i and θ_{i+1}
W	Value of width
S	Width of square twist unit
H	Value of height
L	Value of length
l	Length of crease

V_{in} , V_{SL}

In-plane Poisson's ratios

V_{out} , V_{HL}

Out-of-plane Poisson's ratios

Greek letter

α_{ij} Angle between axes z_i and z_j .

α_{ij}^k Angle between axes z_i and z_j in linkage k ($k = a, b, c, d$).

α_{ij}^{Be} Angle between axes z_i and z_j in Bennett linkage.

α_{ij}^{My} Angle between axes z_i and z_j in Myard linkage.

α_{ij}^{Br} Angle between axes z_i and z_j in Bricard linkage.

θ_i Rotation between two panels joined by a crease or revolute joint z_i

θ_i^k Rotation between two panels joined by a crease or revolute joint z_i in linkage k ($k = a, b, c, d$).

θ_i^{Be} Rotation between two panels joined by a crease or revolute joint z_i in Bennett linkage

θ_i^{My} Rotation between two panels joined by a crease or revolute joint z_i in Myard linkage

θ_i^{Br} Rotation between two panels joined by a crease or revolute joint z_i in Bricard linkage

φ_i Dihedral angle between two panels joined by a crease or revolute joint z_i

φ_i^{Be} Dihedral angle between two panels joined by a revolute joint z_i in Bennett linkage

φ_i^{My} Dihedral angle between two panels joined by a revolute joint z_i in Myard linkage

φ_i^{Br} Dihedral angle between two panels joined by a revolute joint z_i in Bricard linkage

$\alpha, \beta, \gamma, \delta$ Sector angles

θ, φ Dihedral angles

English abbreviation

DOF	Degree of freedom
$S4R$	Spherical $4R$ linkage
$S5R$	Spherical $5R$ linkage
$S6R$	Spherical $6R$ linkage
Be	Bennett linkage
Br	Bricard linkage
My	Myard linkage

Chapter 1 Introduction

1.1 Background and Significance

Deployable structures are structures that have the ability to transform themselves from a small closed or folded configuration to a much larger or deployed configuration, so that they have a compact form for, e.g., transportation or storage, but can then expand for their final use^[1]. Simple examples include umbrellas or tents, but more highly engineered deployable structures are used in inhospitable environments. A good example is the use of booms, solar arrays and antennas on spacecraft, metamaterial of absorbing energy. Thus, architectural engineers, mechanical scientists and many researchers in different fields are working on it.

Many mechanical engineers have invented large number of novel mechanism to constitute a network, then to achieve the deployable structures, such as network of angulated scissor-like beam pairs, Bennett linkages, Bricard linkages, etc. These structures are based on planar mechanism and spatial mechanism. However, spherical mechanism is rarely used in discovering new structures. As the names imply, a spherical mechanism is a mechanical system in which the bodies move in a way that the trajectories of points in the system lie on concentric spheres. The rotational axes of hinged joints that connect the bodies in the system pass through the center of these spheres. The spherical $4R$ linkage is a kind of spherical mechanism which has 4 revolute joints in this system. It has only one-DOF. For instance, Hooke's universal joint is a spherical $4R$ linkage. The single spherical $4R$ linkage is widely used in manufacturing industry, network of spherical $4R$ linkages is hard to constructed because this is a overconstrained system.

On the other hand, origami is the traditional art of paper folding, which started in the 17th century AD and was popularized in the mid-1900s. Ori means "folding", and gami means "paper". Generally, the paper has deformation or bend during the folding process. However, there is a special kind of origami, Rigid Origami, which has a quadrilateral mesh surface. Every facets of it is rigid and only rotate around the crease, such as Miura-ori and eggbox patterns. This deployable structures without relying on flexible materials can be built from rigid or thick material, very useful in the field of packaging, such as satellite antenna, solar panel, shelters. Because of rigid origami's characteristics, we can treat the vertex with four fold lines as a spherical $4R$ linkage, the paper creases act as joints and paper panels act as linkages. We can use mechanism theories to analyze rigid origami problems and the rigid origami patterns offer us examples of spherical $4R$ linkages' network. So, the rigid origami patterns are actually the network of spherical $4R$ linkages in the view of mechanism engineers, such as Miura-ori, eggbox patterns, etc.

Research in the field of deployable structures focuses on the construction of planar mechanisms. As the space techniques develop rapidly, the deployable structures in satellites require larger deploy-fold ratios and complex shapes to achievement more functions. Furthermore, in order to make it easy to control the folding process of deployable structures, its corresponding mechanisms should be one degree of freedom (DOF).

The planar mechanisms have limits to satisfy all these requirements. As spherical linkages and overconstrained spatial linkages have the characters of one-DOF and spatial shapes, they have the application potentials for these fields, but it is a big challenge to propose the compatible conditions of tilling these linkages to constituting large mobile structures. Referring to the mobile networks of spherical linkages, new rigid origami patterns and their folding processes can be obtained, and more origami-based metamaterials will be proposed. In return, the known rigid origami patterns give inspirations for building mobile networks and deployable structures. Origami patterns are commonly created for a zero-thickness sheet, for real engineering applications where thickness cannot be disregarded, new kinematic model of origami need to be proposed.

1.2 Review of Previous Work

1.2.1 Linkages and Kinematic Notations

The mechanisms to be discussed here are formed from a succession of rigid parts coupled end to end to form a single closed chain. This single closed chain is called a linkage, the individual component of it is called link. The connection of two adjacent links is a joint. It includes spherical joints, planar joints, cylindrical joints, screw joints, revolute joints, prismatic joints. Our attention is the system constituted only by revolute joints. This joint allows one-DOF rotation about its axis.

An approach to the problem of rationalizing kinematics into a science by means of a symbolic language was proposed by Denavit and Hartenberg in 1966^[2]. The coordinate systems, geometrical parameters and variables related to the links connected by revolute joint are shown in Fig. 1-1. Here, $a_{i(i+1)}$ is the shortest distance between axes z_i and z_{i+1} , also referred as length of link $i(i+1)$. R_i is the distance from link $(i-1)i$ to link $i(i+1)$ positively about z_i , also referred as offset of joint i . And θ_i is the revolute variable of the linkage, which is the angle of rotation from x_{i-1} to x_i positively about z_i .

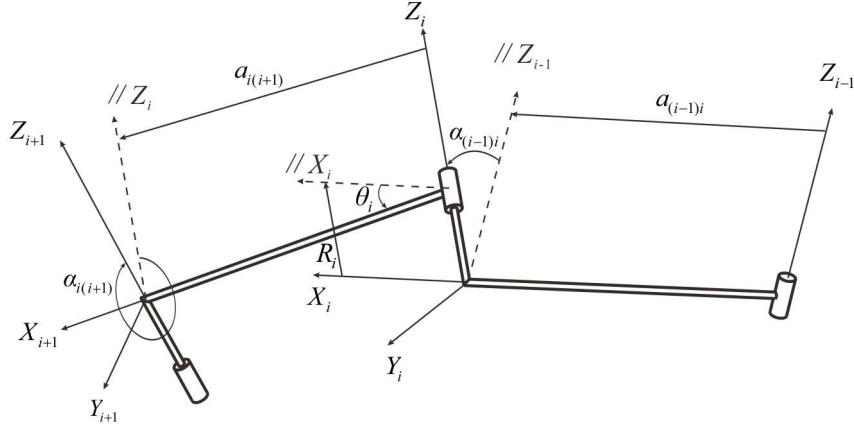


Figure 1-1 Coordinate systems, parameters and variables for two adjacent links connected by revolute joints.

In this method, they pointed out that for a closed loop in a linkage, the necessary and sufficient mobility condition is the product of the transform matrices equals the unit matrix, i.e.,

$$\mathbf{T}_{12} \mathbf{T}_{23} \mathbf{T}_{34} \cdots \mathbf{T}_{n1} = \mathbf{I}_4 \quad (1-1)$$

where $\mathbf{T}_{i(i+1)}$ is the transfer matrix between the system of link $(i-1)i$ to the system of link $i(i+1)$, if $i+1 > n$, $i+1$ is replaced by 1.

$$\mathbf{T}_{i(i+1)} = \begin{bmatrix} \cos \theta_i & -\cos \alpha_{i(i+1)} \sin \theta_i & \sin \alpha_{i(i+1)} \sin \theta_i & a_{i(i+1)} \cos \theta_i \\ \sin \theta_i & \cos \alpha_{i(i+1)} \cos \theta_i & -\sin \alpha_{i(i+1)} \cos \theta_i & a_{i(i+1)} \sin \theta_i \\ 0 & \sin \alpha_{i(i+1)} & \cos \alpha_{i(i+1)} & R_i \\ 0 & 0 & 0 & 1 \end{bmatrix} \quad (1-2)$$

Note that the transfer matrix between the system of link $i(i+1)$ and the system of link $(i-1)i$ is the inverse of $\mathbf{T}_{i(i+1)}$. That is

$$\mathbf{T}_{(i+1)i} = \mathbf{T}_{i(i+1)}^{-1} \quad (1-3)$$

The mobility m of a system composed of n links with p joints can be determined by Kutzbach mobility criterion^[3],

$$m = 6(n - p - 1) + \sum f \quad (1-4)$$

where, $\sum f$ is the sum of kinematic variables in the mechanism. For an n -link closed loop linkage with revolute joints, $p = n$, and the kinematic variable $\sum f = n$, then Eqn. (1-1) can be simplified,

$$m = n - 6 \quad (1-5)$$

Obviously, if the closed loop with revolute joints is mobile, i.e., $m > 0$, the number of links n must be greater than 6. According to this criterion, we can not find an available with less than seven links.

However, Eqn. (1-4) is not a necessary condition because it considers only the topology of the assembly. There are many mobile linkages without this criterion because of special geometry conditions^[4]. These linkages are called overconstrained linkages, e.g. Bennett linkage, Myard linkage, Bricard linkage, etc. These overconstrained linkages only have one-DOF^[5, 6].

1.2.2 Deployable Structure Constituting by Revolute Hinges

Deployable structures have the characteristic of transforming themselves from a small configuration to large scale shape as we need. These magic structures' ability attracts many engineers and scientists to devote themselves to invent new ones in different researching areas, especially in the application such as antenna reflectors and solar arrays on spacecraft, retractable roofs, etc^[7].

The deployable structures can be classified by rigid and flexible assemblies^[8]. The rigid assemblies are the ones in which rigid elements are assembled via rigid joints. Flexible assemblies may or may not include rigid parts or subassemblies. Several types of flexible assemblies exist: cable-strut assemblies, tensegrity structures^[9], inflatable systems^[10]. The large structures require high rigidity, so we prefer the rigid assemblies and put our attention on the network constituted by revolute hinges.

1.2.2.1 Planer Linkages and Their Networks

A simple, plate foldable structure can be made from two sets of parallel, straight rods connected by pivots, or scissor hinges. A scissor hinge is a revolute joint whose axis is perpendicular to the plane of the structure. The Hoberman's invention of the simple angulated element in Fig. 1-2(a), consisting of a pair of identical angulated rods connected together by a scissor hinge, extends this type of structure. The angle α follows $\alpha = 2 \arctan \overline{EF} / \overline{AF}$. It is obvious that α becomes a constant because the length of EF and AC does not varies in a scissor hinge. So, the assembly is still mobile if we assemble the scissor hinges in the circumferential direction to achieve an radially retractable plate structure showing in Fig. 1-2(b)^[11-13].

Based on Hoberman's general scissor joint, You and Pellegrino had discovered a family of mobile assemblies^[14, 15]. The shape of the assembly is not necessary to be a circle. We can use the scissor joint to get more shapes as we need. Consisting a series of scissor joints can also make a planar closed loop which is made of a serious of loop parallelograms. Whether the number of intersecting scissor-like pairs is even or odd, the assembly is mobile if it is satisfied with the conditions in ^[15].

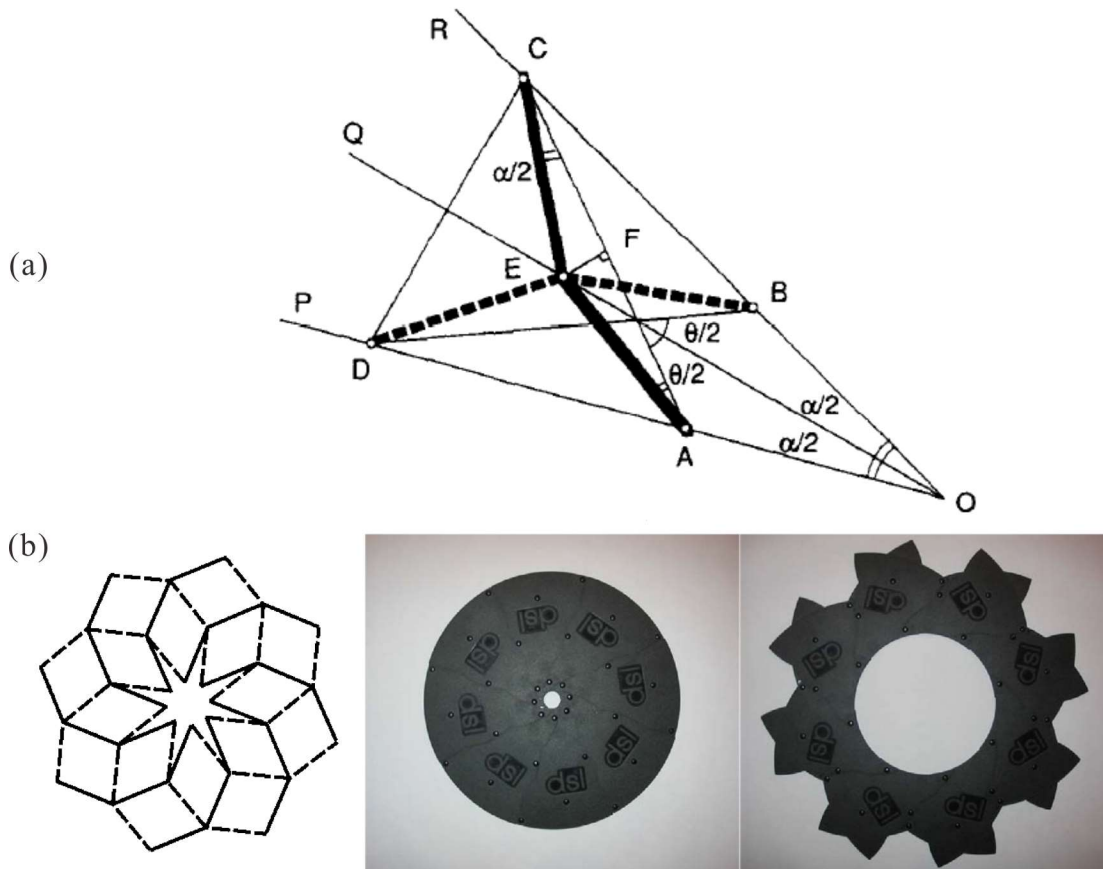


Figure 1-2 Plate foldable structure, (a) basic component of scissor hinge with a constant angle of embrace, (b) a model of retractable structure.

The deployable structures based on scissor joints have two-dimension shapes. The two-dimensional solutions are easily extended to three-dimensional solution onto a surface with the required shape, see Fig. 1-3(a). During this process each angulated element becomes curved out of its plane, all hinges of scissors must be parallel to the direction of projection in order to maintain the same freedom as in the two-dimensional structure^[16].

Another way to creating three-dimension shape by using scissor joints is to use more interconnected plate structures^[17]. We consider two such identical plate structures positioned above one another, which are to be rigidly connected. Note that the bottom layer of the top structure is connected to the top layer of the bottom structure, as the adjacent structures have the identical motions. The model is shown in Fig. 1-3(b).

In the past, deployable structural mechanisms made from pantographic elements of straight struts could form only certain shapes because of restrictions imposed by geometric compatibility conditions, which prohibit the concepts from being used in applications such as antenna reflectors where nodes of the structure usually lie on a parabolic surface. Considering a parallelogram element made of two pairs of struts with a pivot in the middle, a model with curved profile is made by You^[18].

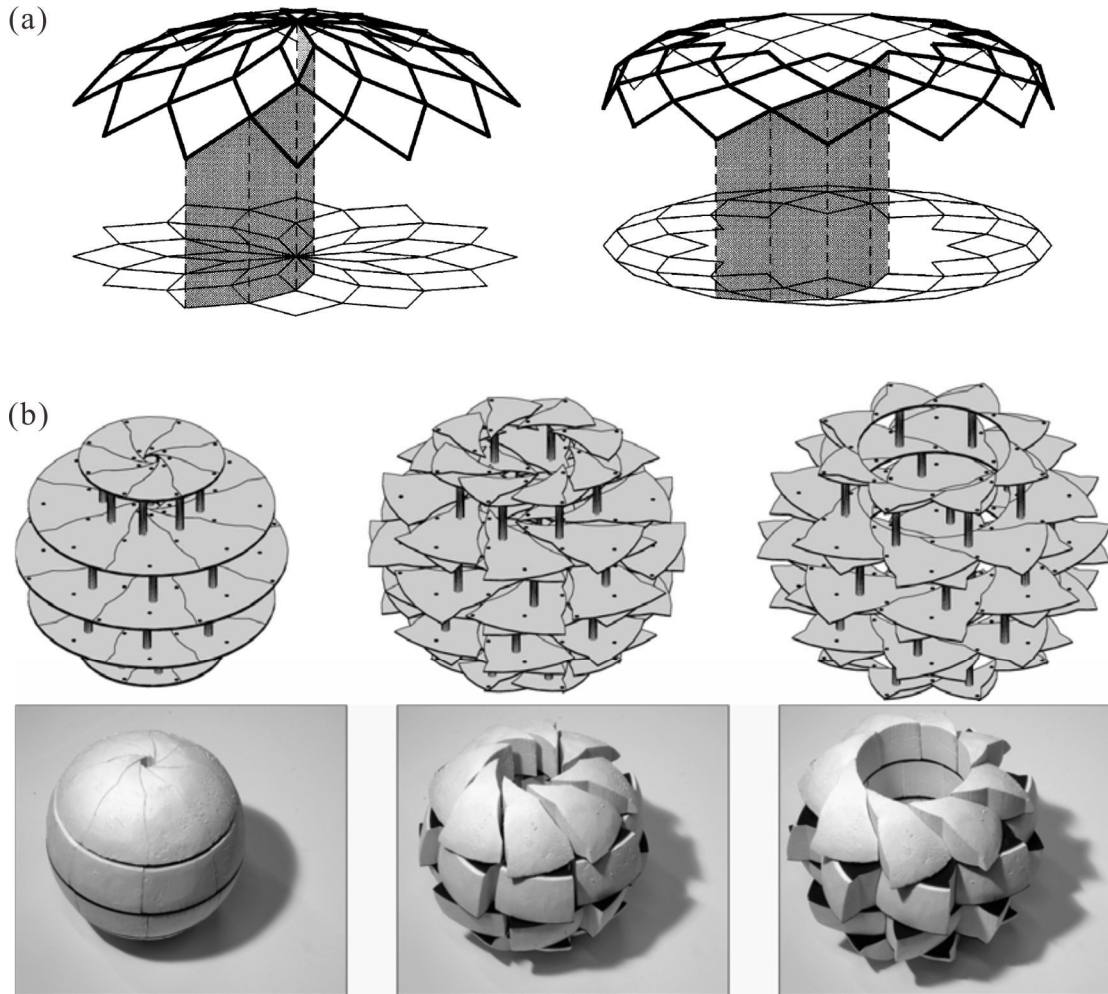


Figure 1-3 Three-dimension shape structure based on scissor joints, (a) two configurations of a two-dimensional foldable structure, projected onto a curved surface, (b) expandable spherical structure.

1.2.2.2 Overconstrained Linkages and Their Networks

The planer $4R$ linkage is the most common $4R$ loops, the rotation axes of this linkage are all parallel. Spherical $4R$ linkage is a kind of four-bar linkage in which all the links are connected by rotation joints. The joint axes intersect at a single point and the links move on concentric spheres^[19]. A model of this linkage is shown below and it has four design parameters, α_{12} , α_{23} , α_{34} , α_{41} . The conditions of this linkage are

$$\begin{aligned} a_{12} = a_{23} = a_{34} = a_{41} = 0, \\ R_1 = R_2 = R_3 = R_4 = 0. \end{aligned} \quad (1-6)$$

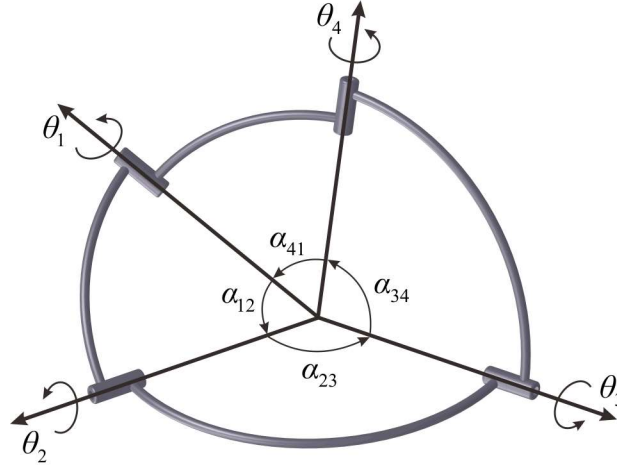


Figure 1-4 A spherical 4R linkage.

Besides of these planer and spherical linkages, the 4R closed loop linkages are usually not mobile. The Bennett linkage is the only one exception and shown in Fig. 1-5 [20]. Its geometric conditions in the DH coordinate systems are,

$$\begin{aligned} a_{12} &= a_{34} = a, \\ a_{23} &= a_{41} = b, \end{aligned} \quad (1-7a)$$

$$\begin{aligned} \alpha_{12} &= \alpha_{34} = \alpha, \\ \alpha_{23} &= \alpha_{41} = \beta, \end{aligned} \quad (1-7b)$$

$$R_i = 0 (i = 1, 2, 3, 4) \quad (1-7c)$$

In order to have mobility, the lengths and twists of this linkage should satisfy the condition

$$\frac{\sin \alpha}{a} = \frac{\sin \beta}{b} \quad (1-7d)$$

The kinematics of this linkage are [21]

$$\begin{aligned} \theta_1 + \theta_3 &= 2\pi, \\ \theta_2 + \theta_4 &= 2\pi, \\ \tan \frac{\theta_1}{2} \cdot \tan \frac{\theta_2}{2} &= \frac{\sin \frac{\alpha_{23} + \alpha_{12}}{2}}{\sin \frac{\alpha_{23} - \alpha_{12}}{2}}. \end{aligned} \quad (1-8)$$

Connecting two similar Bennett linkages together with only revolute joints has been achieved [21, 22]. The assembly has only one-DOF and has been verified. Further, the network of Bennett linkages is used to form large structural mechanisms and

possible to achieve the highest expansion ratio^[23-25]. Regular polygonal linkages and regular polyhedral linkages can also be constructed by assemblies of Bennett loops^[26]. The Bennett linkage even can be used in nanoscale geometries for programmable motion of DNA origami mechanisms^[27].

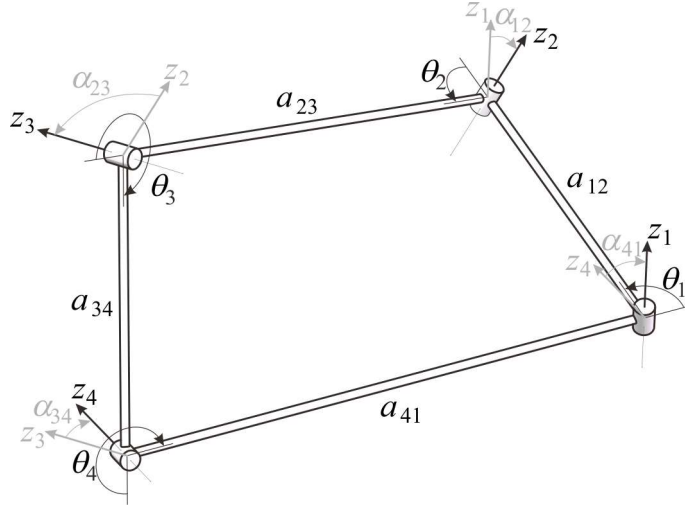


Figure 1-5 Bennett linkage.

Some spatial $5R$ linkages are proposed by Myard and Goldberg^[28, 29]. All these linkages are based on Bennett linkage. By connecting two Bennett linkages together and taking out the common links, the remaining composite loop is the overconstrained $5R$ linkage. Myard linkage is a plane-symmetric $5R$ linkage constituted by this technique in Fig. 1-6(a) and its geometric conditions are

$$\begin{aligned} \alpha_{23} &= \alpha_{45} = \frac{\pi}{2}, \\ \alpha_{51} &= \pi - \alpha_{12}, \\ \alpha_{34} &= \pi - 2\alpha_{12}, \end{aligned} \quad (1-9a)$$

$$\begin{aligned} a_{34} &= 0, a_{12} = a_{51}, a_{23} = a_{45}, \\ \frac{\sin \alpha_{12}}{a_{12}} &= \frac{\sin \alpha_{51}}{a_{51}} \end{aligned} \quad (1-9b)$$

$$R_i = 0 \quad (i = 1, 2, 3, 4, 5) \quad (1-9c)$$

According to the process of constituting the $5R$ linkages, Myard linkage can be treated as the connection of two Bennett linkages a and b, some limits of geometric conditions can be ignored, an extended Myard linkage is obtained and shown in Fig. 1-6(b)^[30]. Its geometric conditions are,

$$\begin{aligned}
 a_{12}^m &= a_{34}^m = a^m, a_{23}^m = a_{41}^m = b^m, \\
 \alpha_{12}^m &= \alpha_{34}^m = \alpha^m, \alpha_{23}^m = \alpha_{41}^m = \beta^m, \\
 \frac{\sin \alpha^m}{a^m} &= \frac{\sin \beta^m}{b^m},
 \end{aligned} \tag{1-10}$$

Where $m = a$ or b .

Liu and Chen have presented a way to build deployable assemblies using the Myard linkage^[31]. A family of mobile assemblies of Myard linkages with one-DOF has been developed. These assemblies can be used as large scale deployable structures which deploy to a planar configuration and fold to a compact bundle^[32].

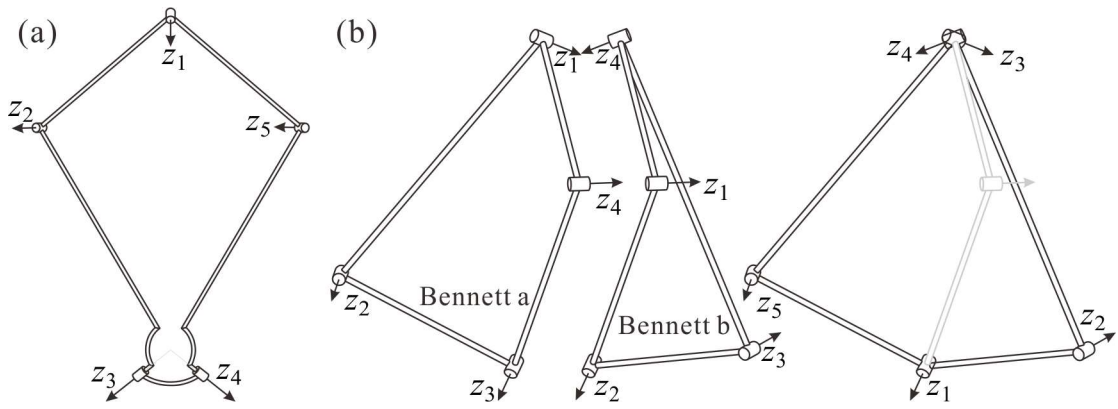


Figure 1-6 Original Myard linkage and extended Myard linkage, (a) Myard linkage, (b) extended Myard linkage.

The first spatial $6R$ overconstrained linkage is the Sarrus linkage^[33]. This linkage has two limbs, each limb has three parallel joints. Connect two spherical $4R$ linkages or one spherical $4R$ linkage and one planer $4R$ linkages, remove the common joints, give the Bennett $6R$ hybrid linkage^[34]. Combining Bennett linkages produces the Goldberg $6R$ linkages^[28]. In the process of finding deployable polyhedrons, Bricard proposed six distinct types of mobile $6R$ linkages^[35-37]. The geometric conditions of these six cases are as follows.

(i) the line-symmetric case,

$$\begin{aligned}
 a_{12} &= a_{45}, a_{23} = a_{56}, a_{34} = a_{61}, \\
 \alpha_{12} &= \alpha_{45}, \alpha_{23} = \alpha_{56}, \alpha_{34} = \alpha_{61}, \\
 R_1 &= R_4, R_2 = R_5, R_3 = R_6,
 \end{aligned} \tag{1-11a}$$

(ii) the plane-symmetric case,

$$\begin{aligned}
 a_{12} &= a_{61}, a_{23} = a_{56}, a_{34} = a_{45}, \\
 \alpha_{12} + \alpha_{61} &= \pi, \alpha_{23} + \alpha_{56} = \pi, \alpha_{34} + \alpha_{45} = \pi, \\
 R_1 = R_4 &= 0, R_2 = R_6 = 0, R_3 = R_5,
 \end{aligned} \tag{1-11b}$$

(iii) the trihedral case,

$$\begin{aligned}
 a_{12}^2 + a_{34}^2 + a_{56}^2 &= a_{23}^2 + a_{45}^2 + a_{61}^2, \\
 \alpha_{12} = \alpha_{34} = \alpha_{56} &= \frac{\pi}{2}, \alpha_{23} = \alpha_{45} = \alpha_{61} = \frac{3\pi}{2}, \\
 R_i &= 0 \quad (i = 1, 2, \dots, 6),
 \end{aligned} \tag{1-11c}$$

(iv) the line-symmetric octahedral case,

$$\begin{aligned}
 a_{12} = a_{23} = a_{34} = a_{45} = a_{56} = a_{61}, \\
 R_1 + R_4 = R_2 + R_5 = R_3 + R_6 = 0,
 \end{aligned} \tag{1-11d}$$

(v) the plane-symmetric octahedral case and

$$\begin{aligned}
 a_{12} = a_{23} = a_{34} = a_{45} = a_{56} = a_{61} &= 0, \\
 R_2 = -\frac{\sin \alpha_{34}}{\sin(\alpha_{12} + \alpha_{34})} \cdot R_1, R_3 &= \frac{\sin \alpha_{12}}{\sin(\alpha_{12} + \alpha_{34})} \cdot R_1, R_4 = -R_1, \\
 R_5 = \frac{\sin \alpha_{61}}{\sin(\alpha_{45} + \alpha_{61})} \cdot R_1, R_6 &= -\frac{\sin \alpha_{45}}{\sin(\alpha_{45} + \alpha_{61})},
 \end{aligned} \tag{1-11e}$$

(vi) the doubly collapsible octahedral case.

$$\begin{aligned}
 a_{12} = a_{23} = a_{34} = a_{45} = a_{56} = a_{61} &= 0, \\
 R_1 \cdot R_3 \cdot R_5 + R_2 \cdot R_4 \cdot R_6 &= 0.
 \end{aligned} \tag{1-11f}$$

By using the combinations or derivatives of these six basic Bricard linkages, the other linkages are proposed. The Schatz linkage discovered and patented by Schatz is used for the Turbula machine and is derived from a special trihedral Bricard linkage^[38]. Three-fold symmetric Bricard linkage has three planes of symmetry and is a particular type of the plane-symmetric case. As the linkage can be folded completely to a bundle and expanded to a planar equilateral triangle, this particular feature makes the three-fold symmetric Bricard linkage a good choice as the basic mechanism for the construction of deployable structures as shown in Fig. 1-7^[39]. One-DOF single-loop mechanisms with two operation modes can be proposed by combining two overconstrained linkages^[40].

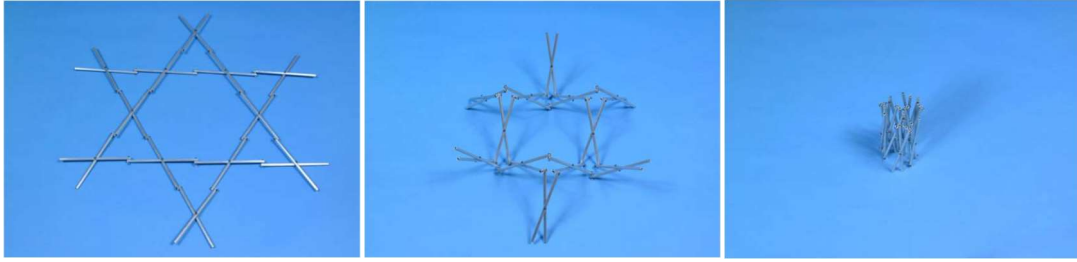


Figure 1-7 Model of a network of three-fold Bricard linkages.

1.2.3 Origami

In order to fold a large scale membrane into a smaller size one, the traditional art, origami, is a suitable technology for this application. The origami pattern can be folded by human hands, robot^[41], memory alloy actuator^[42], even cells^[43]. Rigid origami is a special branch of origami which is concerned with folding structures using flat rigid sheets joined by hinges. Besides of facet origami, origami is also used to fold a patterned cylinder to achieve the deployable structures. The cylinders are classified by two rigid assemblies and flexible assemblies. The panels of these rigid assembly cylinders are rigid without deformation.

The facet origami and cube origami are both widely applied in the area of packaging^[44], such space antennas^[45, 46], solar panel arrays^[47], energy absorbing^[48, 49], sandwich structures^[50], folded shell^[51-53], sunshield for space telescopes^[54], etc.

1.2.3.1 Facet Origami Pattern

The surfaces constituted by quadrilaterals are our interests. Origami is a mathematical process giving a flat piece of paper appropriate folds and vertexes joining several folds, which results in a polyhedral surface. Koryo Miura^[55] has studied a cured surface by means of the fundamental magnitudes of the first order and the consequent Christoffel symbols and Gaussian curvature.

In rigid origami, the transformation of a piece of paper does not include any extensional deformation during the folding process, so the Gaussian curvature K is zero which is the conditions of rigid origami.

Thomas Hull^[56] has showed a more simpler method to judge a pattern which is rigid or nonrigid. The preliminary judgment can be completed by it. Creases are classified by two types, mountain crease and valley crease. As Maekawa and Justin's theory says, in an origami pattern, mountain crease is convex and its number is M , valley crease is convex and its number is V . The relationship between M and V should satisfies,

$$M - V = \pm 2 \quad (1-12)$$

For a flat-foldability pattern, As Kawasaki and Justin's theory tells, let v be a vertex of degree $2n$ in an origami crease pattern and let $\alpha_1, \dots, \alpha_{2n}$ be the consecutive angles between the creases. Then the creases adjacent to v will fold flat if and only if

$$\alpha_1 - \alpha_2 + \alpha_3 - \dots - \alpha_{2n} = 0 \quad (1-13)$$

Origami is an art of folding paper. It has gained popularity among scientists and engineers recently as the origami technique can be utilised to create shape-changing structures. Rigid origami is a restricted form of origami where any deformation of the paper (or panel) is prohibited except their rotation about the creases, such as Miura-ori pattern which is from unfolding tree leaves^[57]. Rigidness judgement of origami patterns are necessary for the application of this technology. Diagram method and numerical method which can choose the rigid foldable patterns are proposed by Watanabe and Kawaguchi^[58]. Tachi pointed out that a rigidly foldable origami pattern can be generalized to find a valid three-dimensional state^[59]. The quaternions and dual quaternions are used to modelling rigid origami^[60]. By treating the paper as links and the creases as the joints, kinematics theories can be used to analyse the rigidity and the folding motion of origami patterns^[61, 62]. The Bar and hinges models are also used to analyse origami^[63].

1.2.3.2 Cylinders by Rigid Origami

Some folding patterns in cylindrical shells has been developed by Nojima^[64]. By his method, a pattern in cylindrical shell is been built according to the given spiral configurations. Wang and Chen^[65] also design several origami patterns to fold one piece of flat paper into closed patterned cylinder. The patterned cylinder formed by their method is a static structure without further flat foldability same as the Nojima's. This kind of cylinders can be used to design the deployable mast in the space engineering. As this is a static structure, the mobility is based on the material's flexibility. A model made by Guest is shown Fig. 1-8(a)^[66]. By covering the origami cylinder by Ecoflex as shown in Fig. 1-8(b), the composite structures are used as pneumatic actuators and they are inexpensive, simple to fabricate, light in weight and easy to actuate^[67].

When the structure is made by shape memory alloy foil, a self-deployable origami stent grafts with the biomedical application has been obtained^[68]. This deployable structures will be more useful for minimum invasive surgery, such as vascular surgery using an endoscope. The experiment is shown in Fig. 1-9. This cylinder is from rigid origami. Unlike Guest's model, the plane of this structure has no deformation and is rigid. However, its degree of freedom is more than one.

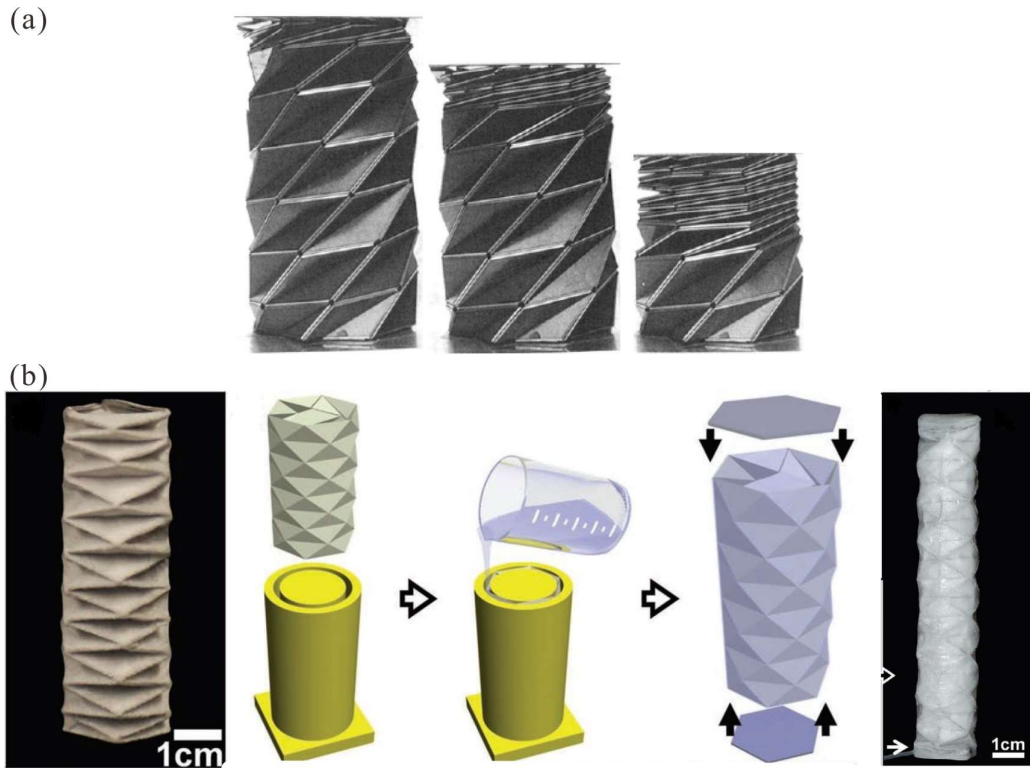


Figure 1-8 Origami cylinder structure, (a) folding of triangulated cylinders, (b) origami cylinder actuator.

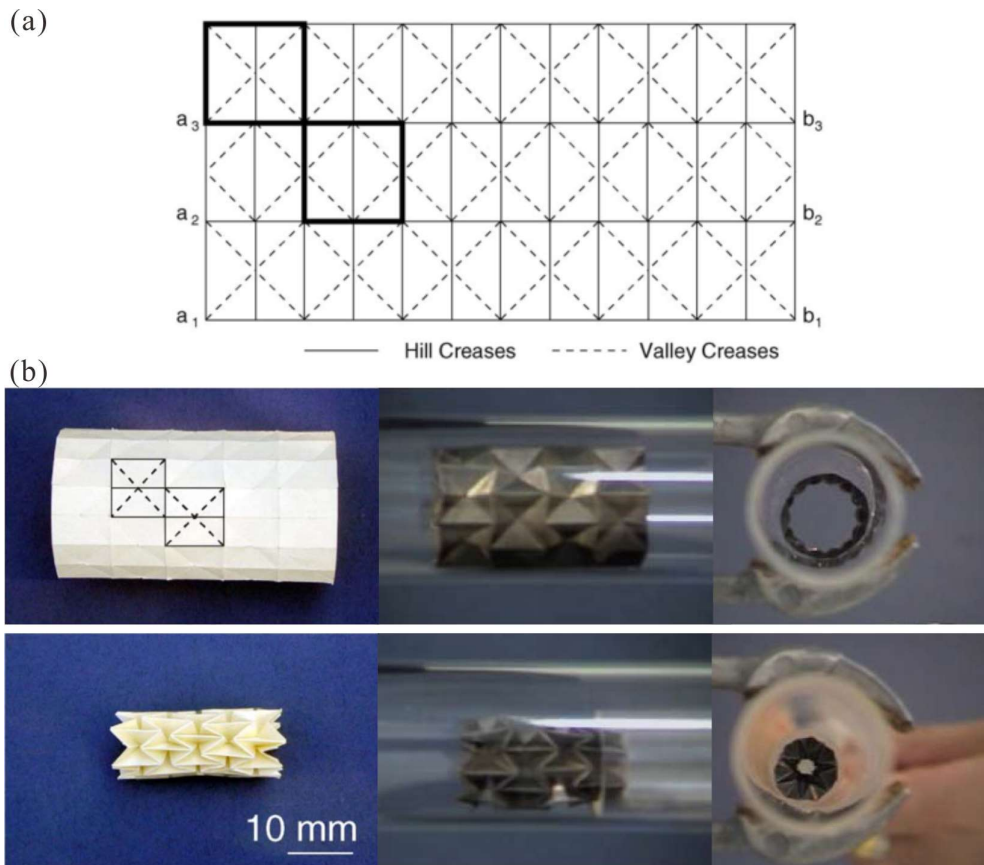


Figure 1-9 Origami tent, (a) design of the cylinder, (b) self-deployment of the tent.

Comparing with the flexible foldable cylinders or the multi-DOF cylinders, rigid foldable cylinders with only one-DOF has better controllability. We can accurately control the processing of their deploying or folding because their facets have no deformation and the control algorithm is simple as they have only one-DOF. Because of the overconstrained conditions, not many cylinders are found. A kind of one-DOF cylindrical deployable structures with rigid quadrilateral panels is proposed by Tachi and is shown in Fig. 1-10(a) ^[69, 70]. The cross sections of Tachi's cylinders are parallelograms or zonogons. Liu and Chen have found some novel patterns and Tachi's is the special case of their ^[71]. The cross section of Chen's basic cylinder is kite in Fig. 1-10(b). The axis of Chen's tubes can be a straight line, i.e., the cylinder or not. Another star-polyhedron cylinder with a synchronized motion ^[72, 73] is in Fig. 1-10(c). All these cylinders have three characteristics, flat-foldable, rigid-foldable and one-DOF. The shape flattens into a compact 2D configuration, each element does not deform throughout the transformation, and the mechanisms have exactly one degree of freedom.

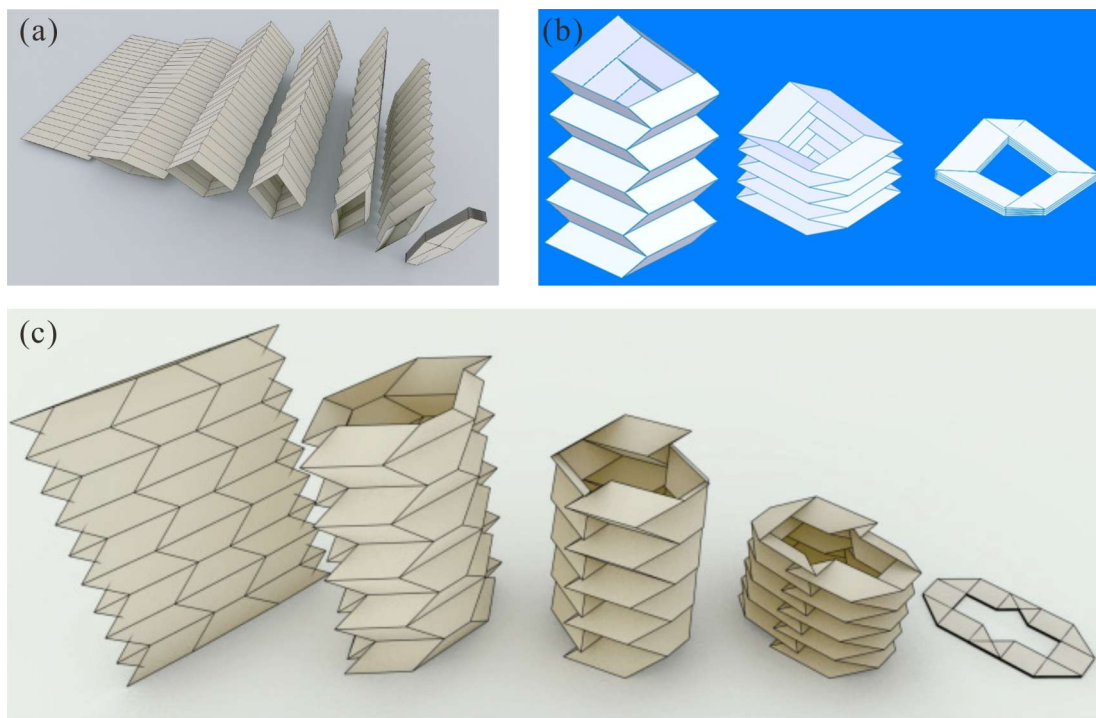


Figure 1-10 Rigid-foldable cylindrical structures.

1.2.3.3 Thick Origami

When the origami vertex has to be flat-foldable, the intersection problem can not be avoided. There are many thick folding techniques proposed. By shifting hinges out of plane of the origami pattern, the material thickness will be accommodated. The method is shown in Fig. 1-11(a) ^[74]. The method is only suitable for the simple zig-zag

pattern. The kinematics of thick origami model is different from its corresponded zig-zag origami pattern. The offset panel technique is shown in Fig. 1-11(b) ^[75]. The hinges of thick model and the origami pattern creases have the same position. The thick panels are out panel of the origami facets. The thick model and the origami pattern have the same folding process. Volume trimming is another method to avoid the material intersection in the folding process of the thick model ^[76]. A kind of volume trimming method is shown in Fig. 1-11(c).

These methods though often result in surfaces that are either not entirely flat or with openings to accommodate thickness. There are only two exceptions. One is a technique introduced by Hoberman to fold the Miura-ori ^[77] in Fig. 1-12(a), and the other by De Temmerman for the diamond origami pattern ^[78] Fig. 1-12(b). In both of them, all of the folding lines do not meet at a point, and thus, the vertices no longer exist. This indicates that their folding cannot be simply treated as the motion of spherical linkage assemblies.

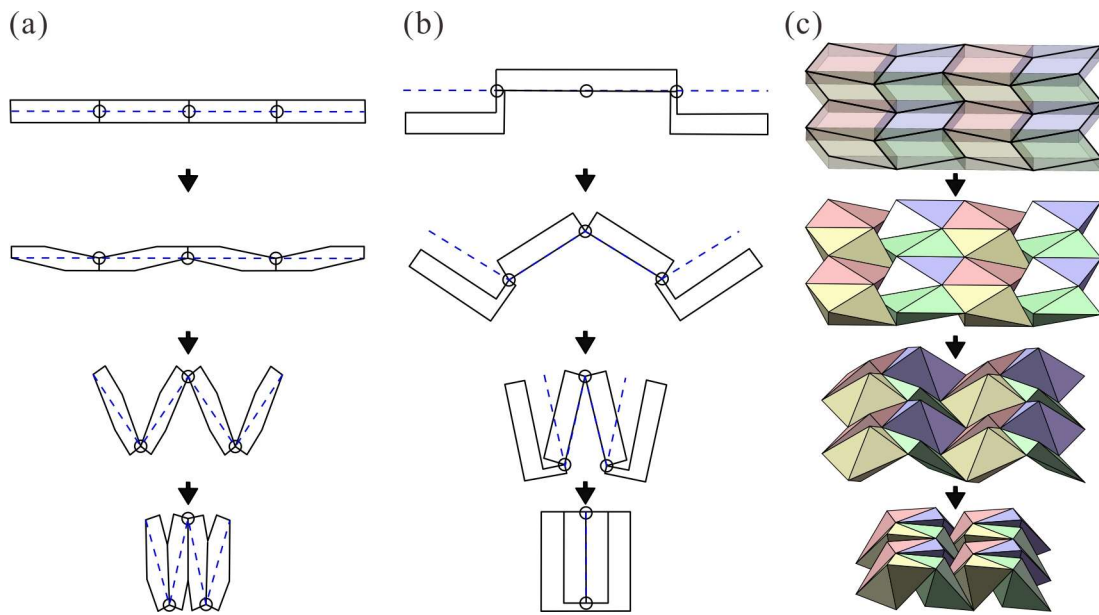


Figure 1-11 Current methods for thick panel origami based on zero-thickness model, (a) hinge shift method, (b) panel offset method, (c) volume trimming method.

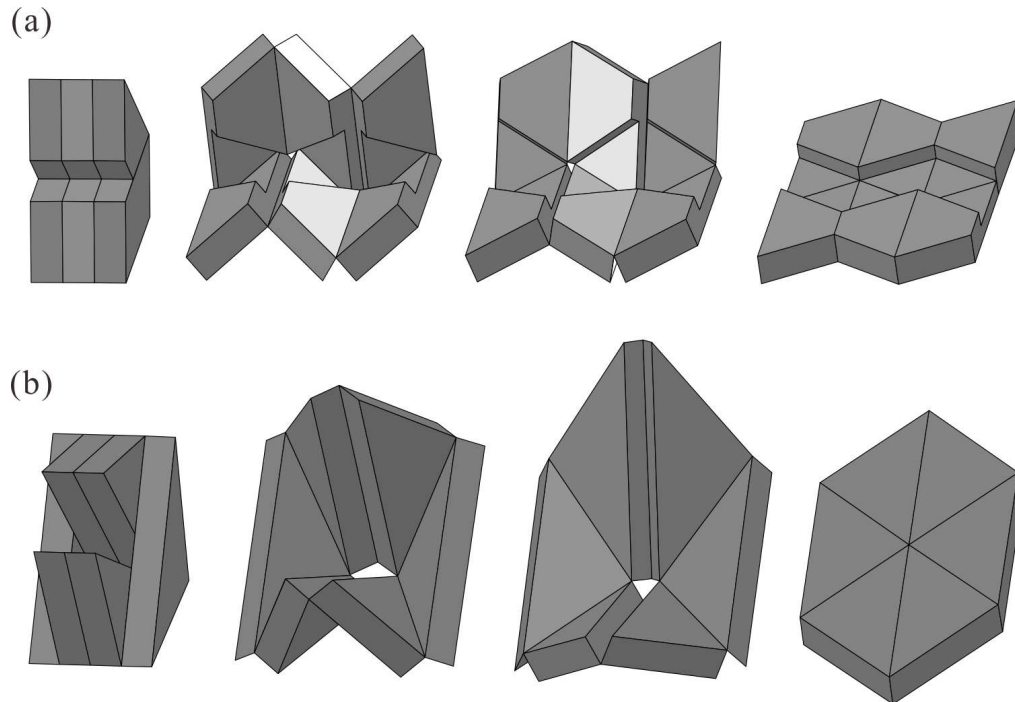


Figure 1-12 Thick panel model, (a) thick panel model of miura-ori pattern, (b) thick panel model of diamond pattern.

1.2.3.4 Origami Application

Origami has probably the widest application potential in engineering structures ranging from solar panels, space antenna reflectors, air craft wings to robots. This technique also gives inspiration for designing new metamaterials^[79-81].

Space missions require ultra-low-mass and large space platforms or structures, such as antenna and solar panel arrays. Koryo Miura presents a new concept of packing and deployment of large membranes in space by using origami technique^[82]. A solar panels arrays based on Miura-ori pattern has been launched and tested in orbit as shown in Fig. 1-13^[83]. Origami-type structures have large fold-deploy ratios. A deployable solar array for space application with a ratio of deployed-to-stowed diameter of 9.2m is designed in^[84]. This model is demonstrated in hardware as a 1/20th scale prototype.

Origami can fold paper into complex 3D shapes, this technique helps to use this 2-D fabrication method to build 3D robotic systems. A self-folding robot with embedded electronics is designed in Fig. 1-14(a)^[85]. A similar self-folding robot is controlled by an alternating external magnetic field as shown in Fig. 1-14(b), it can walk, swim and degrade^[86]. Besides design new patterns, some traditional patterns are also useful for building robot systems. E.g., the famous waterbomb pattern has been used to design parallel robot^[87], worm-like robots^[88, 89], the floating equipment of aerial vehicles^[90], or the deformable wheel of a robot^[91].

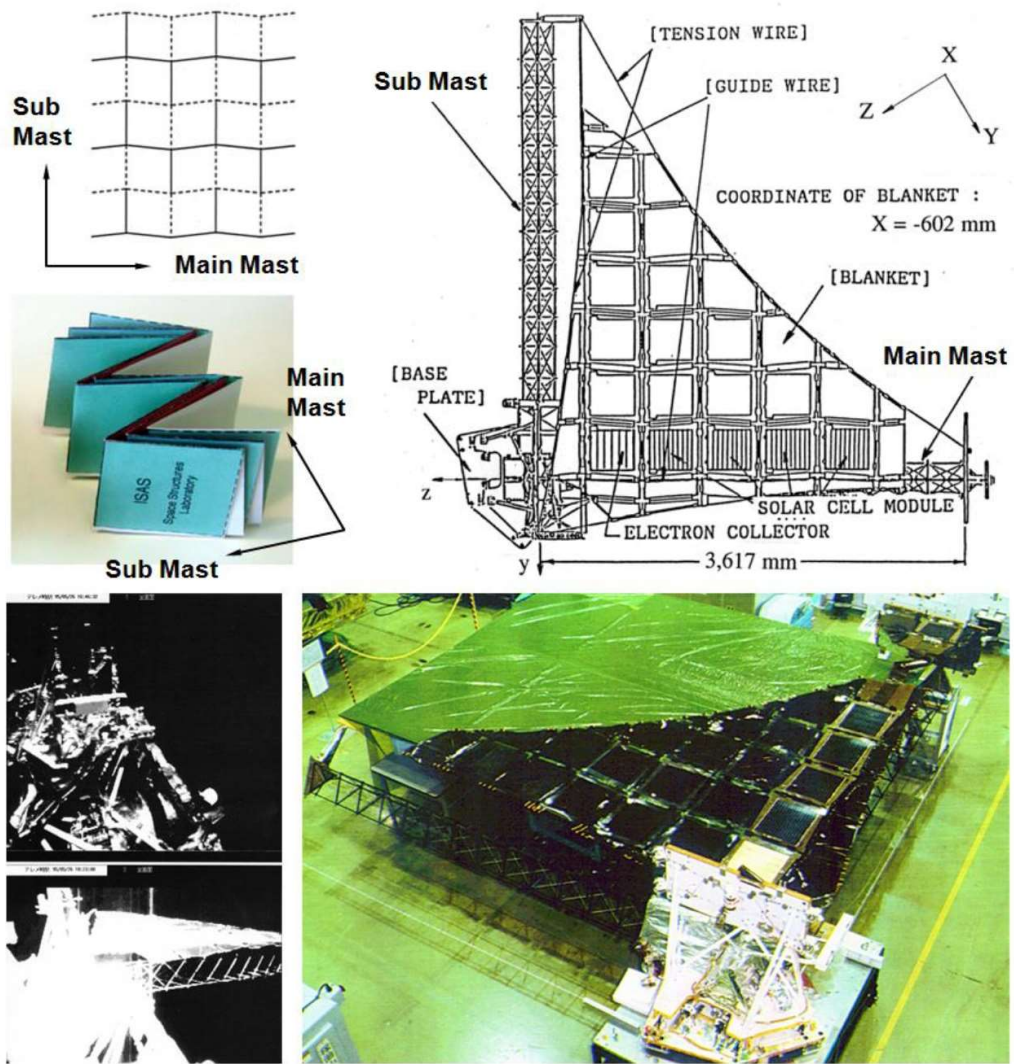


Figure 1-13 Miura-ori solar panel arrays.

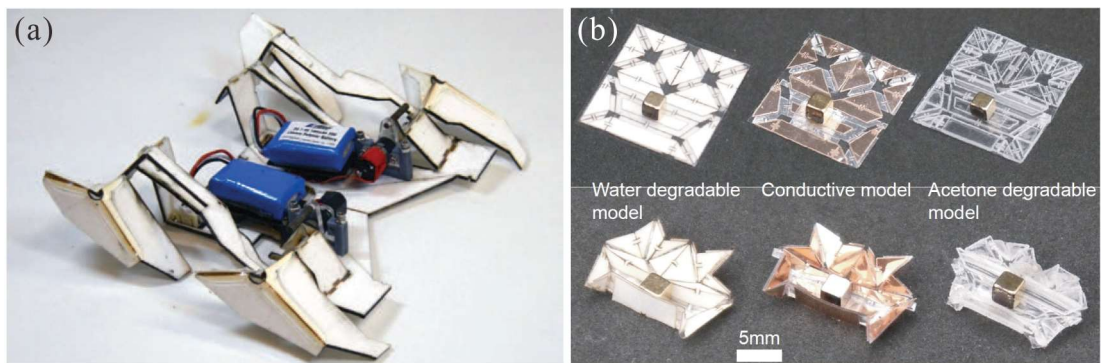


Figure 1-14 Origami robot, (a)electric drive robot, (b) magnetic drive robot.

By stacking many layers of the famous Miura-ori pattern, a metamaterial is proposed in Fig. 1-15 [92]. This metamaterial provides negative Poisson's ratio for both in-plane and out-of-plane deformations, and is used as the core for blast-resistant sandwich beams [93]. The Poisson's ratio and the bending stiffness of the miura-ori pattern are also analysed in [94]. By adding defects in the original miura-ori pattern structure, this mechanical metamaterial can be reprogrammable [95]. Besides the periodic Miura-ori pattern, a non-periodic Ron Resch pattern has unusually strong load bearing capability which can attribute to build mechanical metamaterials [96]. The rigid origami tubes also can be used as the basic units to construct metamaterials [97-99]. Besides of to design metamaterials, the square-twist pattern [100], the single vertexes in miura-ori pattern [101] and waterbomb pattern [102] can be used to multistability structures.

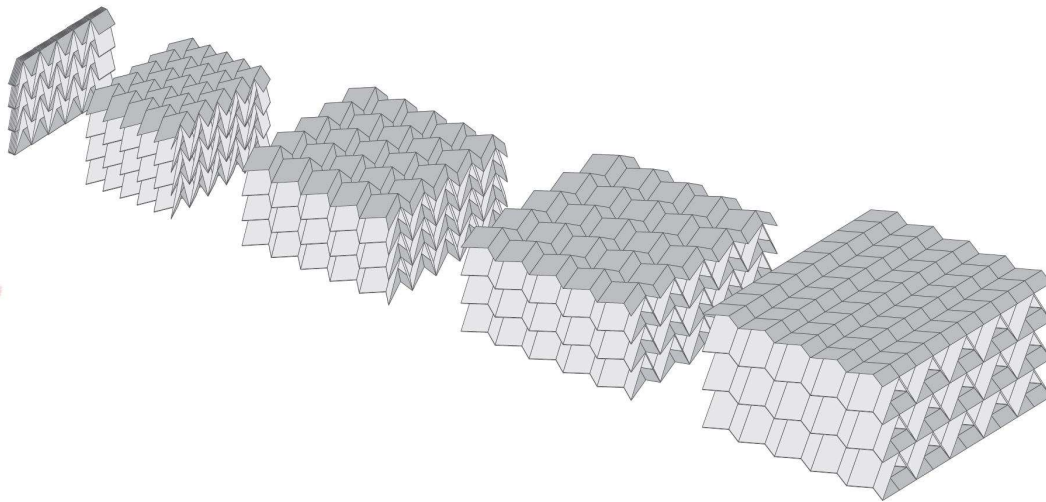


Figure 1-15 Miura-folded metamaterial.

1.3 Aim and Scope

This thesis is to explore the possibility of constructing mobile mechanism using spherical $4R$ linkages and use mechanism theory to analyse rigid origami problems.

In this process, we first analyse the kinematics of spherical $4R$ linkage and build three cases of mobile network of four spherical $4R$ linkages, i.e., two-fold symmetric case, symmetric case and rotational symmetric case, then we generalize the conditions of these mobile networks. According to the relationship between spherical linkages and rigid origami, we use the kinematic compatible conditions to present the effect of mountain-valley fold assignments on the rigidity of flat foldable origami patterns. Finally, we propose a novel and comprehensive kinematic synthesis for rigid origami of thick panels.

1.4 Outline of Thesis

This thesis consists five chapters.

Chapter 1 presents a brief review of existing works. It includes the mechanism theory for analyzing the linkages, the compatible condition for closed loop linkages and the deployable structures constituting by revolute hinges. As origami is a special technique for design deployable structures, its definition and applications are also introduced in this chapter.

Chapter 2 is aiming to develop a family of mobile assemblies with spherical $4R$ linkages and form the corresponding rigid origami patterns. The kinematics of spherical $4R$ linkage will be studied firstly. It is followed by the one-DOF mobile assemblies of four identical or different spherical $4R$ linkages. Based on these mobile assemblies, their corresponding rigid origami patterns are proposed.

Chapter 3 proposes a kinematic method to study the effect of mountain-valley fold assignments on the rigidity of flat foldable origami patterns. Here the double corrugated pattern is taken as the study case firstly. Based on the kinematic models of spherical $4R$ linkage ($S4R$) assemblies, the analysis on the rigidity of its basic units is conducted. Then the tessellations of the double corrugated patterns and their metamaterials are explored. The square-twist pattern and its metamaterials are also discussed to show the generalization of this method.

Chapter 4 describes the construction process of thick panel origami models for four-crease origami vertex by using Bennett linkage, five-crease origami vertex by using Myard linkage, and six-crease origami vertex by using Bricard linkage. The kinematic equivalent of the thick panels model and origami vertex has been proved. Thick panel models for multi-vertex patterns by this technique are also presented in this chapter.

Chapter 5 makes a conclude of this whole thesis and shows the future research works.

Chapter 2 Network of Spherical 4R Linkages

2.1 Introduction

A spherical 4R linkage has four revolute axes which must intersect in a single point to provide one degree-of-freedom (one-DOF) rotational movement. The trajectories of these links lie on concentric spheres as shown in Fig. 1-4. Due to its one-DOF mobility, the spherical 4R linkage has been used as basic element to construct other mechanisms, such as Hooke's linkage or universal joint, double Hooke's linkage^[103], Bennett hybrid 6R linkage^[34], and so on. Most of the previous research focused on the single spherical 4R linkage or the combination of two such linkages. Recent research attempted on the mobile assemblies of spherical 4R linkages, which could involve unlimited number of identical or similar spherical 4R linkages.

In this chapter, we are aiming to develop a family of mobile assemblies with spherical 4R linkages and form the corresponding rigid origami patterns. The layout of this chapter is as follows. Firstly, the kinematics of spherical 4R linkage will be studied in section 2.2. Section 2.3 derives the one-DOF mobile assemblies of four identical spherical 4R linkages. In section 2.4, by considering the kinematic characteristics of spherical 4R linkages, the assemblies of four different spherical 4R linkages are proposed. Based on the assemblies in section 2.3 and 2.4, section 2.5 is devoted to design corresponding rigid origami patterns. The conclusions and discussion in section 2.6 end this chapter.

2.2 The Kinematics of Spherical 4R Linkage

For spherical linkages, the distances between adjacent links are zero because the axes of revolute joints meet at a point, and thus Eqn. (1-1) reduces to

$$\mathbf{Q}_{12}\mathbf{Q}_{23}\cdots\mathbf{Q}_{n1} = \mathbf{I}_3 \quad (2-1)$$

where

$$\mathbf{Q}_{i(i+1)} = \begin{bmatrix} \cos \theta_i & \sin \theta_i & 0 \\ -\cos \alpha_{i(i+1)} \cdot \sin \theta_i & \cos \alpha_{i(i+1)} \cdot \cos \theta_i & \sin \alpha_{i(i+1)} \\ \sin \alpha_{i(i+1)} \cdot \sin \theta_i & -\sin \alpha_{i(i+1)} \cdot \cos \theta_i & \cos \alpha_{i(i+1)} \end{bmatrix}.$$

There is

$$\mathbf{Q}_{(i+1)i} = \mathbf{Q}_{i(i+1)}^{-1} = \begin{bmatrix} \cos \theta_i & -\cos \alpha_{i(i+1)} \cdot \sin \theta_i & \sin \alpha_{i(i+1)} \cdot \sin \theta_i \\ \sin \theta_i & \cos \alpha_{i(i+1)} \cdot \cos \theta_i & -\sin \alpha_{i(i+1)} \cdot \cos \theta_i \\ 0 & \sin \alpha_{i(i+1)} & \cos \alpha_{i(i+1)} \end{bmatrix} \quad (2-2)$$

Eqns. (1-1) and (2-1) have been used to obtain closure equations in all of the subsequent derivations.

For spherical 4R linkage, Eqn. (2-1) can also be written as

$$\mathbf{Q}_{12}\mathbf{Q}_{23} = \mathbf{Q}_{14}\mathbf{Q}_{43} \quad (2-3)$$

because of Eqn. (2-2), which amounts to a total of nine equations. Note that the kinematic twists (angles) under DH notation can be made to be identical to their respective sector angles for any the spherical linkage. The relationships between kinematic variables θ_i and θ_{i+1} ($i=1, 2, 3, 4$) can be obtained,

$$\begin{aligned} & \cos \alpha_{23} \cdot \sin \alpha_{41} \cdot \sin \alpha_{12} \cdot \cos \theta_1 + \cos \alpha_{41} \cdot \sin \alpha_{12} \cdot \sin \alpha_{23} \cdot \cos \theta_2 \\ & + \cos \alpha_{12} \cdot \sin \alpha_{23} \cdot \sin \alpha_{41} \cdot \cos \theta_1 \cdot \cos \theta_2 - \sin \alpha_{23} \cdot \sin \alpha_{41} \cdot \sin \theta_1 \cdot \sin \theta_2 \\ & + \cos \alpha_{34} - \cos \alpha_{12} \cdot \cos \alpha_{23} \cdot \cos \alpha_{41} = 0; \end{aligned} \quad (2-4a)$$

$$\begin{aligned} & \cos \alpha_{34} \cdot \sin \alpha_{12} \cdot \sin \alpha_{23} \cdot \cos \theta_2 + \cos \alpha_{12} \cdot \sin \alpha_{23} \cdot \sin \alpha_{34} \cdot \cos \theta_3 \\ & + \cos \alpha_{23} \cdot \sin \alpha_{12} \cdot \sin \alpha_{34} \cdot \cos \theta_2 \cdot \cos \theta_3 - \sin \alpha_{12} \cdot \sin \alpha_{34} \cdot \sin \theta_2 \cdot \sin \theta_3 \\ & + \cos \alpha_{41} - \cos \alpha_{12} \cdot \cos \alpha_{23} \cdot \cos \alpha_{34} = 0; \end{aligned} \quad (2-4b)$$

$$\begin{aligned} & \cos \alpha_{41} \cdot \sin \alpha_{23} \cdot \sin \alpha_{34} \cdot \cos \theta_3 + \cos \alpha_{23} \cdot \sin \alpha_{34} \cdot \sin \alpha_{41} \cdot \cos \theta_4 \\ & + \cos \alpha_{34} \cdot \sin \alpha_{23} \cdot \sin \alpha_{41} \cdot \cos \theta_3 \cdot \cos \theta_4 - \sin \alpha_{23} \cdot \sin \alpha_{41} \cdot \sin \theta_3 \cdot \sin \theta_4 \\ & + \cos \alpha_{12} - \cos \alpha_{23} \cdot \cos \alpha_{34} \cdot \cos \alpha_{41} = 0; \end{aligned} \quad (2-4c)$$

$$\begin{aligned} & \cos \alpha_{12} \cdot \sin \alpha_{34} \cdot \sin \alpha_{41} \cdot \cos \theta_4 + \cos \alpha_{34} \cdot \sin \alpha_{41} \cdot \sin \alpha_{12} \cdot \cos \theta_1 \\ & + \cos \alpha_{41} \cdot \sin \alpha_{12} \cdot \sin \alpha_{34} \cdot \cos \theta_4 \cdot \cos \theta_1 - \sin \alpha_{12} \cdot \sin \alpha_{34} \cdot \sin \theta_4 \cdot \sin \theta_1 \\ & + \cos \alpha_{23} - \cos \alpha_{12} \cdot \cos \alpha_{34} \cdot \cos \alpha_{41} = 0; \end{aligned} \quad (2-4d)$$

which can be represented as

$$\begin{aligned} & \cos \alpha_{(i+1)(i+2)} \cdot \sin \alpha_{(i-1)i} \cdot \sin \alpha_{i(i+1)} \cdot \cos \theta_i \\ & + \cos \alpha_{(i-1)i} \cdot \sin \alpha_{i(i+1)} \cdot \sin \alpha_{(i+1)(i+2)} \cdot \cos \theta_{i+1} \\ & + \cos \alpha_{i(i+1)} \cdot \sin \alpha_{(i+1)(i+2)} \cdot \sin \alpha_{(i-1)i} \cdot \cos \theta_i \cdot \cos \theta_{i+1} \\ & - \sin \alpha_{(i+1)(i+2)} \cdot \sin \alpha_{(i-1)i} \cdot \sin \theta_i \cdot \sin \theta_{i+1} \\ & + \cos \alpha_{(i+2)(i+3)} - \cos \alpha_{i(i+1)} \cdot \cos \alpha_{(i+1)(i+2)} \cdot \cos \alpha_{(i-1)i} = 0. \end{aligned} \quad (2-5)$$

And later, we will use $\theta_{i+1} = f_{i(i+1)}(\theta_i)$ to present this relationship in the analysis of mobile assemblies.

By changing the link twists α_{ij} , into α_{ij} , $\pi - \alpha_{ij}$, $-\pi + \alpha_{ij}$, or $-\alpha_{ij}$, there are 256 ($= 4 \times 4 \times 4 \times 4$) variations on the geometric parameters for each spherical 4R linkage.

Similarly, for each kinematic variables θ_i , there are four variations, i.e., θ_i , $\pi - \theta_i$, $-\pi + \theta_i$ and $-\theta_i$. If the basic relationship between two adjacent joints' kinematic variables is θ_i v.s. θ_{i+1} , there are totally 16 ($= 4 \times 4$) types of different relationship R_i by combining the four variations in a single kinematic variables, as shown in table 2-1.

Table 2-1. Relationships between θ_i and θ_{i+1}

Types	Relationships
R1	θ_i v.s. θ_{i+1}
R2	θ_i v.s. $(\pi - \theta_{i+1})$
R3	θ_i v.s. $(-\pi + \theta_{i+1})$
R4	θ_i v.s. $-\theta_{i+1}$
R5	$(\pi - \theta_i)$ v.s. θ_{i+1}
R6	$(\pi - \theta_i)$ v.s. $(\pi - \theta_{i+1})$
R7	$(\pi - \theta_i)$ v.s. $(-\pi + \theta_{i+1})$
R8	$(\pi - \theta_i)$ v.s. $-\theta_{i+1}$
R9	$-\theta_i$ v.s. $-\theta_{i+1}$
R10	$-\theta_i$ v.s. $(-\pi + \theta_{i+1})$
R11	$-\theta_i$ v.s. $(\pi - \theta_{i+1})$
R12	$-\theta_i$ v.s. θ_{i+1}
R13	$(-\pi + \theta_i)$ v.s. $-\theta_{i+1}$
R14	$(-\pi + \theta_i)$ v.s. $(-\pi + \theta_{i+1})$
R15	$(-\pi + \theta_i)$ v.s. $(\pi - \theta_{i+1})$
R16	$(-\pi + \theta_i)$ v.s. θ_{i+1}

For example, taking the spherical 4R linkage with the geometric parameters α_{12} , α_{23} , α_{34} or α_{41} as the basic geometric condition, a variant spherical 4R linkage can be obtained, when

$$\alpha'_{12} = \alpha_{12}, \alpha'_{23} = \pi - \alpha_{23}, \alpha'_{34} = \pi - \alpha_{34}, \alpha'_{41} = \alpha_{41} \quad (2-6)$$

By substituting (2-6) into (2-4), we can get

$$\begin{aligned} & \cos(\pi - \alpha_{23}) \cdot \sin \alpha_{41} \cdot \sin \alpha_{12} \cdot \cos \theta'_1 \\ & + \cos \alpha_{41} \cdot \sin \alpha_{12} \cdot \sin(\pi - \alpha_{23}) \cdot \cos \theta'_2 \\ & + \cos \alpha_{12} \cdot \sin(\pi - \alpha_{23}) \cdot \sin \alpha_{41} \cdot \cos \theta'_1 \cdot \cos \theta'_2 \\ & - \sin(\pi - \alpha_{23}) \cdot \sin \alpha_{41} \cdot \sin \theta'_1 \cdot \sin \theta'_2 \\ & + \cos(\pi - \alpha_{34}) - \cos \alpha_{12} \cdot \cos(\pi - \alpha_{23}) \cdot \cos \alpha_{41} = 0; \end{aligned} \quad (2-7a)$$

$$\begin{aligned} & \cos(\pi - \alpha_{34}) \cdot \sin \alpha_{12} \cdot \sin(\pi - \alpha_{23}) \cdot \cos \theta'_2 \\ & + \cos \alpha_{12} \cdot \sin(\pi - \alpha_{23}) \cdot \sin(\pi - \alpha_{34}) \cdot \cos \theta'_3 \\ & + \cos(\pi - \alpha_{23}) \cdot \sin \alpha_{12} \cdot \sin(\pi - \alpha_{34}) \cdot \cos \theta'_2 \cdot \cos \theta'_3 \\ & - \sin \alpha_{12} \cdot \sin(\pi - \alpha_{34}) \cdot \sin \theta'_2 \cdot \sin \theta'_3 \\ & + \cos \alpha_{41} - \cos \alpha_{12} \cdot \cos(\pi - \alpha_{23}) \cdot \cos(\pi - \alpha_{34}) = 0; \end{aligned} \quad (2-7b)$$

$$\begin{aligned} & \cos \alpha_{41} \cdot \sin(\pi - \alpha_{23}) \cdot \sin(\pi - \alpha_{34}) \cdot \cos \theta'_3 \\ & + \cos(\pi - \alpha_{23}) \cdot \sin(\pi - \alpha_{34}) \cdot \sin \alpha_{41} \cdot \cos \theta'_4 \\ & + \cos(\pi - \alpha_{34}) \cdot \sin(\pi - \alpha_{23}) \cdot \sin \alpha_{41} \cdot \cos \theta'_3 \cdot \cos \theta'_4 \\ & - \sin(\pi - \alpha_{23}) \cdot \sin \alpha_{41} \cdot \sin \theta'_3 \cdot \sin \theta'_4 \\ & + \cos \alpha_{12} - \cos(\pi - \alpha_{23}) \cdot \cos(\pi - \alpha_{34}) \cdot \cos \alpha_{41} = 0; \end{aligned} \quad (2-7c)$$

$$\begin{aligned} & \cos \alpha_{12} \cdot \sin(\pi - \alpha_{34}) \cdot \sin \alpha_{41} \cdot \cos \theta'_4 \\ & + \cos(\pi - \alpha_{34}) \cdot \sin \alpha_{41} \cdot \sin \alpha_{12} \cdot \cos \theta'_1 \\ & + \cos \alpha_{41} \cdot \sin \alpha_{12} \cdot \sin(\pi - \alpha_{34}) \cdot \cos \theta'_4 \cdot \cos \theta'_1 \\ & - \sin \alpha_{12} \cdot \sin(\pi - \alpha_{34}) \cdot \sin \theta'_4 \cdot \sin \theta'_1 \\ & + \cos(\pi - \alpha_{23}) - \cos \alpha_{12} \cdot \cos(\pi - \alpha_{34}) \cdot \cos \alpha_{41} = 0; \end{aligned} \quad (2-7d)$$

Comparing the basic and variant spherical 4R linkages, with the same input, i.e.,

$$\theta'_1 = \theta_1 \quad (2-8)$$

According to Eqns. (2-4) and (2-7), the output is

$$\begin{aligned} \theta'_2 &= -\pi + \theta_2, \\ \theta'_3 &= -\theta_3, \\ \theta'_4 &= \pi - \theta_4. \end{aligned} \quad (2-9)$$

By considering Eqns. (2-8) and (2-9), these two sets of relationships among revolute variables are shown in Fig. 2-1. It is shown that the relationship between θ_i and θ_{i+1} is central symmetric, i.e.,

$$f_{i(i+1)}(-\theta_i) = -f_{i(i+1)}(\theta_i) = -\theta_{i+1} \quad (2-10)$$

which reveals that the geometric parameters for Ri and $R(i+8)$ in table 2-1 are exactly the same. So we only consider $R1$ to $R8$ in the later analysis.

We use $R1$ and $R9$ as the example to explain that the geometric parameters for Ri and $R(i+8)$ are exactly same. We put points $(\theta_i^0, \theta_{i+1}^0)$ and $(-\theta_i^0, -\theta_{i+1}^0)$ into (2-5), obtain

$$\begin{aligned} & \cos \alpha_{(i+1)(i+2)} \cdot \sin \alpha_{(i-1)i} \cdot \sin \alpha_{i(i+1)} \cdot \cos \theta_i^0 \\ & + \cos \alpha_{(i-1)i} \cdot \sin \alpha_{i(i+1)} \cdot \sin \alpha_{(i+1)(i+2)} \cdot \cos \theta_{i+1}^0 \\ & + \cos \alpha_{i(i+1)} \cdot \sin \alpha_{(i+1)(i+2)} \cdot \sin \alpha_{(i-1)i} \cdot \cos \theta_i^0 \cdot \cos \theta_{i+1}^0 \\ & - \sin \alpha_{(i+1)(i+2)} \cdot \sin \alpha_{(i-1)i} \cdot \sin \theta_i^0 \cdot \sin \theta_{i+1}^0 \\ & + \cos \alpha_{(i+2)(i+3)} - \cos \alpha_{i(i+1)} \cdot \cos \alpha_{(i+1)(i+2)} \cdot \cos \alpha_{(i-1)i} = 0. \end{aligned} \quad (2-11a)$$

$$\begin{aligned} & \cos \alpha_{(i+1)(i+2)} \cdot \sin \alpha_{(i-1)i} \cdot \sin \alpha_{i(i+1)} \cdot \cos(-\theta_i^0) \\ & + \cos \alpha_{(i-1)i} \cdot \sin \alpha_{i(i+1)} \cdot \sin \alpha_{(i+1)(i+2)} \cdot \cos(-\theta_{i+1}^0) \\ & + \cos \alpha_{i(i+1)} \cdot \sin \alpha_{(i+1)(i+2)} \cdot \sin \alpha_{(i-1)i} \cdot \cos(-\theta_i^0) \cdot \cos(-\theta_{i+1}^0) \\ & - \sin \alpha_{(i+1)(i+2)} \cdot \sin \alpha_{(i-1)i} \cdot \sin(-\theta_i^0) \cdot \sin(-\theta_{i+1}^0) \\ & + \cos \alpha_{(i+2)(i+3)} - \cos \alpha_{i(i+1)} \cdot \cos \alpha_{(i+1)(i+2)} \cdot \cos \alpha_{(i-1)i} = 0. \end{aligned} \quad (2-11b)$$

After simplifying Eqn. (2-11b), we can see that Eqns. (2-11a) and (2-11b) are same, which means $R1$ and $R9$ have the same link twist angles α_{ij} .

The variations of the kinematic relationships and their corresponding geometric parameters are listed in Table A1 of appendix, which can be used to vary the rotation transmission between θ_i and θ_{i+1} when geometric parameters are changed. For each Ri , there are 16 corresponding solutions as listed in the appendix. All rest variant linkages offer rather complicated changes in kinematic variables and are not considered in this chapter.

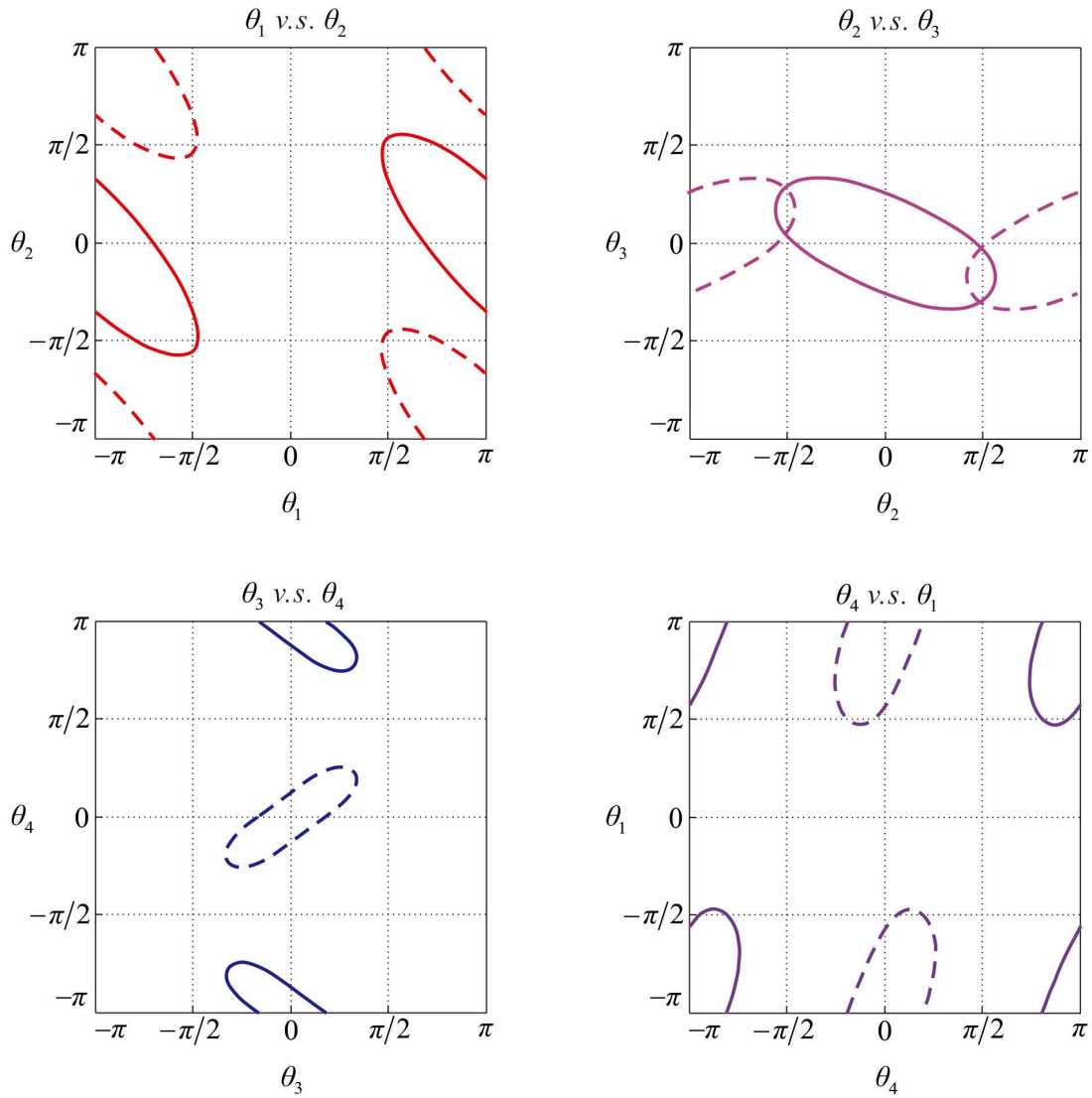


Figure 2-1 Relationship among the revolute variables of spherical 4R linkages.

(solid line: $\alpha_{12} = \pi/9, \alpha_{23} = 2\pi/9, \alpha_{34} = 4\pi/9, \alpha_{41} = 2\pi/3,$

dash line: $\alpha'_{12} = \pi/9, \alpha'_{23} = 7\pi/9, \alpha'_{34} = 5\pi/9, \alpha'_{41} = 2\pi/3.$)

By using Eqn. (2-6), the basic spherical 4R linkage is changed to a variant type and the rotation transmission loop is also changed. The closed loop of rotation transmission in the basic spherical 4R linkage is,

$$\begin{array}{c}
 (\theta_1) \rightarrow (\theta_2) \rightarrow (\theta_3) \rightarrow (\theta_4) \\
 \uparrow \hspace{10em} \downarrow \\
 \hline
 \end{array}
 \tag{2-12}$$

And that in the variant spherical 4R linkage is

$$\begin{array}{c}
 (\theta'_1) \rightarrow (\theta'_2) \rightarrow (\theta'_3) \rightarrow (\theta'_4) \\
 \uparrow \hspace{10em} \downarrow \\
 \hline
 \end{array}
 \tag{2-13a}$$

i.e.,

$$(\theta_1) \rightarrow (-\pi + \theta_2) \rightarrow (-\theta_3) \rightarrow (-\pi + \theta_4) \quad (2-13b)$$

2.3 One-DOF Mobile Assemblies of Four Identical Spherical 4R Linkages

In order to construct one-DOF mobile assemblies with a tessellation of unlimited number of spherical 4R linkages, a closed loop of four spherical 4R linkages is considered first. The connection between two spherical 4R linkages is constructed through the aligned revolute joint. For example, two spherical 4R linkages are connected in Fig. 2-2. Link 12 of linkage A and link 14 of linkage B are connected rigidly into one body. So are the link 14 of linkage A and link 12 of linkage B. As a result, the joint a_1 of linkage A and joint b_1 of linkage B are aligned into one revolute joint with the same motion, i.e., $\theta_1^a = \theta_1^b$.

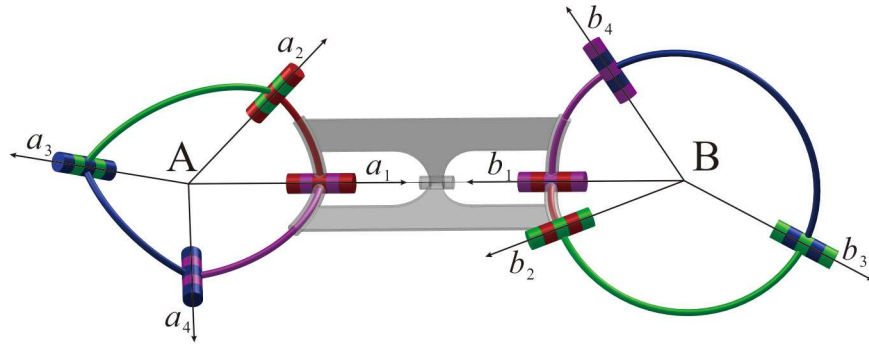


Figure 2-2 Assembly of two spherical 4R linkages.

To start from the simplest situation, we can set that the four spherical 4R linkages are identical, i.e., the geometric parameters of the linkages satisfy

$$\begin{aligned}
 \alpha_{12}^a &= \alpha_{12}^b = \alpha_{12}^c = \alpha_{12}^d = \alpha_{12}, \\
 \alpha_{23}^a &= \alpha_{23}^b = \alpha_{23}^c = \alpha_{23}^d = \alpha_{23}, \\
 \alpha_{34}^a &= \alpha_{34}^b = \alpha_{34}^c = \alpha_{34}^d = \alpha_{34}, \\
 \alpha_{41}^a &= \alpha_{41}^b = \alpha_{41}^c = \alpha_{41}^d = \alpha_{41}.
 \end{aligned} \quad (2-14)$$

As connection between two joints shown in Fig. 2-2, the joints with the same subscript are assembled. For example, the rotation of joint a_2 of linkage A and joint b_2 of linkage B are exactly the same after assembling. So the same as the joint b_1 of linkage B and the joint c_1 of linkage C, joint c_2 of linkage C and joint d_2 of linkage D, joint d_1

of linkage D and joint a_1 of linkage A. Then, a closed loop of spherical 4R linkages A, B, C and D is obtained. This is an assembly strategy corresponding to Path1 in Fig. 2-3. Other three types of available assemblies are also shown in it.

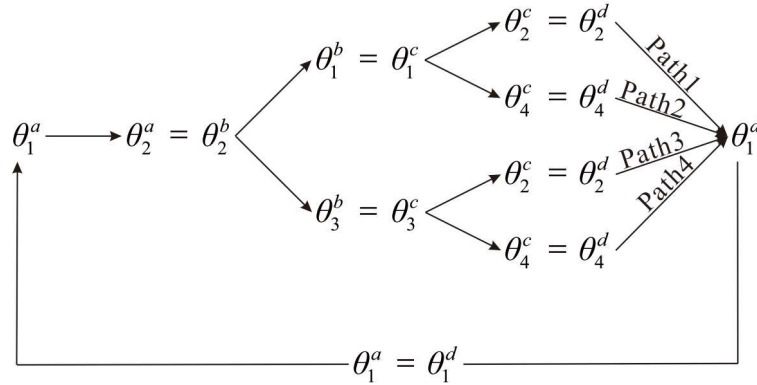


Figure 2-3 Assemblies of four spherical 4R linkages.

The corresponding graph representations of these four assemblies are shown in Fig. 2-4. The nodes in the graph represent the joints connecting the ends of the links. The straight lines are the axes of the joints intersecting at the dark points. The distributions of the four spherical 4R linkages in the assemblies are shown in Fig. 2-4. The distributions of spherical 4R linkages A and D, B and C are symmetric about the horizontal direction in Fig. 2-4 (b). The distributions of A and B are symmetric with D and C about the vertical direction in Fig. 2-4 (c). Because of having the same symmetric characteristics, Path2 and Path3 are the same in fact. In summary, there are only three assemblies available, i.e., Path1, Path3 and Path4 in Fig. 2-4.

In Fig. 2-4(a), the distribution of spherical 4R linkages C and D are the mirror of A and B, B and C are the mirror of A and D, so we name it twofold-symmetric case. In Fig. 2-4(c), the distribution of spherical 4R linkages C and D is the mirror of A and B so we call it symmetric case. In Fig. 2-4(d), the distribution of four joints of each linkages is center clockwise about the sphere center, so we name it rotational case.

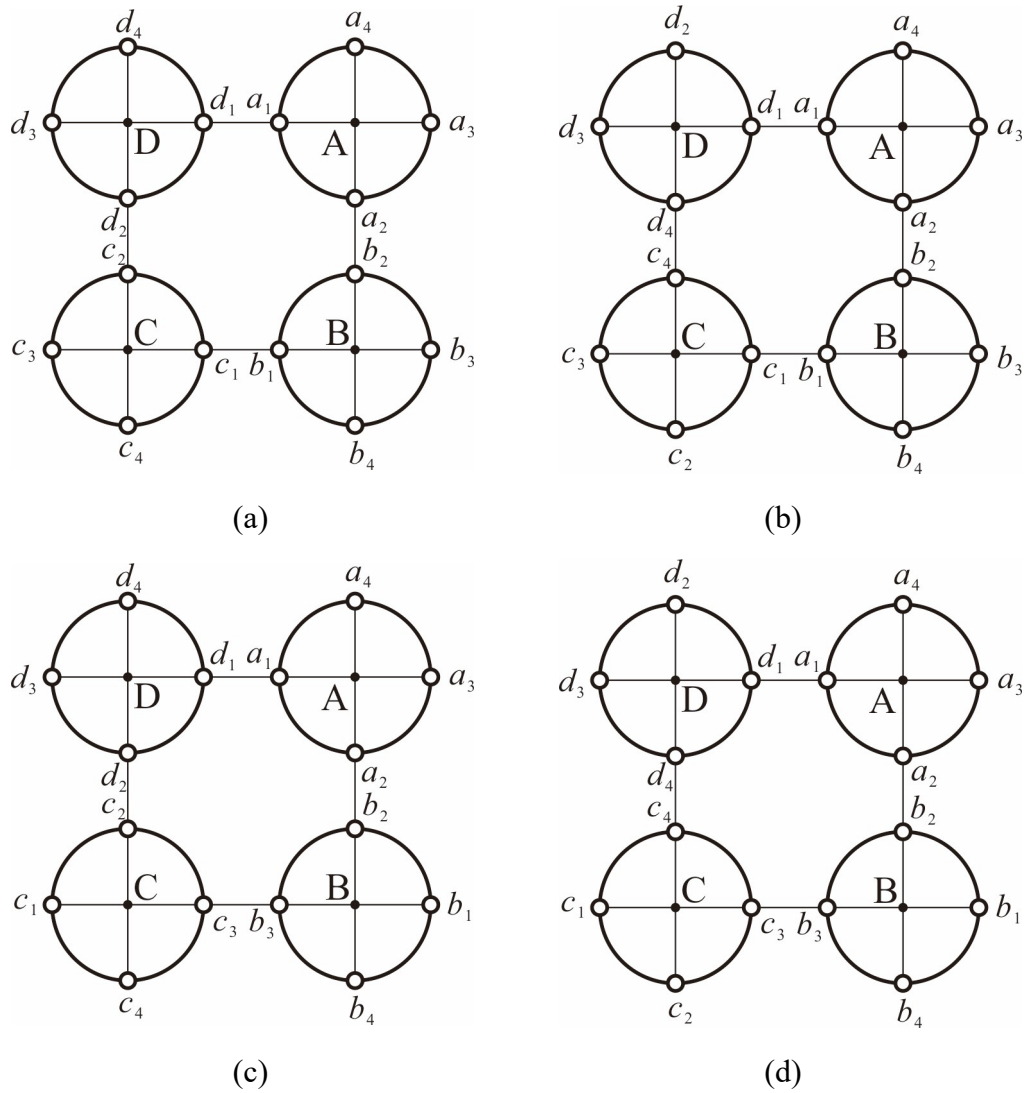


Figure 2-4 Graph representation of the assemblies.

(a) Path1: Twofold-symmetric case; (b) Path2: similar as Path3; (c) Path3: Symmetric case; (d) Path4: Rotational case.

Referring to Fig. 2-4 (a), an assembly of four spherical 4R linkages is shown in Fig. 2-5. The joints a_2 and b_2 , b_1 and c_1 , c_2 and d_2 , d_1 and a_1 are respectively connected collinearly with the same motion. The DH notation systems' property causes that rotation angles and kinematic variables are not simply the same all the time. E.g., the rotation angles of joints a_2 and b_2 in Fig. 2-5 are equal, but $\theta_2^a = -\theta_2^b$. After connecting, we have

$$\theta_2^a = -\theta_2^b, \theta_1^b = -\theta_1^c, \theta_2^c = -\theta_2^d, \theta_1^d = -\theta_1^a. \quad (2-15)$$

In order to keep this assembly one-DOF, the kinematical compatibility conditions must be set up. If taking θ_1^a as input, the rotational motion transfers through the collinear joints, and back to θ_1^a at last. The transmission loop is

Referring to Fig. 2-4(d), an assembly of four spherical 4R linkages is shown in Fig. 2-7. The joints a_2 and b_2, b_3 and c_3, c_4 and d_4, d_1 and a_1 are respectively collinear. For this assembly, we have

$$\theta_2^a = \theta_2^b, \theta_3^b = \theta_3^c, \theta_4^c = \theta_4^d, \theta_1^d = \theta_1^a. \quad (2-23)$$

The transmission loop is

$$\begin{aligned} (\theta_1^a) \rightarrow (\theta_2^a) = (\theta_2^b) \rightarrow (\theta_3^b) = (\theta_3^c) \rightarrow (\theta_4^c) = (\theta_4^d) \rightarrow (\theta_1^d) \\ \uparrow \hspace{15em} \downarrow \\ (\theta_1^a) = (\theta_1^d) \end{aligned} \quad (2-24)$$

Then, the transmission loop is represented as

$$f_{41}^D(f_{34}^C(f_{23}^B(f_{12}^A(\theta_1^a)))) = \theta_1^a \quad (2-25)$$

Simplified by the identical conditions of linkages A, B, C and D, then gives

$$f_{41}(f_{34}(f_{23}(f_{12}(\theta_1)))) = \theta_1 \quad (2-26)$$

which can obviously exist. Thus, the compatibility condition of rotation case is satisfied, i.e., this assembly is mobile with one DOF.

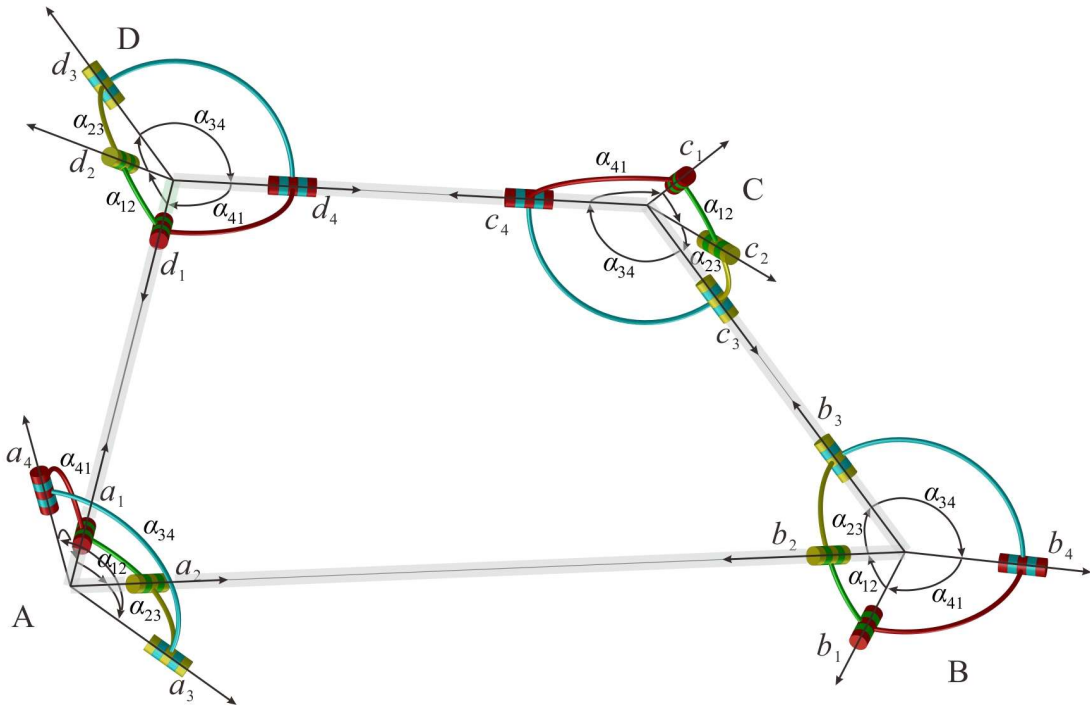


Figure 2-7 Rotation case of four identical spherical 4R linkages' assembly.

$$(\alpha_{12} = 2\pi/9, \alpha_{23} = 3\pi/9, \alpha_{34} = 13\pi/18, \alpha_{41} = 5\pi/9)$$

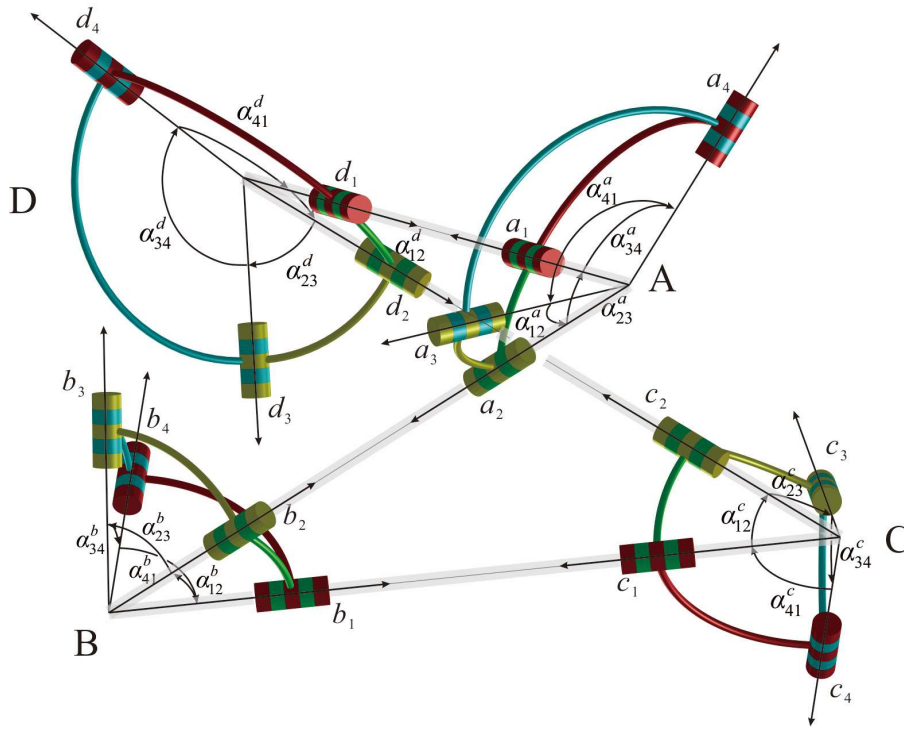


Figure 2-8 A kind of variant two-fold symmetric case.

Table 2-2. Variant relations for two-fold symmetric case

Transmission types	method
t_1^{2R}	$R2 - R2$
t_2^{2R}	$R3 - R3$
t_3^{2R}	$R4 - R4$
t_4^{2R}	$R5 - R5$
t_5^{2R}	$R12 - R12$
t_6^{2R}	$R16 - R16$
t_1^{3R}	$R2 - R6 - R2$
t_2^{3R}	$R2 - R7 - R3$
t_3^{3R}	$R2 - R8 - R4$
t_4^{3R}	$R3 - R13 - R4$
t_5^{3R}	$R3 - R14 - R3$
t_6^{3R}	$R3 - R15 - R2$
t_7^{3R}	$R4 - R9 - R4$
t_8^{3R}	$R4 - R10 - R3$
t_9^{3R}	$R4 - R11 - R2$

Table 2-4. Variant relations for rotation case

Transmission types	method
t_1^{2R}	$R2 - R5$
t_2^{2R}	$R3 - R16$
t_3^{2R}	$R4 - R12$
t_1^{3R}	$R2 - R6 - R5$
t_2^{3R}	$R2 - R7 - R16$
t_3^{3R}	$R2 - R8 - R12$
t_4^{3R}	$R3 - R13 - R12$
t_5^{3R}	$R3 - R14 - R16$
t_6^{3R}	$R3 - R15 - R5$
t_7^{3R}	$R4 - R9 - R12$
t_8^{3R}	$R4 - R10 - R16$
t_9^{3R}	$R4 - R11 - R5$

2.5 The Corresponding Rigid Origami Patterns

Rigid origami is an overconstrained system which is immobile generally. The analysis of its mobility relies on an equivalent mechanism with that the paper creases act as joints and paper panels act as links. The vertex with four creases can be treated as a spherical 4R linkage. Thus, the origami pattern in Fig. 2-11 can correspond to the network in Fig. 2-7. For example, the creases AE_1 and AE_2 correspond to joints $a4$ and $a3$ respectively. The crease AB is the combination of the coaxial joints $a2$ and $b2$. By this way, all the creases have the one-to-one relationships with the joints of spherical 4R linkages' network. If the corresponding assembly of spherical 4R linkages meets the compatibility conditions, the origami pattern is rigid.

In the process of designing rigid origami pattern inspired from mobile assemblies, some extra conditions should be added. For origami, the panel ABCD in Fig. 2-11 should be a planar quadrilateral obeying

$$\alpha_{12}^a + \alpha_{23}^b + \alpha_{34}^c + \alpha_{41}^d = 2\pi \quad (2-32)$$

If the pattern is flat-deployable, i.e., we can fold this pattern from a flat paper, the conditions are

$$\begin{aligned} \alpha_{12}^k + \alpha_{23}^k + \alpha_{34}^k + \alpha_{41}^k &= 2\pi, \\ 0 < \alpha_{ij}^k < \pi. \end{aligned} \quad (2-33)$$

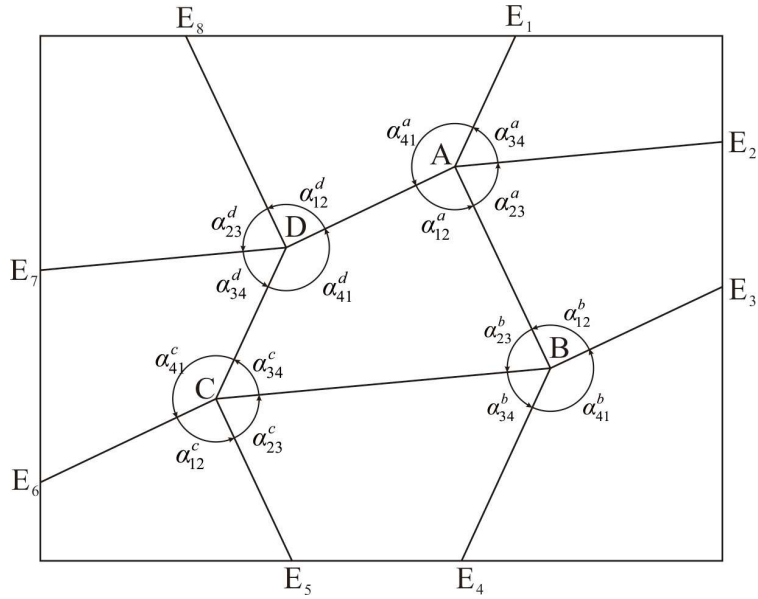


Figure 2-11 Crease pattern inspired by rotation case.

Combining Eqns. (2-13), (2-32) and (2-33), we obtain the conditions for this kind of origami pattern. An example is

$$\begin{aligned}
 \alpha_{12}^a &= \alpha_{12}^b = \alpha_{12}^c = \alpha_{12}^d = \pi/2, \\
 \alpha_{23}^a &= \alpha_{23}^b = \alpha_{23}^c = \alpha_{23}^d = 7\pi/18, \\
 \alpha_{34}^a &= \alpha_{34}^b = \alpha_{34}^c = \alpha_{34}^d = \pi/3, \\
 \alpha_{41}^a &= \alpha_{41}^b = \alpha_{41}^c = \alpha_{41}^d = 7\pi/9.
 \end{aligned}
 \tag{2-34}$$

The paper model is

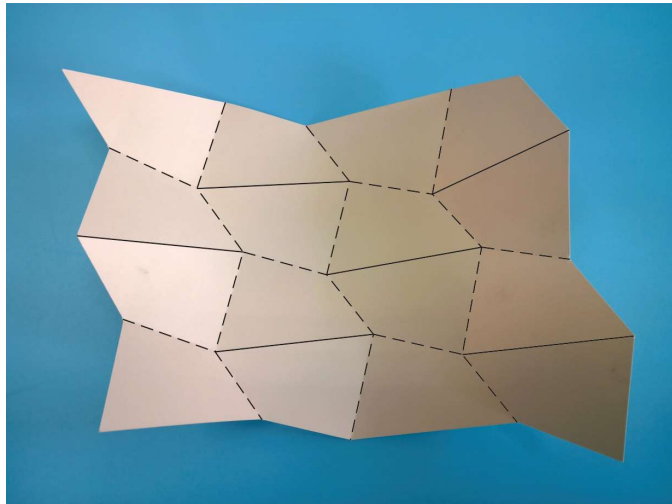


Figure 2-12 An origami pattern inspired by rotation case.

The networks of spherical 4R linkages based on variant relationships can also be used to design new origami patterns. For example, we modify the assembly in Fig. 2-7

2-13 relying on rotation case and variant type, all mobile networks of identical or different four spherical $4R$ linkages mentioned in sections 2.3 and 2.4 can be used to design origami patterns in the same way. In order to make the structure to be one DOF, the nonadjacent creases should not be collinear, i.e., the orthogonal creases can not exit^[55].

Rigid origami is a special case of Kokotsakis meshes. The Kokotsakis meshes satisfy that the plane ABCD is flat and every angle of each vertex is less than π . By using the varied transmission loops of the mobile assemblies of spherical $4R$ linkages, we can get the geometrical conditions of their corresponding Kokotsakis meshes in the Appendix table A2-A4. If every vertex of Kokotsakis mesh is flat, this mesh is a kind of rigid origami pattern. Referring to the tables, only one new rigid origami pattern is found and shown in Fig. 2-13.

2.6 Conclusion

In this chapter, we establish three basic mobile assemblies of four identical spherical $4R$ linkages. Kinematics is used to prove the mobility and the compatibility conditions have been presented. Based on the research of a single spherical $4R$ linkage's kinematics, we propose 16 variations of relationships R_i in Table 2-1 to alter the rotation transmission paths of the basic assemblies. According to table A1 in appendix, we find suitable parameters of spherical $4R$ linkages to meet the new transmission paths. Finally, we achieve to constitute the mobile assemblies of four different spherical $4R$ linkages.

The relationship between network of spherical $4R$ linkages and rigid origami makes it possible to use the mobile assemblies of spherical $4R$ linkages to design origami patterns. By combining the kinematic compatibility conditions of mobile assemblies and geometrical conditions of origami patterns, we get the conditions for rigid origami patterns. Two examples of this method have been shown in section 2.5.

The theory we have proposed in the chapter can give us large number of mobile assemblies of spherical $4R$ linkages. We modify the rotation transmission path firstly, find suitable spherical $4R$ linkages to meet it, then a network of spherical $4R$ linkages has been constituted. To the inverse process, we can use it to judge the mobility of assemblies and rigidity of origami patterns. For an assembly of spherical $4R$ linkages, we firstly check which R_i the linkages respectively belong to according to table A1 in appendix, then we use Table 2-1 to get the rotation transmission path. If the path can be closed, this assembly is mobile and its corresponding origami pattern is rigid.

Chapter 3 Rigid Foldability Origami Pattern and Metamaterials

3.1 Introduction

Flat foldability and rigidity are two specific and independent characteristics of origami pattern, both of which are decided or affected not only by the geometric angles of the crease pattern, but also by the assignment of mountain (convex) and valley (concave) fold lines on the creases^[104, 105]. Hull developed recursive functions to count the number of valid mountain and valley assignments for a single vertex pattern^[56]. Yet, for multi-vertex patterns, such as the square-twist pattern^[106, 107], there are a number of arguments on its foldability and rigidity^[100].

This chapter proposes a kinematic method to study the effect of mountain-valley fold assignments on the rigidity of flat foldable origami patterns in this chapter. In section 3.2, the double corrugated pattern is taken as the study case as it has more complicated mountain-valley fold assignments than Miura-ori, square-twist, or other periodic origami patterns. All the possible mountain-valley assignments for the basic units in the pattern are presented with the flat foldability condition. The analysis on the rigidity is conducted based on the kinematic models of spherical 4R linkage (S4R) assemblies. Subsequently, the tessellations of the double corrugated patterns and their metamaterials are explored. In section 3.3, to demonstrate the generalization of this method, the square-twist pattern and its metamaterials are also discussed. The conclusions in section 3.4 end this chapter.

3.2 Double corrugated pattern

For a typical four-fold vertex such as vertex A in Fig. 3-1(a), four creases divide the sheet into four portions, with sector angles α , β , γ and δ , respectively, and the sum of these angles equals 2π . To be flat foldable—the folded origami can be pressed flat eventually — $\alpha + \gamma = \beta + \delta = \pi$ must be satisfied^[59]. At the same time, the mountain and valley assignment must be considered for the flat-foldability condition, which requires, first, the difference between the numbers of mountain and valley creases should be 2 according to Maekawa-Justin theory^[108], and second, the two creases forming the minimum sector angle should have different mountain-valley parity while the other two are of the same one referring to the Big-Little-Big Angle theorem^[56].

The double corrugated pattern in Fig. 3-1(a) consists two types of vertices with the

same set of four sector angles, and in vertices A, C, E, α , β , γ and δ are set in the counter-clockwise order, while in vertices B, D, F, they are set in the clockwise order. There are two different quadrilaterals in the general double corrugated pattern, which can be considered as two basic units, P with vertices A, B, C, D and Q with vertices A, B, E, F. Here γ is taken as the minimum angle among the four sector angles. According to the above flat-foldability condition, all possible mountain and valley folds can be assigned to each unit. Notice that mountain and valley folds are relative to each other depending on viewing them from the top or bottom of the paper. After removing such repeating ones, there are ten distinct assignments for the P unit in Fig. 3-1(b) and six for the Q unit in Fig. 3-1(c).

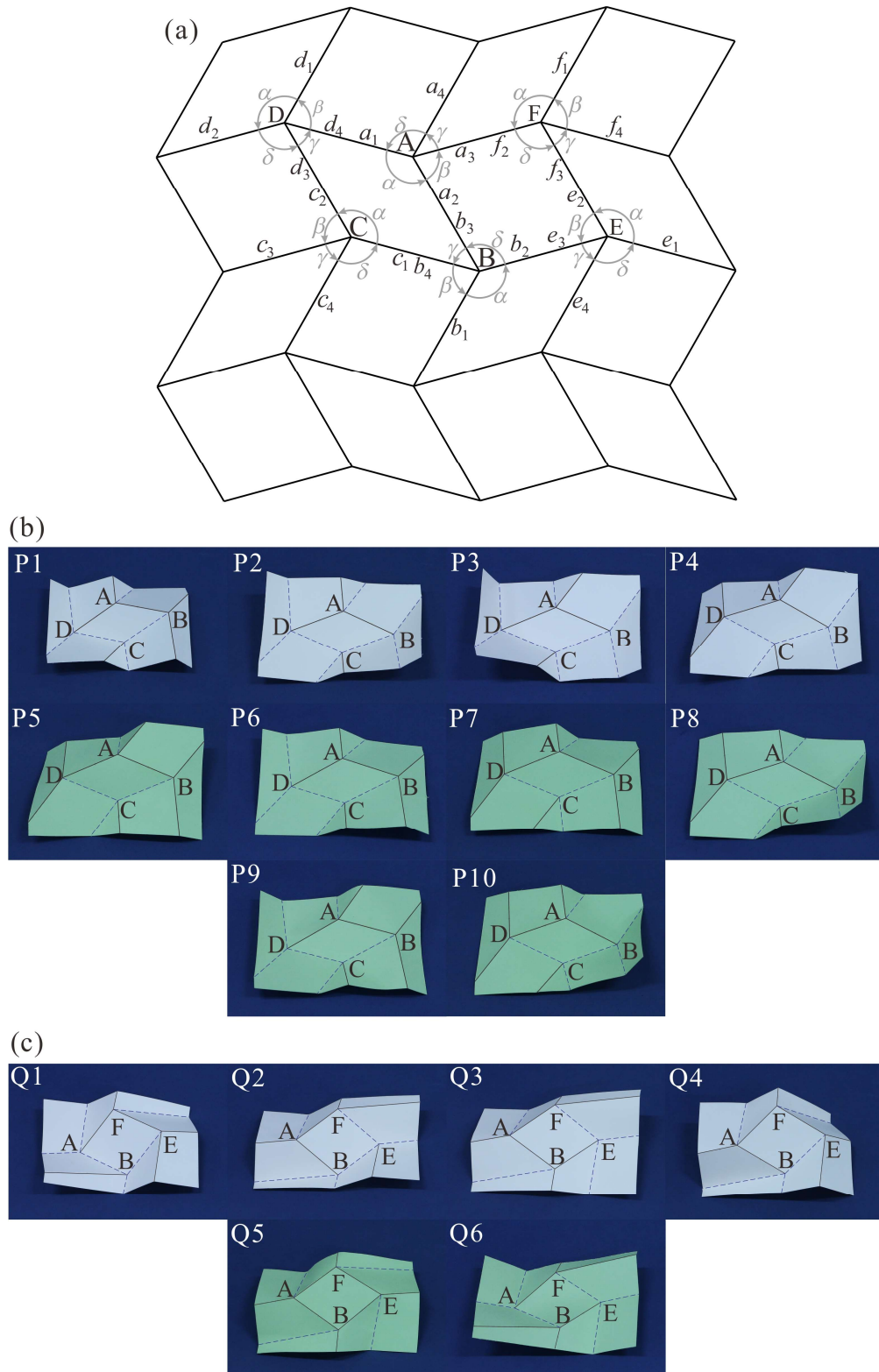


Figure 3-1 Double corrugated pattern and its basic unit patterns, (a) double corrugated pattern (b) mountain-valley assignments of unit P, (c) mountain-valley assignments of unit Q.

3.2.1 Kinematics of Origami Vertex for Double Corrugated Pattern

As mentioned above that there are two types of vertices in the double corrugated pattern with sector angles α , β , γ and δ setting counter-clockwise or clockwise. Kinematics, respectively they have to be considered as two different spherical 4R linkages by taking the paper panels as rigid links and the creases as revolute joints as shown in Figs. 3-2(a) and 3-2(b), named as types I and II, respectively. Hence, vertices A, C, E are modelled as type I linkage and B, D, F as type II.

The vertical angles are complementary in each vertexes of the double corrugated pattern. According to this character, we assume $\alpha_{12} + \alpha_{34} = \pi, \alpha_{23} + \alpha_{41} = \pi$ in spherical 4R linkage. Replacing (2-5) by the trigonometric functions,

$$t_i = \tan \frac{\theta_i}{2}, t_{i+1} = \tan \frac{\theta_{i+1}}{2},$$

$$\sin \theta_i = \frac{2t_i}{1+t_i^2}, \cos \theta_i = \frac{1-t_i^2}{1+t_i^2}, \sin \theta_{i+1} = \frac{2t_{i+1}}{1+t_{i+1}^2}, \cos \theta_{i+1} = \frac{1-t_{i+1}^2}{1+t_{i+1}^2}.$$

A simple equation is obtained

$$\frac{\tan \frac{\theta_i}{2}}{\tan \frac{\theta_{i+1}}{2}} = \frac{-\sin \alpha_{(i+1)(i+2)} \pm \sin \alpha_{i(i+1)}}{\sin(\alpha_{(i+1)(i+2)} + \alpha_{i(i+1)})} \quad (3-1)$$

The compatible condition of spherical 4R linkage is

$$\frac{\tan \frac{\theta_1}{2}}{\tan \frac{\theta_2}{2}} \cdot \frac{\tan \frac{\theta_2}{2}}{\tan \frac{\theta_3}{2}} \cdot \frac{\tan \frac{\theta_3}{2}}{\tan \frac{\theta_4}{2}} \cdot \frac{\tan \frac{\theta_4}{2}}{\tan \frac{\theta_1}{2}} = 1 \quad (3-2)$$

So, we have two solutions for this spherical 4R linkage

$$\frac{\tan \frac{\theta_1}{2}}{\tan \frac{\theta_2}{2}} = -\frac{\sin \frac{\alpha_{23} - \alpha_{12}}{2}}{\sin \frac{\alpha_{23} + \alpha_{12}}{2}}, \frac{\tan \frac{\theta_2}{2}}{\tan \frac{\theta_3}{2}} = \frac{\sin \frac{\alpha_{23} + \alpha_{12}}{2}}{\sin \frac{\alpha_{23} - \alpha_{12}}{2}},$$

$$\frac{\tan \frac{\theta_3}{2}}{\tan \frac{\theta_4}{2}} = \frac{\sin \frac{\alpha_{23} - \alpha_{12}}{2}}{\sin \frac{\alpha_{23} + \alpha_{12}}{2}}, \frac{\tan \frac{\theta_4}{2}}{\tan \frac{\theta_1}{2}} = -\frac{\sin \frac{\alpha_{23} + \alpha_{12}}{2}}{\sin \frac{\alpha_{23} - \alpha_{12}}{2}}, \quad (3-3a)$$

$$\begin{aligned}
 \frac{\tan \frac{\theta_1}{2}}{\tan \frac{\theta_2}{2}} &= -\frac{\cos \frac{\alpha_{23} - \alpha_{12}}{2}}{\cos \frac{\alpha_{23} + \alpha_{12}}{2}}, \frac{\tan \frac{\theta_2}{2}}{\tan \frac{\theta_3}{2}} = -\frac{\cos \frac{\alpha_{23} + \alpha_{12}}{2}}{\cos \frac{\alpha_{23} - \alpha_{12}}{2}}, \\
 \frac{\tan \frac{\theta_3}{2}}{\tan \frac{\theta_4}{2}} &= \frac{\cos \frac{\alpha_{23} - \alpha_{12}}{2}}{\cos \frac{\alpha_{23} + \alpha_{12}}{2}}, \frac{\tan \frac{\theta_4}{2}}{\tan \frac{\theta_1}{2}} = \frac{\cos \frac{\alpha_{23} + \alpha_{12}}{2}}{\cos \frac{\alpha_{23} - \alpha_{12}}{2}}.
 \end{aligned} \tag{3-3b}$$

For the linkage type I, we have $\alpha_{12} = \alpha$ and $\alpha_{23} = \beta$, so Eqn. (3-3) is simplified as,

$$\begin{aligned}
 \frac{\tan \frac{\theta_1}{2}}{\tan \frac{\theta_2}{2}} &= -\frac{\cos \frac{\beta - \alpha}{2}}{\cos \frac{\beta + \alpha}{2}}, \frac{\tan \frac{\theta_2}{2}}{\tan \frac{\theta_3}{2}} = -\frac{\cos \frac{\beta + \alpha}{2}}{\cos \frac{\beta - \alpha}{2}}, \\
 \frac{\tan \frac{\theta_3}{2}}{\tan \frac{\theta_4}{2}} &= \frac{\cos \frac{\beta - \alpha}{2}}{\cos \frac{\beta + \alpha}{2}}, \frac{\tan \frac{\theta_4}{2}}{\tan \frac{\theta_1}{2}} = \frac{\cos \frac{\beta + \alpha}{2}}{\cos \frac{\beta - \alpha}{2}},
 \end{aligned} \tag{3-4a}$$

$$\begin{aligned}
 \frac{\tan \frac{\theta_1}{2}}{\tan \frac{\theta_2}{2}} &= -\frac{\sin \frac{\beta - \alpha}{2}}{\sin \frac{\beta + \alpha}{2}}, \frac{\tan \frac{\theta_2}{2}}{\tan \frac{\theta_3}{2}} = \frac{\sin \frac{\beta + \alpha}{2}}{\sin \frac{\beta - \alpha}{2}}, \\
 \frac{\tan \frac{\theta_3}{2}}{\tan \frac{\theta_4}{2}} &= \frac{\sin \frac{\beta - \alpha}{2}}{\sin \frac{\beta + \alpha}{2}}, \frac{\tan \frac{\theta_4}{2}}{\tan \frac{\theta_1}{2}} = -\frac{\sin \frac{\beta + \alpha}{2}}{\sin \frac{\beta - \alpha}{2}}.
 \end{aligned} \tag{3-4b}$$

For the linkage type II, we have $\alpha_{12} = \alpha$ and $\alpha_{23} = \delta$, so Eqn. (3-3) is simplified as,

$$\begin{aligned}
 \frac{\tan \frac{\theta_1}{2}}{\tan \frac{\theta_2}{2}} &= -\frac{\sin \frac{\delta - \alpha}{2}}{\sin \frac{\delta + \alpha}{2}}, \frac{\tan \frac{\theta_2}{2}}{\tan \frac{\theta_3}{2}} = \frac{\sin \frac{\delta + \alpha}{2}}{\sin \frac{\delta - \alpha}{2}}, \\
 \frac{\tan \frac{\theta_3}{2}}{\tan \frac{\theta_4}{2}} &= \frac{\sin \frac{\delta - \alpha}{2}}{\sin \frac{\delta + \alpha}{2}}, \frac{\tan \frac{\theta_4}{2}}{\tan \frac{\theta_1}{2}} = -\frac{\sin \frac{\delta + \alpha}{2}}{\sin \frac{\delta - \alpha}{2}},
 \end{aligned} \tag{3-5a}$$

$$\begin{aligned}
 \frac{\tan \frac{\theta_1}{2}}{\tan \frac{\theta_2}{2}} &= -\frac{\cos \frac{\delta - \alpha}{2}}{\cos \frac{\delta + \alpha}{2}}, \quad \frac{\tan \frac{\theta_2}{2}}{\tan \frac{\theta_3}{2}} = -\frac{\cos \frac{\delta + \alpha}{2}}{\cos \frac{\delta - \alpha}{2}}, \\
 \frac{\tan \frac{\theta_3}{2}}{\tan \frac{\theta_4}{2}} &= \frac{\cos \frac{\delta - \alpha}{2}}{\cos \frac{\delta + \alpha}{2}}, \quad \frac{\tan \frac{\theta_4}{2}}{\tan \frac{\theta_1}{2}} = \frac{\cos \frac{\delta + \alpha}{2}}{\cos \frac{\delta - \alpha}{2}}.
 \end{aligned} \tag{3-5b}$$

Here, θ_i is the bilateral angle on the crease. In general, $-\pi \leq \theta_i < \pi$. Yet, in origami, the paper cannot physically penetrate through each other. So for the mountain fold, $0 \leq \theta_M \leq \pi$ and for the valley fold, $-\pi \leq \theta_V \leq 0$. Generally, the spherical 4R linkage is one degree of freedom, i.e., one input angle can decide the rest three as the output. There are two sets of equations in the kinematic input-output relationship of type I linkage, which correspond to two different input-output curves, types I₁ and I₂ as shown in Fig. 3-2(a). A close look reveals that they present the motion paths of type I linkage with different mountain-valley assignments. As γ is the minimum angle among the four sector angles, the creases of θ_3 and θ_4 must be different. In type I₁, θ_1 , θ_2 , and θ_3 are of the same crease while θ_4 is the opposite. When θ_1 , θ_2 , and θ_3 are mountain folds and θ_4 is valley fold, the folding path is the solid line in the first quadrant with θ_1 , θ_2 both positive. Certainly, the four creases in this type I₁ linkage can be all reversed with θ_1 , θ_2 , and θ_3 valley folds and θ_4 mountain fold, and then the folding path is still on the solid line but in the third quadrant with θ_1 , θ_2 both negative. Similarly, in type I₂, θ_1 , θ_2 , and θ_4 are of the same crease while θ_3 is the opposite, and the folding path is the dash line. In the same manner, the curves in Fig 2b can be interpreted for the type II₁ and II₂ linkages, where the curves are the relationship between θ_3 and θ_4 whose signs are always positive.

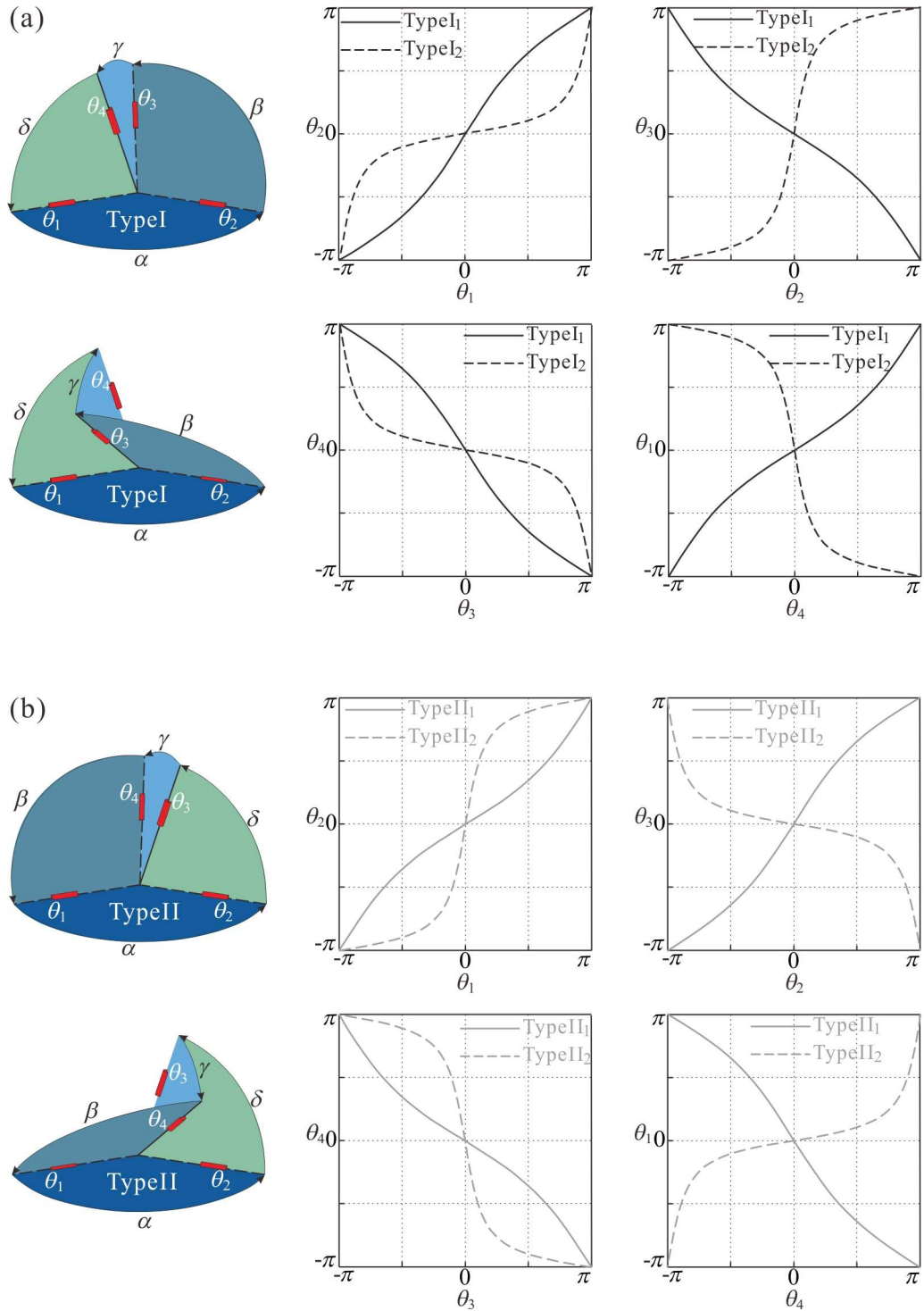


Figure 3-2 Spherical 4R linkage and its kinematics, (a) Type I of spherical 4R linkage and its kinematics, (b) Type II of spherical 4R linkage and its kinematics.

$$\left(\alpha = \frac{3\pi}{4}, \beta = \frac{\pi}{3}, \gamma = \frac{\pi}{4}, \delta = \frac{2\pi}{3}\right)$$

If an object appears identical after a rotation of 180° , then it is said to have a two-fold rotational symmetry. Mathematically, this means that for a curve $y = f(x)$ to be two-fold rotational symmetric, the necessary and sufficient condition is that for any arbitrary point (x_0, y_0) on the curve which satisfies $y_0 = f(x_0)$, the rotation of it by 180° , which is $(-x_0, -y_0)$, is also on the same curve and therefore $-y_0 = f(-x_0)$ holds. All the curves in Fig. 3-2 are two-fold rotational symmetric. In order to prove this, we assume that an arbitrary point (θ_i, θ_{i+1}) is on the curve. According to Eqn. (3-1), we have

$$\tan \frac{\theta_{i+1}}{2} = \frac{\sin(\alpha_{(i+1)(i+2)} + \alpha_{i(i+1)})}{-\sin \alpha_{(i+1)(i+2)} \pm \sin \alpha_{i(i+1)}} \cdot \tan \frac{\theta_i}{2}, \quad (3-6)$$

Adding a negative sign on both sides of Eqn. (3-6)

$$-\tan \frac{\theta_{i+1}}{2} = \frac{\sin(\alpha_{(i+1)(i+2)} + \alpha_{i(i+1)})}{-\sin \alpha_{(i+1)(i+2)} \pm \sin \alpha_{i(i+1)}} (-\tan \frac{\theta_i}{2}), \quad (3-7)$$

Since $-\tan \frac{\theta_i}{2} = \tan \frac{-\theta_i}{2}$, $-\tan \frac{\theta_{i+1}}{2} = \tan \frac{-\theta_{i+1}}{2}$, Eqn. (3-7) can be rewritten as

$$\tan \frac{-\theta_{i+1}}{2} = \frac{\sin(\alpha_{(i+1)(i+2)} + \alpha_{i(i+1)})}{-\sin \alpha_{(i+1)(i+2)} \pm \sin \alpha_{i(i+1)}} \tan \frac{-\theta_i}{2}, \quad (3-8)$$

Comparing Eqn. (3-8) and Eqn. (3-1), we can see that $(-\theta_i, -\theta_{i+1})$ is also on the curves, and therefore the curves in Fig. 3-2 drawn from Eqn. (3-1) are two-fold rotational symmetric.

The definition of four-fold rotational symmetry is that an object repeats itself after 90° of rotation. Mathematically, this means that a curve $y = f(x)$ of four-fold rotational symmetry, requires that for any arbitrary point (x_0, y_0) on the curve which satisfies $y_0 = f(x_0)$, the rotation of it by 90° , which is $(y_0, -x_0)$, is also on the same curve and therefore $-x_0 = f(y_0)$ holds. Combing two curves of Fig. 3-2 into one figure gives some four-fold rotational symmetric curves. For example, the curve of type I₁ about θ_1 & θ_2 and the curve of type II₁ about θ_3 & θ_4 in Fig. 3-3(a), the curve of type I₂ about θ_1 & θ_2 and the curve of type II₂ about θ_3 & θ_4 in Fig. 3-3(b), the curve of type I₁ about θ_2 & θ_3 and the curve of type II₁ about θ_2 & θ_3 in Fig. 3-3(c), the curve of type I₂ about θ_2 & θ_3 and the curve of type II₂ about θ_2 & θ_3 in Fig. 3-3(d), are all four-fold rotation symmetric. We use Fig. 3-3(a) as an example to prove this conclude. According to Eqn. (3-4a), the function of dark solid curve in Fig. 3-3(a) are

$$\frac{\tan \frac{\theta_{in}}{2}}{\tan \frac{\theta_{out}}{2}} = -\frac{\cos \frac{\beta - \alpha}{2}}{\cos \frac{\beta + \alpha}{2}}, \quad (3-9a)$$

According to Eqn. (3-5a), the function of gray solid curve in Fig. 3-3(a) are

$$\frac{\tan \frac{\theta_{in}}{2}}{\tan \frac{\theta_{out}}{2}} = \frac{\sin \frac{\delta - \alpha}{2}}{\sin \frac{\delta + \alpha}{2}}, \quad (3-9b)$$

Assuming that an arbitrary point (θ_x, θ_y) is on the solid dark curve in Fig. 3-3(a). According to Eqn. (3-9a), we have

$$\tan \frac{\theta_y}{2} = -\frac{\cos \frac{\beta + \alpha}{2}}{\cos \frac{\beta - \alpha}{2}} \tan \frac{\theta_x}{2}, \quad (3-10)$$

Substituting $\beta + \delta = \pi$ into Eqn. (3-10)

$$\tan \frac{\theta_y}{2} = -\frac{\sin \frac{\delta - \alpha}{2}}{\sin \frac{\delta + \alpha}{2}} \tan \frac{\theta_x}{2}, \quad (3-11)$$

Since $-\tan \frac{\theta_x}{2} = \tan \frac{-\theta_x}{2}$, Eqn. (3-11) can be rewritten as

$$\tan \frac{-\theta_x}{2} = \frac{\sin \frac{\delta + \alpha}{2}}{\sin \frac{\delta - \alpha}{2}} \tan \frac{\theta_y}{2}, \quad (3-12)$$

Comparing Eqn. (3-9b) and Eqn. (3-12), it can be found that point $(\theta_y, -\theta_x)$ falls on the gray solid curve.

Assuming that an arbitrary point (θ_x, θ_y) is on the solid gray curve in Fig. 3-3(a). According to Eqn. (3-9b), we have

$$\tan \frac{\theta_y}{2} = \frac{\sin \frac{\delta + \alpha}{2}}{\sin \frac{\delta - \alpha}{2}} \tan \frac{\theta_x}{2}, \quad (3-13)$$

Substituting $\beta + \delta = \pi$ into Eqn. (3-13)

$$-\tan \frac{\theta_y}{2} = -\frac{\cos \frac{\beta - \alpha}{2}}{\cos \frac{\beta + \alpha}{2}} \tan \frac{\theta_x}{2}, \quad (3-14)$$

Since $-\tan \frac{\theta_x}{2} = \tan \frac{-\theta_x}{2}$, Eqn. (3-11) can be rewritten as

$$\tan \frac{-\theta_x}{2} = -\frac{\cos \frac{\beta + \alpha}{2}}{\cos \frac{\beta - \alpha}{2}} \tan \frac{\theta_y}{2}, \quad (3-15)$$

Comparing Eqn. (3-9a) and Eqn. (3-15), it can be found that point $(\theta_y, -\theta_x)$ falls on the dark solid curve.

So that points (θ_x, θ_y) and $(\theta_y, -\theta_x)$ are both on the curve in Fig. 3-3(a), therefore the curve is four-fold rotational symmetric. By the same method, we can prove that Fig. 3-3(b-c) are also four-fold rotational symmetric.

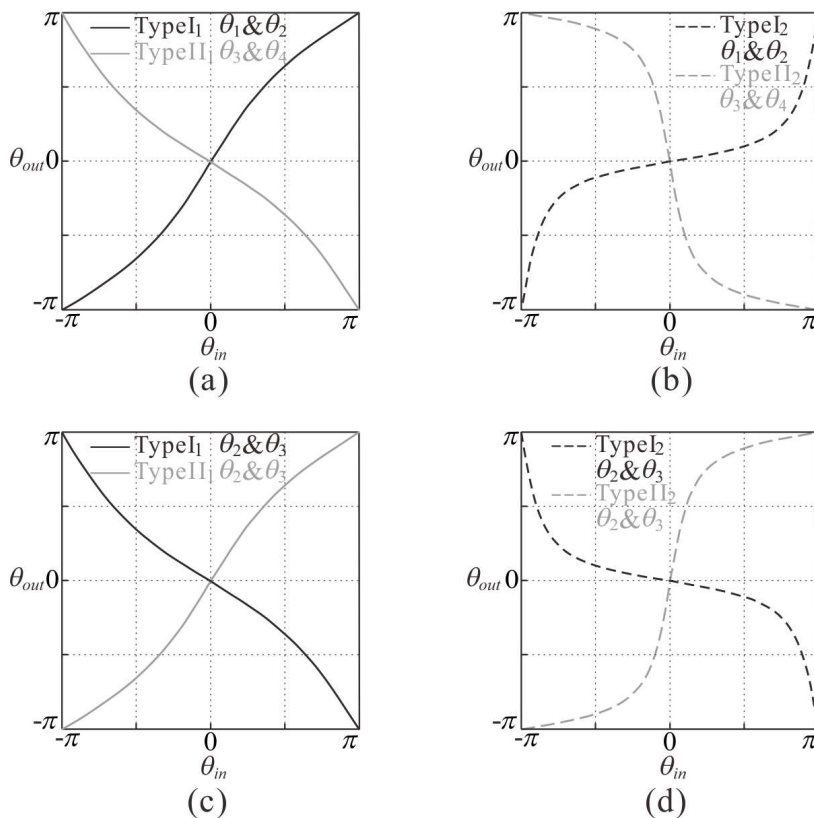


Figure 3-3 Combing curves from Fig. 3-2.

In the closed loop in Fig. 3-4, linkages A and C are type I in Fig. 3-2(a) and B, D are type II in Fig. 3-2(b). So we can use their motion curves to analyze the rigidity of the pattern unit. Take unit P1 in Fig. 3-1(b) as an example. From the mountain-valley assignments of each vertices, we can find their corresponding motion curves in Fig. 2. In vertex A, θ_1^a , θ_2^a , θ_4^a are mountain folds and θ_3^a is valley, so its curve is the first quadrant path of type I₁. The motion curves of vertices B, C, D are the fourth quadrant path of type I₂, the third quadrant path of type I₁, and the second quadrant path of type I₂, respectively. Combining these four curves together, the completed motion path of pattern unit P1 is formed as Fig. 3-4(a). Using the input-output path in Eqn. (3-17), we can allocate the instant configurations of linkages A, B, C, D. On the paths, points A, B, C, and D represent the configurations of four spherical 4R linkages in the closed loop and θ 's are the input/output sector angles. Taking θ_1^a as the initial input of the four-linkage loop and θ_4^d as the final output, if the compatibility condition, $\theta_4^d = \theta_1^a$ marked as the red arch is met. The compatibility condition, $\theta_4^d = \theta_1^a$, is satisfied as shown in Fig. 3-4(a) to 3-4(d), then the pattern units P1-P4 are rigid with one degree of freedom. Otherwise, as shown in Fig. 3-5(a) to 3-5(f), then the units P5-P10 are non-rigid.

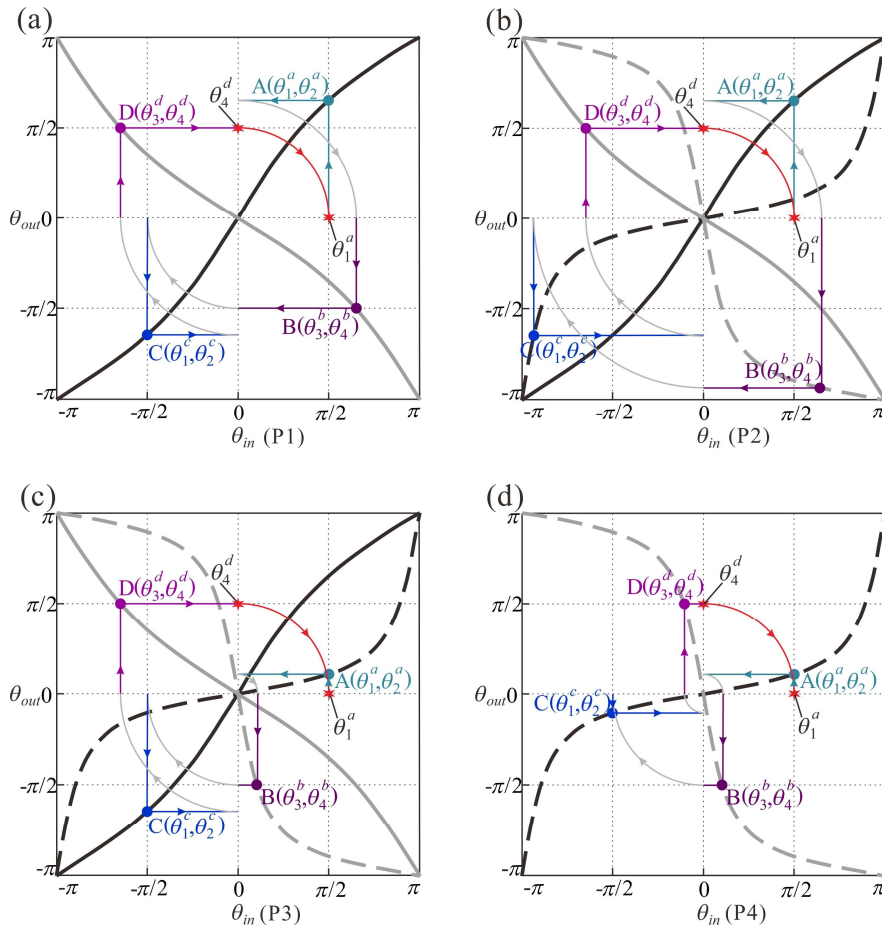


Figure 3-5 The rotation transmission of rigid types of unit P.

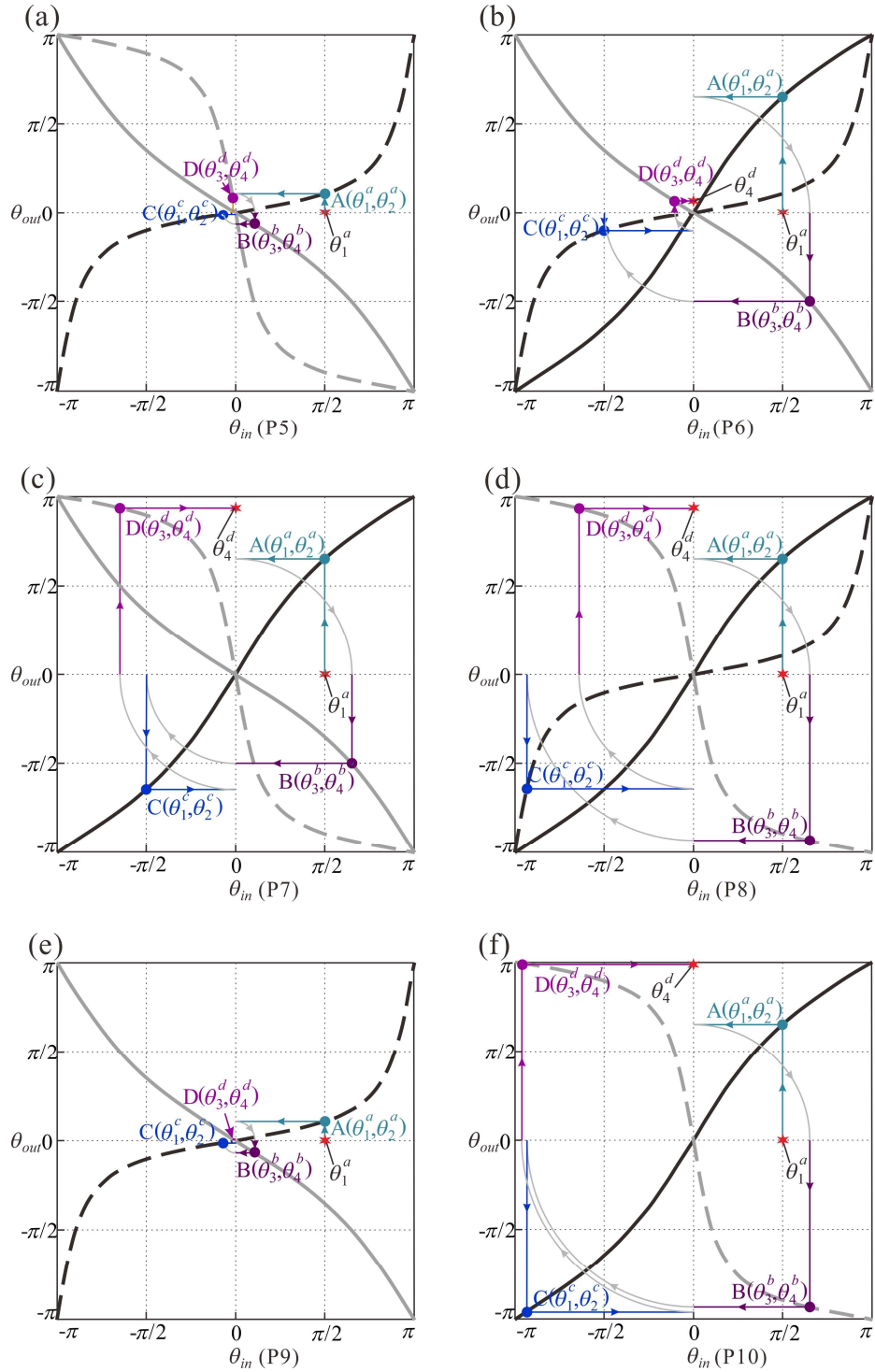


Figure 3-6 The rotation transmission of nonrigid types of unit P.

The curves in Fig. 3-5(b) and 3-5(c) can be treated as the combination of Fig 3-5(a) and 3-5(d). Referring to Fig. 3-3, we can see that the curves in Fig. 3-5 are all four-fold rotational symmetric. Due to the four-fold symmetric property of the motion curves, $\theta_4^d = \theta_1^a$ is met at all configurations on the motion paths of P1-P4 to guarantee the rigidity of the units, i.e., the kinematic compatibility condition Eqn. (3-16) is met at all

configurations on the motion paths of P1-P4.

Therefore, it can be found that in P1, all four vertices are in identical configuration but different orientations. And the same property also applies to unit P4. In P3, vertices A, B and C, D form two pairs of identical configurations. According to this four-fold rotational symmetric character, we have

$$\begin{aligned}\theta_1^a &= -\theta_4^b, \\ \theta_1^c &= -\theta_4^d,\end{aligned}\tag{3-18}$$

If we assume $\theta_2^a = \theta_3^b, \theta_4^b = \theta_1^c, \theta_2^c = \theta_3^d$, the following relationship can be worked out from Eqn. (3-18),

$$\theta_4^d = \theta_1^a\tag{3-19}$$

So the compatible conditions Eqn. (3-16) is satisfied, P1, P3, and P4 are rigid.

While in P2, vertices A, D and B, C forms two pairs of identical configurations, $\theta_4^d = \theta_1^a$ and $\theta_4^b = \theta_1^c$ are obtained. According to the four-fold rotational symmetric character, we have

$$\begin{aligned}\theta_3^d &= -\theta_2^a, \\ \theta_3^b &= -\theta_2^c,\end{aligned}\tag{3-20}$$

If we assume $\theta_4^b = \theta_1^c, \theta_2^c = \theta_3^d, \theta_4^d = \theta_1^a$, the following equation can be obtained from Eqn. (3-20)

$$\theta_2^c = \theta_3^d\tag{3-21}$$

So the compatible conditions Eqn. (3-16) is satisfied, P2 is rigid.

For the curves in Fig. 3-6, the four-fold rotational symmetric character does not exist, so Eqn. (3-16) is not satisfied at all configurations on the motion paths. Therefore, P5-P10 are not rigid patterns.

3.2.1.2 The Rigidity of Unit Q

As in the case of unit P, the vertices of unit Q can also be modelled as spherical 4R linkages with sector angles α , β , γ and δ setting counter-clockwise or clockwise, in which vertices A and E are of type I in Fig. 3-2(a), and vertices B and F are of type II in Fig. 3-2(b).

With each vertex being modelled as a spherical 4R linkage, the whole unit forms a closed loop of four spherical 4R linkages which is shown in Fig. 3-7. And the judgment on the rigidity of the unit is equivalent to the analysis on the compatibility condition of the closed loop of spherical 4R linkages. Kinematically, a closed loop of spherical 4R

linkages should satisfy the following geometric conditions

$$\theta_3^f = \theta_2^e, \theta_3^e = \theta_2^b, \theta_3^b = \theta_2^a, \theta_3^a = \theta_2^f. \quad (3-22)$$

The kinematic compatibility condition of this closed loop of four spherical 4R linkages, F, E, B, A in Fig. 3-7 is represented as

$$\begin{array}{c} \theta_2^f \rightarrow \theta_3^f = \theta_2^e \rightarrow \theta_3^e = \theta_2^b \rightarrow \theta_3^b = \theta_2^a \rightarrow \theta_3^a \\ \leftarrow \theta_2^f = \theta_3^a \rightarrow \end{array} \quad (3-23)$$

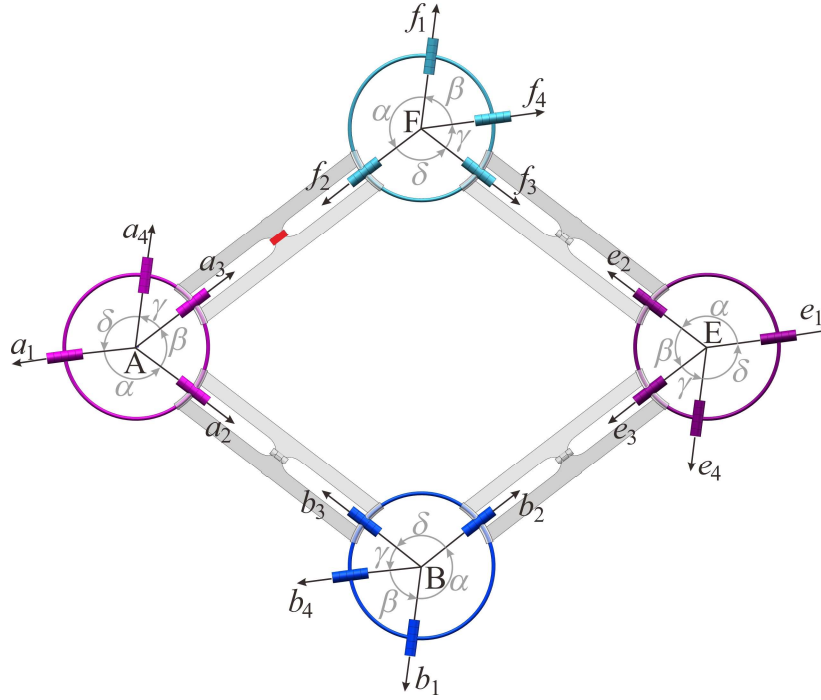


Figure 3-7 Network of spherical 4R linkages for Q pattern.

In this network, linkages A and E are type I, linkages B and F are type II in Fig. 3-2. Similar as the analysis of unit P, their motion curves are used to analyze the rigidity of the pattern unit. We take unit Q1 in Fig. 3-1(c) as an example. From the mountain valley assignments of each vertices, we can find their corresponding motion curves with Fig. 3-2. Combining these four curves together, the completed motion path of pattern unit Q1 is formed as Fig. 3-8(a). Using the input-output path in Eqn. (3-23), we can allocate the instant configurations of linkages F, E, B, A. Taking θ_2^f as the initial input of the four-linkage loop and θ_3^a as the final output, the compatibility condition is $\theta_2^f = \theta_3^a$.

The curves in Fig. 3-8(c) and 3-8(d) can be treated as the combination of Fig 3-8(a) and 3-8(b). Referring to Fig. 3-3, we can see that the curves in Fig. 3-8(a) to Fig. 3-8(d) are all four-fold rotational symmetric. Due to the four-fold symmetric property of the

motion curves, the kinematic compatibility condition Eqn. (3-22) is met at all configurations on the motion paths of Q1-Q4. Then the pattern unit Q1-Q4 is rigid with close transmission loop as shown in Figs. 3-8(a) to Fig. 3-8(d), the unit Q5-Q6 is non-rigid as shown in Fig. 3-8(e) and Fig. 3-8(f). The demonstration is the same as unit P and introduced in the previous section.

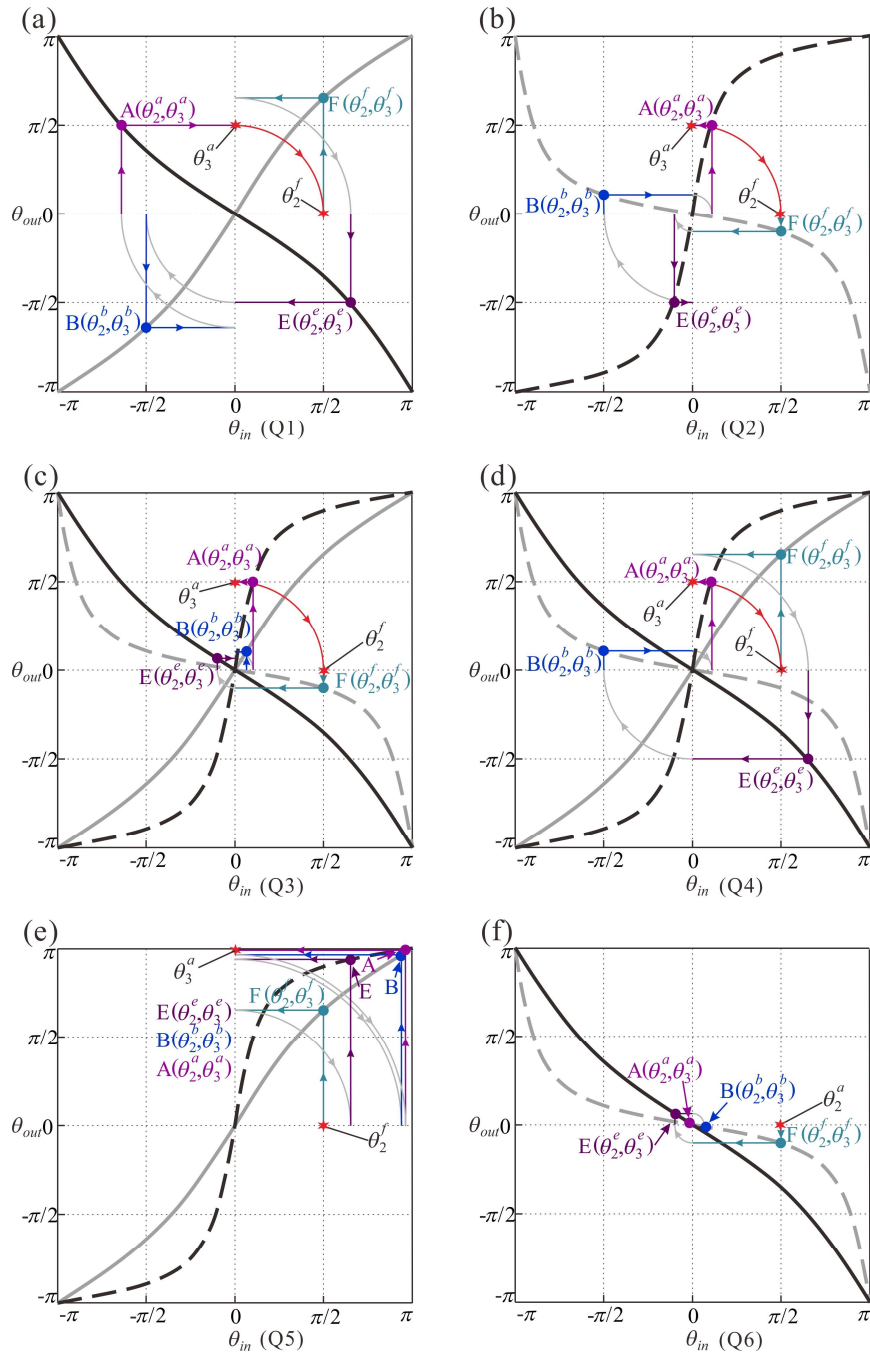


Figure 3-8 (a)-(f) are the transmission loops of the six Q pattern.

3.2.3 Tessellation of Double Corrugated Pattern and Its Metamaterials

The general periodic origami pattern is formed through the tessellating identical or different pattern units. The double corrugated pattern originally referred to in art and mathematics, Fig. 3-9(a), is formed with units P2 and Q1, both of which are rigid, and therefore the whole pattern is rigid as well with one degree of freedom. If one of the units in the pattern is non-rigid, the whole pattern will be non-rigid, see Fig. 3-9(b). Once different rigid units, P1-P4 and Q1-Q4, are mixed together, we can create many varieties of the double corrugated pattern, one of which is shown in Fig. 3-9(c). Therefore, rigid and non-rigid origami patterns based on identical geometric design parameters can be easily obtained just by altering assignments of mountain-valley creases.

For example, two P1 patterns and P2 patterns are used to complete the distribution of Mountain and Valley creases in Fig. 3-9(b) and 3-9(c). The directions of P2 patterns in Fig. 3(a) and (b) are different. After giving the M-V distribution of these four P patterns, the whole M-V distribution of the tessellation are decided, the other five unit patterns are derived and labeled by gray color. As P6 and Q6 are nonrigid pattern, so the tessellation in Fig. 3(b) is nonrigid.

Furthermore, we can stack a number of double corrugated patterns layer by layer to construct origami-based metamaterials. The four models shown in Fig. 3-10 are based on various patterns different from each other only in mountain-valley assignments, but with the same number of identical-sized layers. The patterns on the layers of each metamaterial have either identical or the reverse mountain-valley assignments to meet the mobile compatibility between layers. So once all the patterns forming the metamaterials are rigid, the metamaterials are capable of repeating-performed large deformation by folding and unfolding, which is a desired property. ϕ is the folding angle marked on the pattern. When the metamaterials have the same ϕ , their states are different as shown in Fig. 3-10.

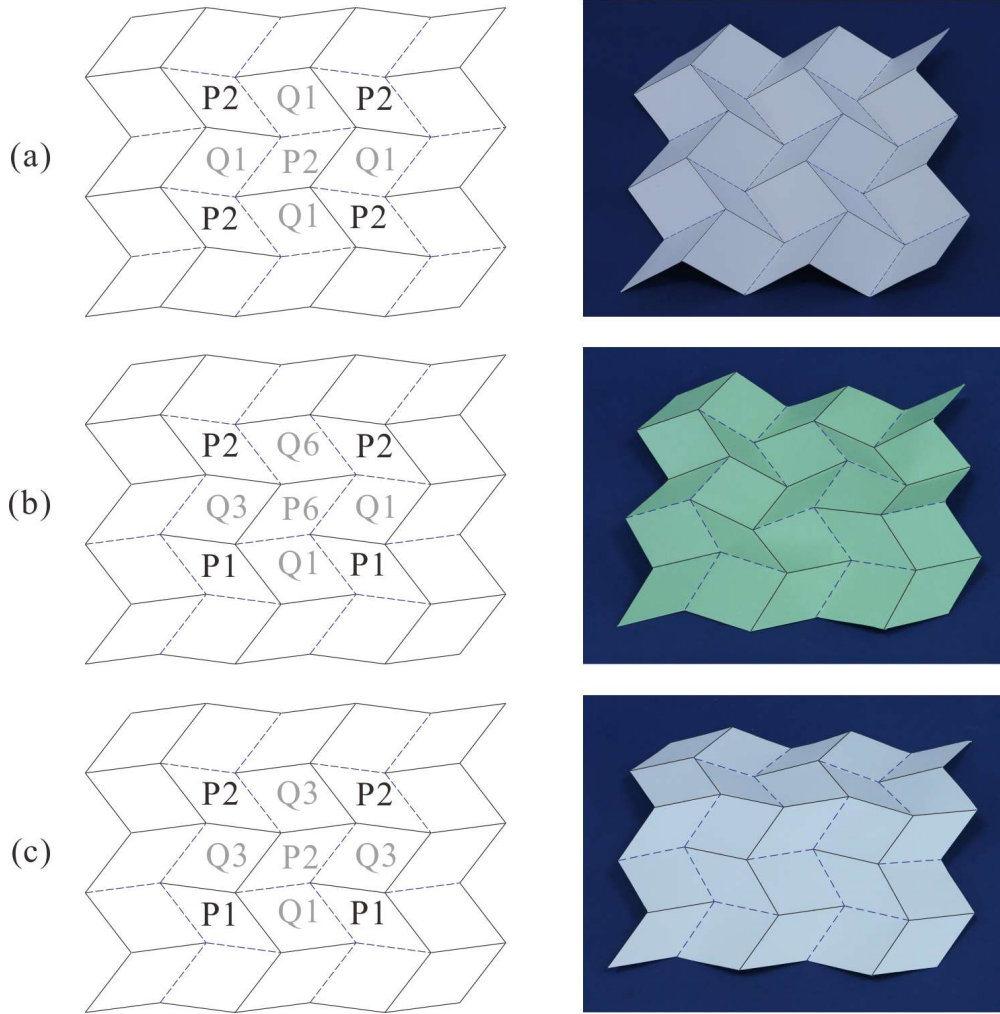


Figure 3-9 Various tessellations of units P and Q.

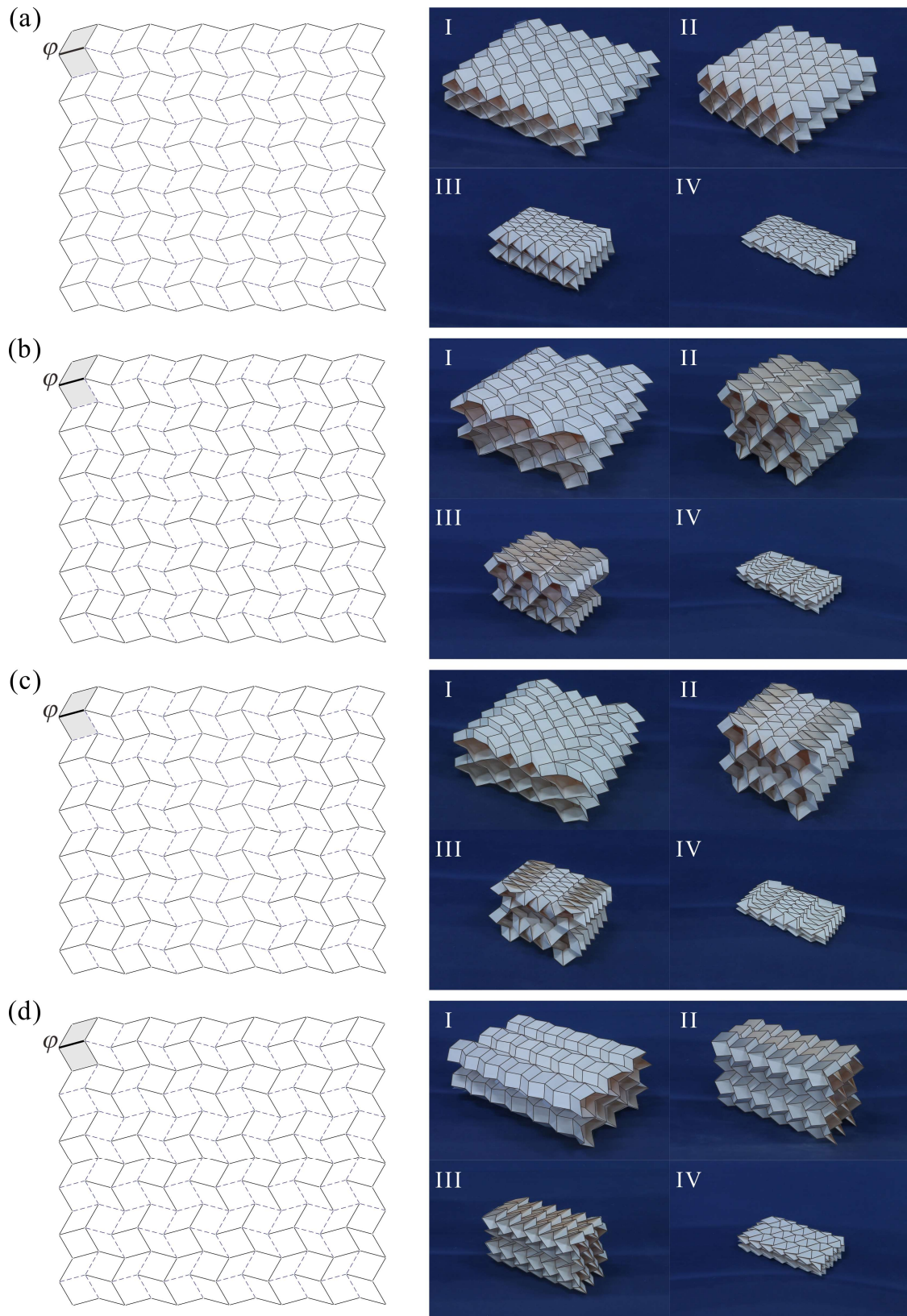


Figure 3-10 Tessellations and their corresponding metamaterials, (a) Metamaterial 1, (b) Metamaterial 2, (c) Metamaterial 3, (d) Metamaterial 4.

The four metamaterials presented in Fig. 3-10 are formed by three basic elements as shown in Fig. 3-11. In order to show more details, the view angle of element 3 rotates about 30° along the Z axis with respect to element 1 and element 2 which have identical view angle. In the photos of these elements, the black solid lines are mountain creases and blue dash lines are valley creases. Specifically, the metamaterial in Fig. 3-10(a) is constructed by element 1, the one in Fig. 3-10(b) by element 2, the one in Fig. 3-10(c) by element 1 and element 2, and the one in Fig. 3-10(d) by element 3. Since all the three basic elements are One-DOF, we use φ which is the dihedral angle of crease A_2B_2 in Fig. 3-11 as the input of these structures. Besides, all the creases in the elements are chosen to have identical length l for simplicity of calculation.

For element 1 in Fig. 3-11(a), its width at any given input angle φ can be calculated as follows

$$\begin{aligned} \cos \angle A_1A_2A_3 &= -\cos \beta \cdot \cos \alpha + \sin \beta \cdot \sin \alpha \cdot \cos \varphi \\ W = A_1A_3 &= 2 \cdot A_1A_2 \cdot \sin \frac{\angle A_1A_2A_3}{2} = 2 \cdot l \cdot \sin \frac{\angle A_1A_2A_3}{2} \end{aligned} \quad (3-24a)$$

The height of element 1 can be obtained as

$$\begin{aligned} \cos \angle B_2PB'_2 &= \frac{-\cos \alpha - \cos \beta \cdot \cos \angle A_1A_2A_3}{\sin \beta \cdot \sin \angle A_1A_2A_3} \\ PB_2 &= l \cdot \sin \beta \\ H = B_2B'_2 &= PB_2 \cdot \sin \angle B_2PB'_2 \end{aligned} \quad (3-24b)$$

The length of element 1 can be obtained as

$$\begin{aligned} PB'_2 &= PB_2 \cdot \cos \angle B_2PB'_2 \\ PA_2 &= l \cdot \cos \beta \\ A_2B'_2 &= \sqrt{(PB'_2)^2 + (PA_2)^2} \\ \angle PA_2B'_2 &= \arctan \frac{PB'_2}{PA_2} \\ \angle C_2A_2B'_2 &= \angle PA_2B'_2 - \frac{\angle A_1A_2A_3}{2} \\ L = A_2C_2 &= 2 \cdot A_2B'_2 \cdot \cos \angle C_2A_2B'_2 \end{aligned} \quad (3-24c)$$

For element 2 in Fig. 3-11(b), since C'_i ($i = 1, 2, 3$) is the reflection of C_i about plane $B_1B_2D_1D_2$, the height of this element is twice of $B_2B'_2$, and the length is twice of $A_2C'_2$. With any input angle φ , the width of element 2 are

$$\begin{aligned} \cos \angle A_1 A_2 A_3 &= -\cos \beta \cdot \cos \alpha + \sin \beta \cdot \sin \alpha \cdot \cos \varphi \\ W = A_1 A_3 &= 2 \cdot A_1 A_2 \cdot \sin \frac{\angle A_1 A_2 A_3}{2} = 2 \cdot l \cdot \sin \frac{\angle A_1 A_2 A_3}{2} \end{aligned} \quad (3-25a)$$

The height of element 2 can be obtained as

$$\begin{aligned} \cos \angle B_2 P B'_2 &= \frac{-\cos \alpha - \cos \beta \cdot \cos \angle A_1 A_2 A_3}{\sin \beta \cdot \sin \angle A_1 A_2 A_3} \\ P B_2 &= l \cdot \sin \beta \\ B_2 B'_2 &= P B_2 \cdot \sin \angle B_2 P B'_2 \\ H &= 2 \cdot B_2 B'_2 \end{aligned} \quad (3-25b)$$

The length of element 2 can be obtained as

$$\begin{aligned} P B'_2 &= P B_2 \cdot \cos \angle B_2 P B'_2 \\ P A_2 &= l \cdot \cos \beta \\ A_2 B'_2 &= \sqrt{(P B'_2)^2 + (P A_2)^2} \\ \angle P A_2 B'_2 &= \arctan \frac{P B'_2}{P A_2} \\ \angle C_2 A_2 B'_2 &= \angle P A_2 B'_2 - \frac{\angle A_1 A_2 A_3}{2} \\ L = A_2 E_2 &= 2 \cdot A_2 C'_2 = 4 \cdot A_2 B'_2 \cdot \cos \angle C_2 A_2 B'_2 \end{aligned} \quad (3-25c)$$

For element 3 in Fig. 3-11(c), A'_3, B'_3, C'_3 are respectively the reflections of A_3, B_3, C_3 about plane $A_2 A_4 B_2 B_4$. And therefore the height of this element is twice of $B_4 B'_4$, and the length is twice of $B_5 B'_3$. Denoting θ as the dihedral angle of crease $B_4 B_5$, the geometric relationship between φ and θ is^[109]

$$\theta = 2 \arctan \left(\frac{\tan \frac{\varphi}{2}}{\cos \frac{\beta - \alpha}{2}} \cdot \cos \frac{\beta + \alpha}{2} \right) \quad (3-26)$$

Then the length of element 3 can be obtained as

$$\begin{aligned} \cos \angle A_5 B_5 C_5 &= \cos \beta \cdot \cos \alpha + \sin \beta \cdot \sin \alpha \cdot \cos \theta \\ L = A_5 C_5 &= 2 \cdot A_5 B_5 \cdot \sin \frac{\angle A_5 B_5 C_5}{2} = 2 \cdot l \cdot \sin \frac{\angle A_5 B_5 C_5}{2} \end{aligned} \quad (3-27a)$$

The height of element 3 can be obtained as

$$\begin{aligned}
 \cos \angle B_4 P B'_4 &= \frac{-\cos \beta + \cos \alpha \cdot \cos \angle A_5 B_5 C_5}{\sin \alpha \cdot \sin \angle A_5 B_5 C_5} \\
 P B_4 &= l \cdot \sin \alpha \\
 B_4 B'_4 &= P B_4 \cdot \sin \angle B_4 P B'_4 \\
 H &= 2 \cdot B_4 B'_4
 \end{aligned} \tag{3-27b}$$

The width of element 3 can be obtained as

$$\begin{aligned}
 P B_5 &= -l \cdot \cos \alpha \\
 P B'_4 &= P B_4 \cdot \cos \angle B_4 P B'_4 \\
 B_5 B'_4 &= \sqrt{(P B'_4)^2 + (P B_5)^2} \\
 \angle P B_5 B'_4 &= \arctan \frac{P B'_4}{P B_5} \\
 \angle B_1 B_5 B'_4 &= \frac{\angle A_5 B_5 C_5}{2} - \angle P B_5 B'_4 \\
 W = B_1 B_5 &= 2 \cdot B_5 B'_4 = 4 \cdot B_5 B'_4 \cdot \cos \angle B_1 B_5 B'_4
 \end{aligned} \tag{3-27c}$$

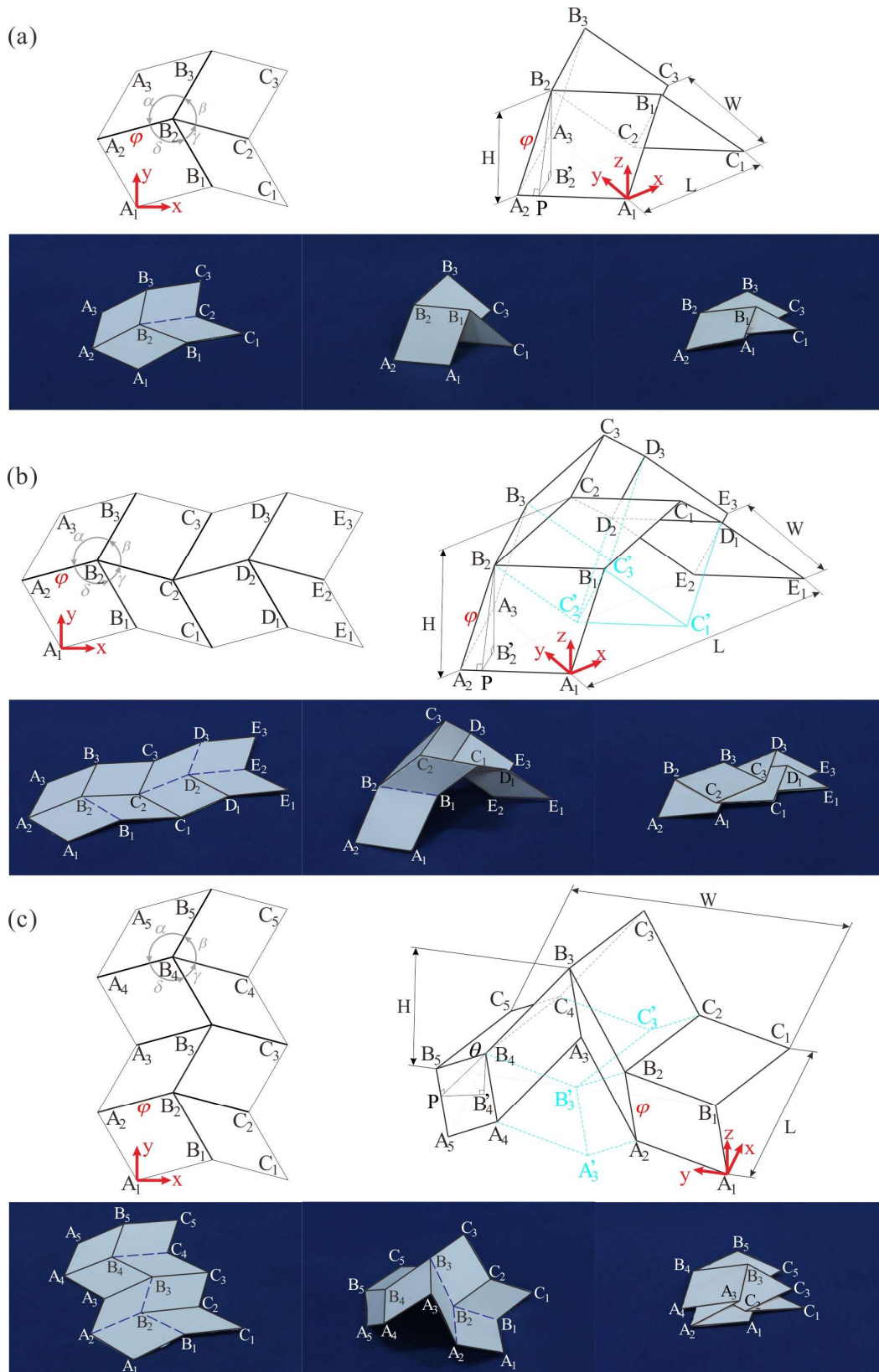


Figure 3-11 Geometrical calculation models and physical folding processes of the three basic element, (a) Element 1, (b) Element 2, (c) Element 3.

With Eqns. (3-24), (3-25) and (3-27), the dimensions of the four materials assembled by the basic elements can be obtained with respect to the dihedral angle ϕ . And the in-plane and out-of-plane Poisson's ratios^[92] can be respectively derived as

$$\begin{aligned}
 \nu_{in} &= -\frac{\varepsilon_L}{\varepsilon_W} = -\frac{\frac{dL}{L}}{\frac{dW}{W}}, \\
 \nu_{out} &= -\frac{\varepsilon_H}{\varepsilon_W} = -\frac{\frac{dH}{H}}{\frac{dW}{W}}.
 \end{aligned} \tag{3-28}$$

According to (3-24), (3-25) (3-27) and (3-28), both the dimension of metamaterial and their Poisson's ratios vs. the folding angle ϕ are shown in Fig. 3-12, in which configuration II is with the maximum height. During the folding between 0 and ϕ_{II} , the metamaterial exhibits a negative Poisson's ratio in 3D, while between ϕ_{II} and π , it has a negative in-plane Poisson's ratio and a positive out-of-plane one. It can be found that metamaterials in Figs. 3-12(a) to 3-12(c) reach maximum height at the same folding angle, and ϕ_{II} of the one in Fig. 3-12(d) is much larger than other three, i.e., this metamaterial has a large range of 3D negative Poisson's ratio. The maximum heights of metamaterials in Figs. 3-12(b) to 3-12(d) are the same and double that in Fig. 3-12(a). The dimension variation curves in Figs. 3-12(b) to 3-12(c) are identical even though they are from different patterns with different deformation details.

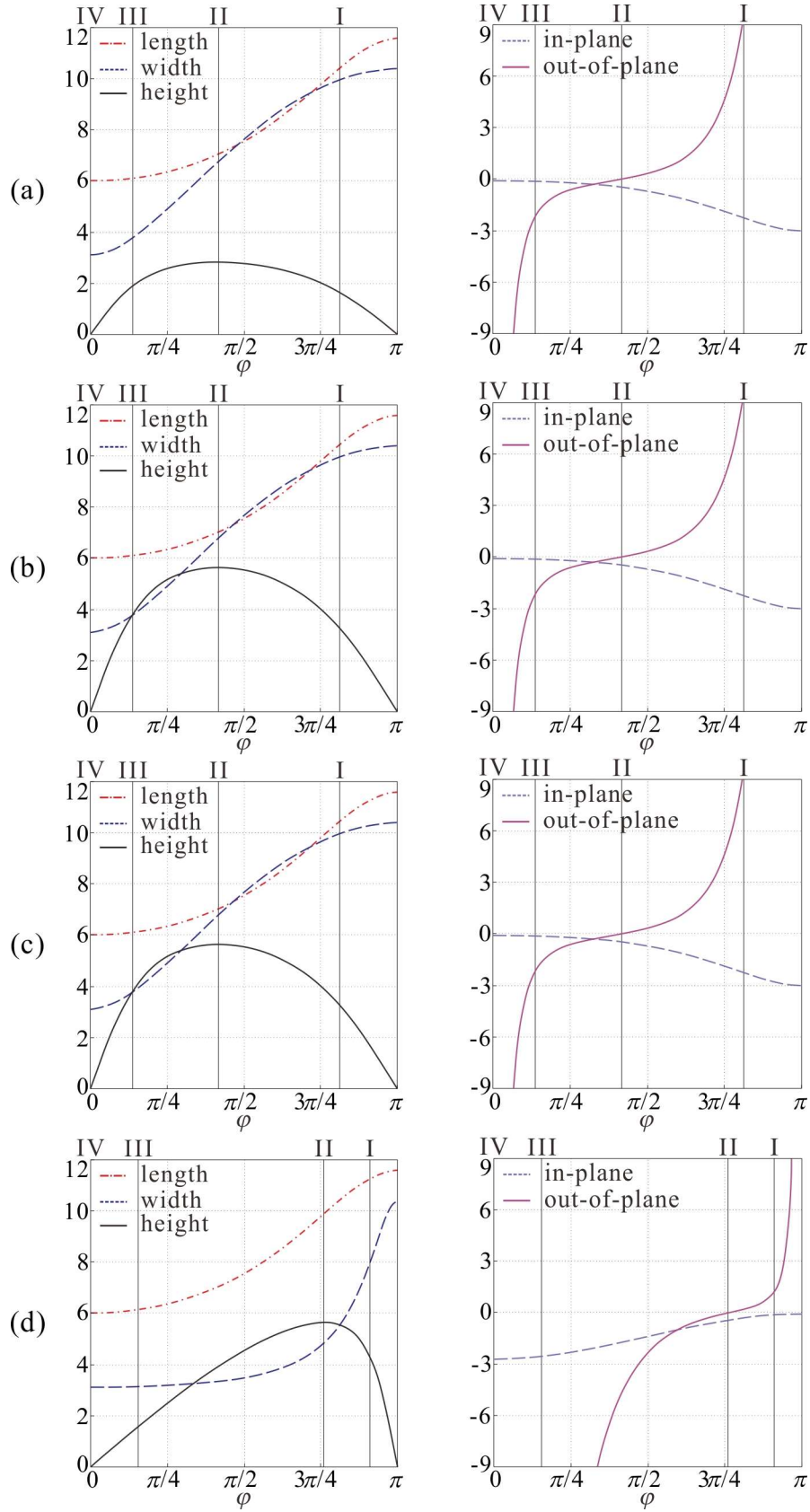


Figure 3-12 Dimensions and Poisson's ratio, (a) Metamaterial 1, (b) Metamaterial 2, (c) Metamaterial 3, (d) Metamaterial 4.

3.3 Square-twist Pattern

A simple example of square-twist pattern is shown in Fig.3-13. In this pattern, a square twists and stays in the middle, the other creases are horizontal or vertical. Each vertex has the same geometric parameters, which are

$$\begin{aligned} \alpha_{12}^a &= \alpha_{12}^c = \alpha, \alpha_{23}^a = \alpha_{23}^c = \frac{\pi}{2}, \\ \alpha_{34}^a &= \alpha_{34}^c = \gamma, \alpha_{41}^a = \alpha_{41}^c = \frac{\pi}{2}, \end{aligned} \quad (3-29a)$$

$$\begin{aligned} \alpha_{12}^b &= \alpha_{12}^d = \alpha, \alpha_{23}^b = \alpha_{23}^d = \frac{\pi}{2}, \\ \alpha_{34}^b &= \alpha_{34}^d = \gamma, \alpha_{41}^b = \alpha_{41}^d = \frac{\pi}{2}, \end{aligned}$$

$$\alpha + \gamma = \pi, \gamma < \frac{\pi}{2}. \quad (3-29b)$$

If $\beta = \delta = \frac{\pi}{2}$ is added to the geometric conditions of the unit Q pattern in section 3.1, the square-twist pattern is obtained, which means that the square-twist pattern is a special case of unit Q pattern.

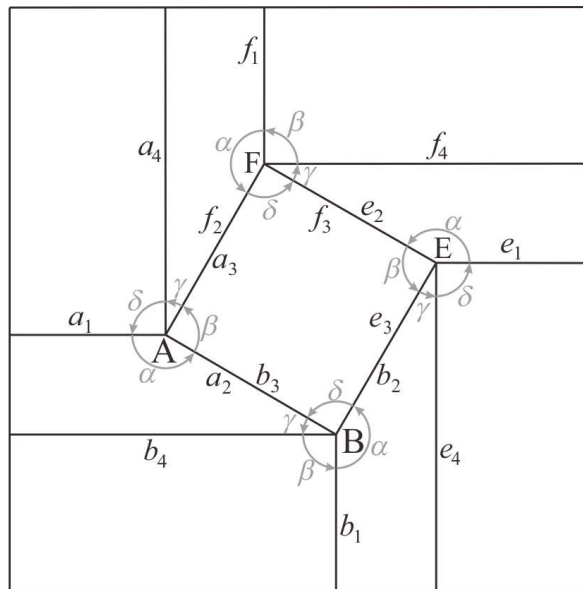


Figure 3-13 Square-twist pattern.

According to the Big-Little-Big Angle theorem and Maekawa-Justin theory, after removing such repeating ones, there are four distinct assignments for the square-twist

pattern in Fig. 3-14, labeled by T1-T4.

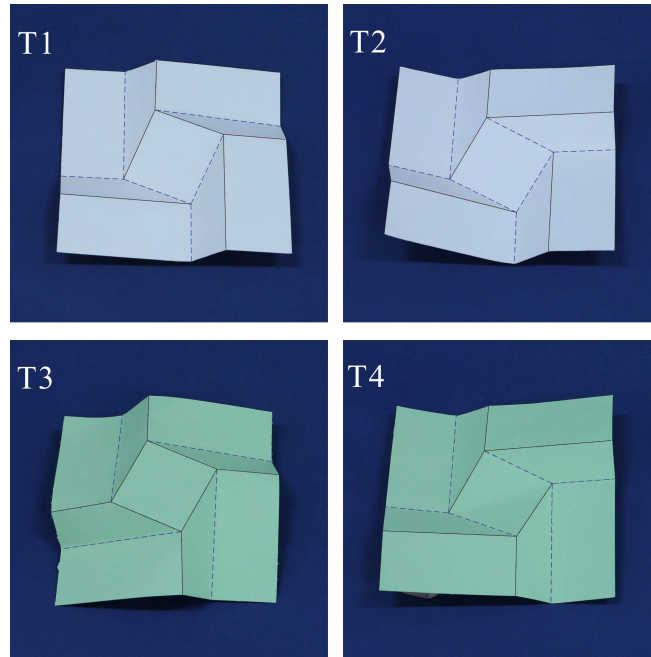


Figure 3-14 Different mountain-valley fold assignments for square-twist pattern.

3.3.1 Rigidity of Square-twist Pattern

As square-twist pattern is special case of unit Q, the compatible condition Eqn. (3-23) is also suitable for square-twist pattern. The kinematics of each vertex is analysed firstly. According to $\beta = \delta$, spherical 4R linkages type I₁ and type II₂, type I₂ and type II₁ are the same. So the relationships of θ_2 & θ_3 in F and B are the same as the relationships in E and A. The kinematics is shown in Fig. 3-15.

According to the kinematic compatibility condition Eqn. (3-23), the four corresponding rotation transmission routes are presented in Fig. 3-16. Taking θ_2^f as the initial input of the four-linkage loop and θ_3^a as the final output, the compatibility condition is $\theta_2^f = \theta_3^a$. Due to the four-fold symmetric property of the motion curves, the kinematic compatibility condition Eqn. (3-22) is met at all configurations on the motion paths of T1 and T2. Then the pattern unit T1 and T2 is rigid with close transmission loop as shown in Figs. 3-16(a) and (b), the unit T3 and T4 is non-rigid as shown in Figs. 3-6(c) and (d).

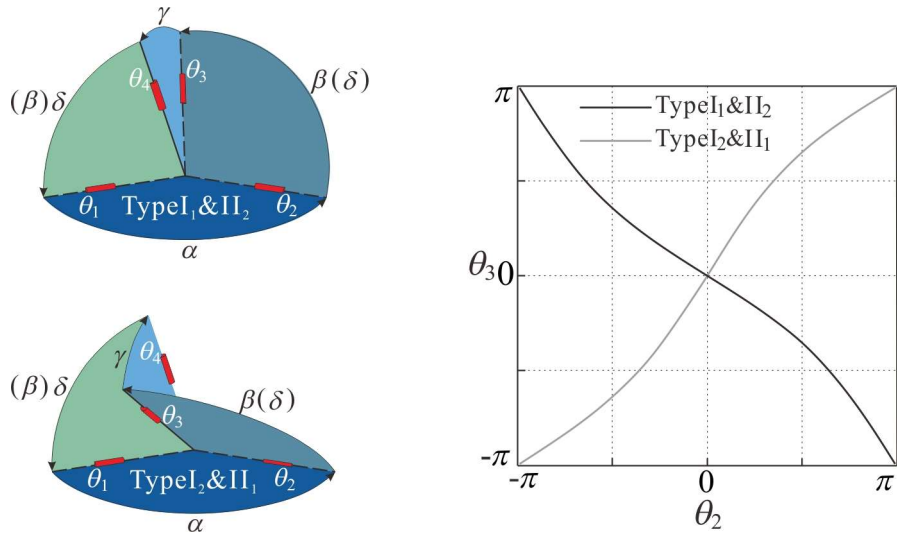


Figure 3-15 Kinematics of spherical 4R linkage in square-twist pattern ($\alpha = \frac{5\pi}{6}$).

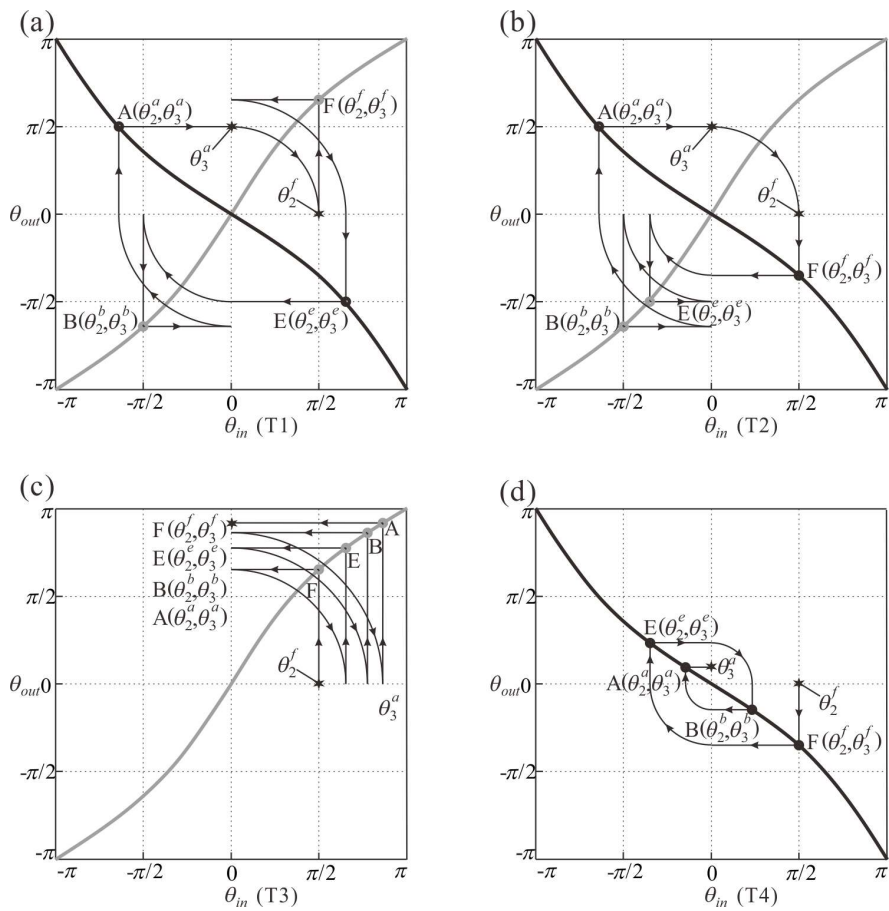


Figure 3-16 The kinematic curves of square twist pattern. (a) T1, (b) T2, (c) T3, (d) T4.

3.3.2 Tessellations of Square-twist Pattern and Its Metamaterials

By repeating the square-twist pattern of Fig. 3-14 in a reflection symmetric manner, we get the corresponding tessellations in in-plane manner and show them in Fig. 3-17. As T1 and T2 are rigid origami pattern, only the tessellation in Fig. 3-17(a) and (b) are rigid.

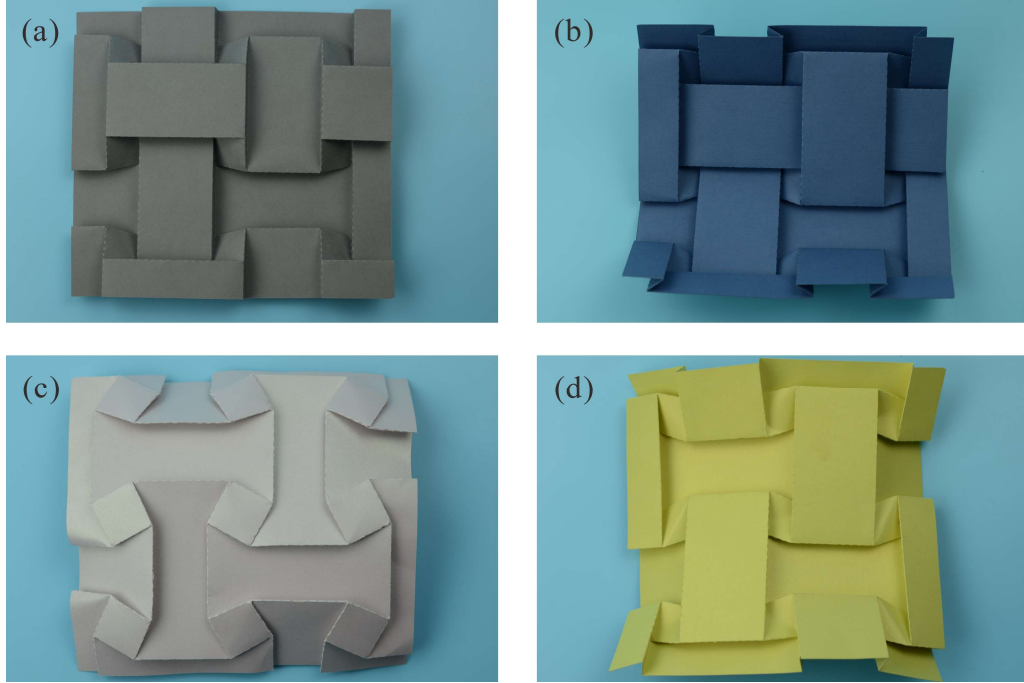


Figure 3-17 Tessellations of square twist pattern. (a) T1, (b) T2, (c) T3, (d) T4.

The rectangle panels in T1 are all parallel to each other, this character also happens in the tessellation of Fig. 3-17(a) and helps to build metamaterials. The overall mechanical behavior of the metamaterial should be linearly related to the square-twist origami unit due to the rigid-foldable characteristics of this origami pattern. Therefore, the Poisson's ratio of the metamaterial can be obtained by study the square-twist origami unit, see Fig. 3-18. The dimensions L , S , H of this unit are the function of the folding configuration parameters, θ and ϕ (both changing from 0 to π during the folding of the pattern).

$$\begin{aligned}
 L &= 2 \cdot c + a \cdot (\cos \alpha + \sin \alpha \cdot \cos \theta), \\
 S &= 2 \cdot b + a \cdot (\cos \alpha + \sin \alpha \cdot \cos \phi), \\
 H &= a \cdot \sin \alpha \cdot (\sin \theta + \sin \phi),
 \end{aligned} \tag{3-30}$$

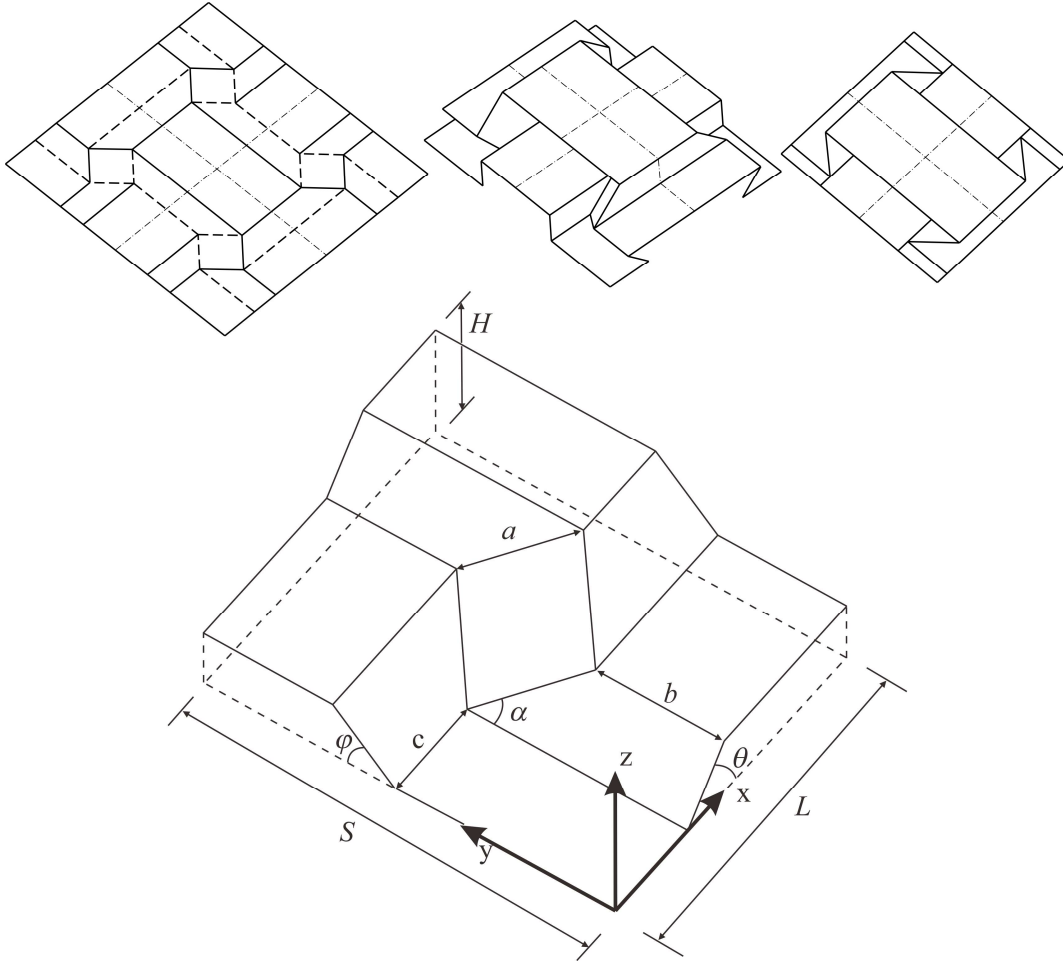


Figure 3-18 Tessellation of T1.

Because the pattern is kinematically one degree of freedom, θ and ϕ are not independent, but related by the kinematic relationship of the spherical 4R linkage on this vertex as

$$-\cos \alpha \cdot \cos \theta + \cos \alpha \cdot \cos \phi - \sin \alpha \cdot \sin \theta \cdot \sin \phi = 0 \quad (3-31)$$

The in-plane Poisson's ratios can be derived as

$$\begin{aligned} \nu_{SL} &= -\frac{\frac{dL}{dS}}{\frac{L}{S}} = -\frac{S}{L} \cdot \frac{dL}{dS} \\ &= -\frac{2b + a \cdot (\cos \alpha + \sin \alpha \cdot \cos \phi)}{2c + a \cdot (\cos \alpha + \sin \alpha \cdot \cos \theta)} \\ &\quad \cdot \frac{\sin \theta \cdot (\cos \alpha \cdot \sin \phi + \sin \alpha \cdot \sin \theta \cdot \cos \phi)}{\sin \phi \cdot (\cos \alpha \cdot \sin \theta - \sin \alpha \cdot \cos \theta \cdot \sin \phi)} \end{aligned} \quad (3-32a)$$

The out-of-plane Poisson's ratios can be derived as

$$\begin{aligned}
 v_{HL} &= -\frac{\frac{dH}{L}}{\frac{dL}{H}} = -\frac{L}{H} \cdot \frac{dH}{dL} \\
 &= -\frac{2c + a \cdot (\cos \alpha + \sin \alpha \cdot \cos \theta)}{a \cdot \sin \alpha \cdot (\sin \theta + \sin \varphi)} \\
 &\quad \cdot \frac{\cos \theta + \cos \varphi \cdot \frac{\cos \alpha \cdot \sin \theta - \sin \alpha \cdot \cos \theta \cdot \sin \varphi}{\cos \alpha \cdot \sin \varphi + \sin \alpha \cdot \sin \theta \cdot \cos \varphi}}{-\sin \theta}
 \end{aligned} \tag{3-32b}$$

In order to show the influence of α , we assume that $a=b=c$. According to (3-32), the in-plane and out-of-plane Poisson's ratios vs. the folding angle θ are shown in Fig. 3-19. The in-plane Poisson's ratios are always negative in Fig. 3-19(a). When the height of the metamaterial reaches the maximum value in the folding process, then the out-of-plane Poisson's ratios become negative, so the metamaterial exhibits a negative Poisson's ratio in 3D. By making α bigger, the in-plane Poisson's ratio changes rapidly but the out-of-plane Poisson's ratio changes gently. As α has such effect on the Poisson's ratios, we can modify it to make the metamaterial has better performance in the practical applications.

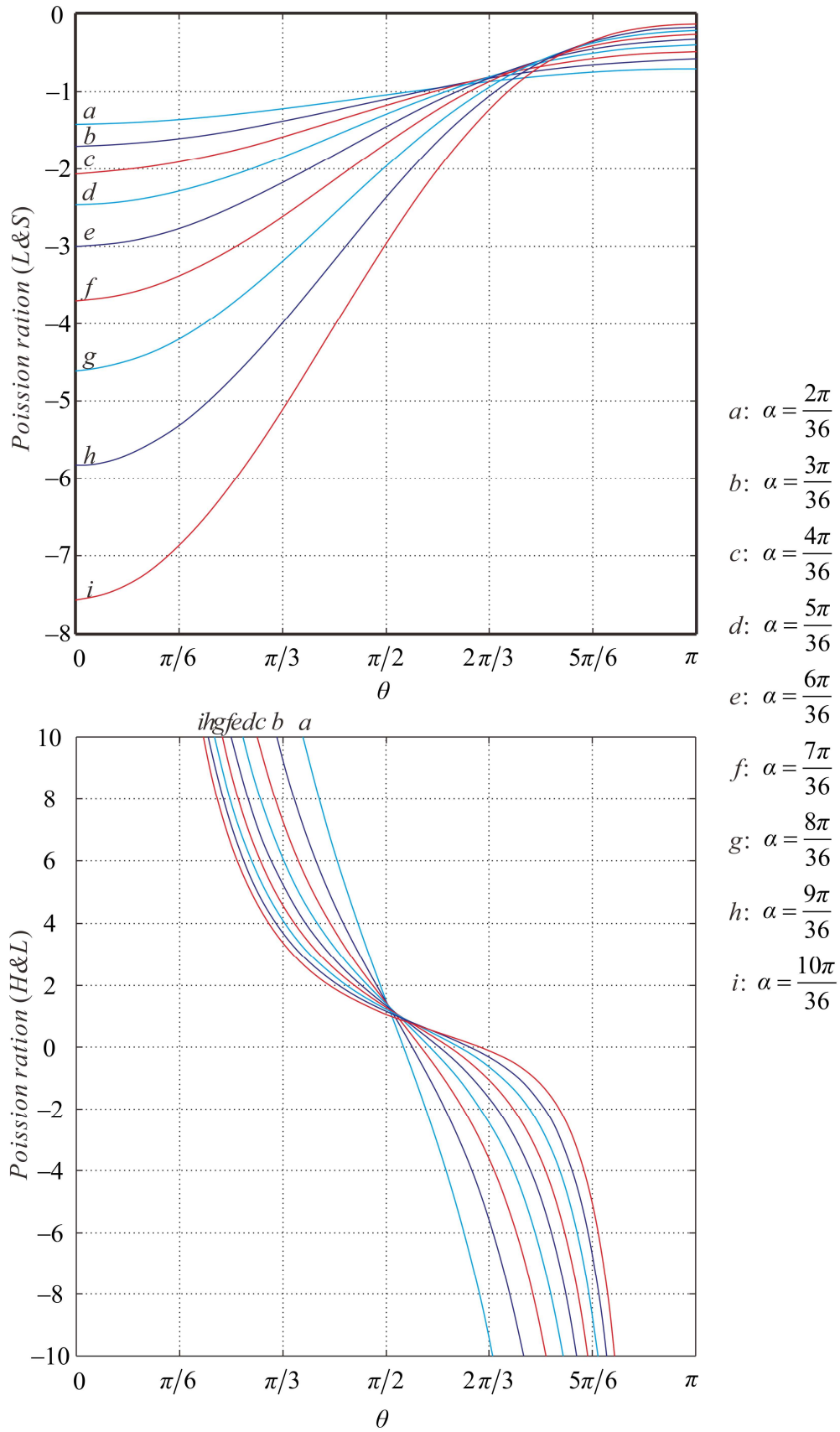


Figure 3-19 Poisson's ratio, (a) in-plane Poisson's ratio, (b) out-of-plane Poisson's ratio.

As we mentioned early, the rectangle panels in the pattern are all parallel to each other to make the folding in a flat profile. Thus we can stack a number of such structures layer by layer in the reflection symmetric manner, see Fig. 3-20(a), to eventually form a metamaterial. Once the geometric parameters in all units are the same, the motion of the whole metamaterial will be compatible with one degree of freedom, i.e., the pattern is rigid. In such a way, we have obtained a metamaterial with square-twist rigid origami pattern, whose physical model made from paper is shown in Fig. 3-20(b).

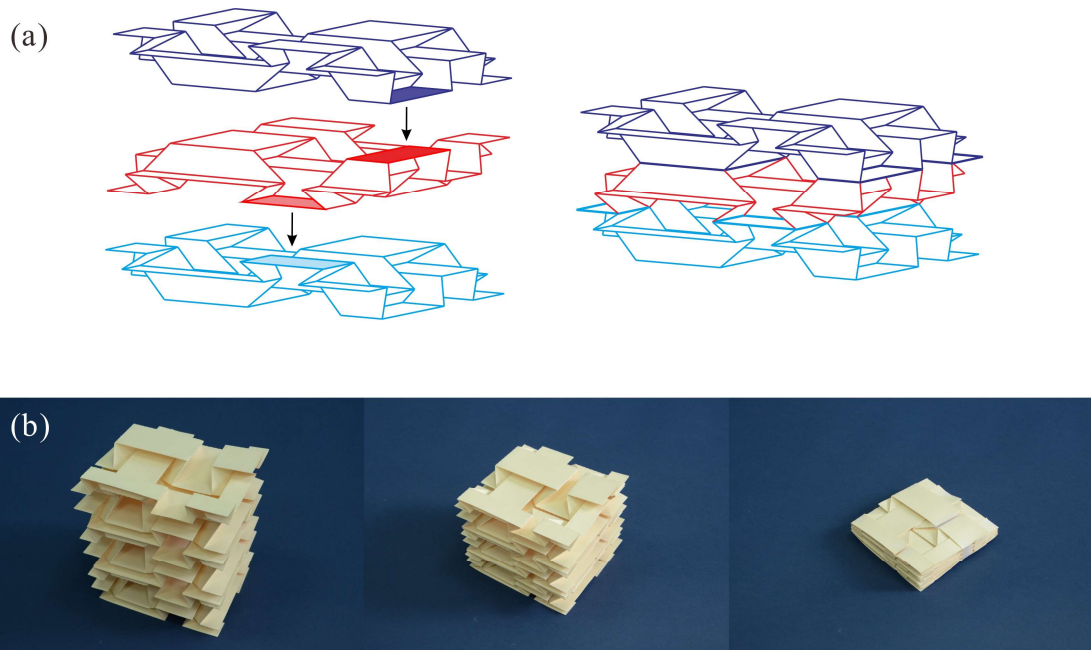


Figure 3-20 Metamaterial and its construction method, (a) construction method of metamaterial for T1 tessellation, (b) metamaterial based on T1.

3.4 Conclusion

We investigated the rigid foldability of origami patterns when different mountain-valley assignments are applied with a kinematic method. Under the condition of flat foldability, mountain and valley folds can be assigned to the creases of origami patterns or their basic units. The kinematics of closed loop of spherical linkages can be applied to analyze the rigidity of the patterns. Metamaterials from the stacks of double corrugated patterns have been proposed with many varieties when changing the mountain-valley assignments. Following the folding of the rigid origami patterns, the metamaterials exhibit negative Poisson's ratio and different mountain-valley assignments can affect the deformation property of origami metamaterials largely. To demonstrate the generalization of this method, the square-twist pattern is also discussed.

A metamaterial based on square-twist pattern is proposed and its Poisson's ratios are analysed. By choosing the suitable folding state, the metamaterial can exhibit Poisson's ratio in 3D direction.

Chapter 4 Origami of Thick Panels

4.1 Introduction

Origami patterns, including the rigid origami patterns where flat inflexible sheets are joined by creases, are primarily created for zero-thickness sheets. In order to apply them to fold structures such as roofs, solar panels and space mirrors, where thickness cannot be disregarded, various methods have been suggested. However, they generally involve adding materials to or offsetting panels away from the idealised sheet without altering the kinematic model used to simulate folding. In this chapter, we develop a comprehensive kinematic synthesis for rigid origami of thick panels that differs from the existing kinematic model but is capable of reproducing motions identical to that of zero-thickness origami. The approach, proven to be effective for typical origami, can be readily applied to fold real engineering structures.

The layout of this chapter is as follows. Section 4.2 describes the construction process of thick panel origami models for four-crease origami vertex by using Bennett linkage. The kinematic equivalent of the thick panels model and origami vertex has been proved. Section 4.3 presents the technique of using Myard linkages to constitute the thick panel models for five-crease origami patterns. The Bricard linkages are used for thick panel models for six-crease origami patterns in section 4.4. The conclusion in section 4.5 ends this chapter.

4.2 Four-crease Origami Pattern and Its Thick Model

A single vertex of origami pattern of zero-thickness panel is shown in Fig. 4-1. The pattern is flat foldable. The mountain and valley creases are denoted by thick solid and dash lines, respectively. The creases divide the sheet into four portions with sector angles. The dihedral angles between adjacent panels are shown when the sheet is partially folded.

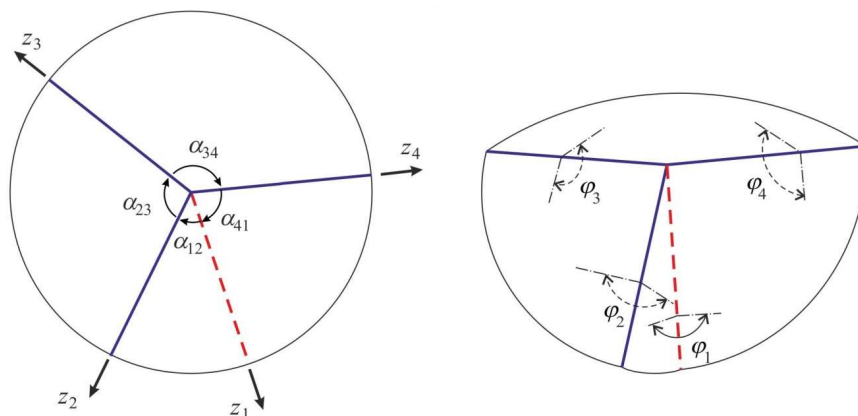


Figure 4-1 A single vertex of four-crease rigid origami pattern.

The fact that the crease corresponding to θ_1 is a valley crease and that to $\theta_2, \theta_3, \theta_4$ are mountain creases, leads to $-\pi \leq \theta_1 \leq 0$ and $0 \leq \theta_2, \theta_3, \theta_4 \leq \pi$. So Eqn. (3-3a) is used for this vertex.

$$\frac{\tan \frac{\theta_1}{2}}{\tan \frac{\theta_3}{2}} = \frac{\tan \frac{\theta_1}{2}}{\tan \frac{\theta_2}{2}} \cdot \frac{\tan \frac{\theta_2}{2}}{\tan \frac{\theta_3}{2}} = -1, \quad (4-1a)$$

$$\frac{\tan \frac{\theta_2}{2}}{\tan \frac{\theta_4}{2}} = \frac{\tan \frac{\theta_2}{2}}{\tan \frac{\theta_3}{2}} \cdot \frac{\tan \frac{\theta_3}{2}}{\tan \frac{\theta_4}{2}} = 1, \quad (4-1b)$$

This yields

$$\theta_1 = -\theta_3, \quad (4-2a)$$

$$\theta_2 = \theta_4, \quad (4-2b)$$

Referring to Eqn. (3-3a) also gives

$$\frac{\tan \frac{\theta_1}{2}}{\tan \frac{\theta_2}{2}} = -\frac{\sin \frac{\alpha_{23} - \alpha_{12}}{2}}{\sin \frac{\alpha_{23} + \alpha_{12}}{2}}, \quad (4-2c)$$

Hence, these three equations in Eqn. (4-2) are the closure equations of this spherical $4R$ linkage.

The corresponding thick origami model is shown in Fig. 4-2. Thick origami model with four creases that do not meet at a point. The dihedral angles are marked along each joint axis. The rigid sheet is divided into four portions with the sector angles α_{12}^{Be} , α_{23}^{Be} , $\pi - \alpha_{34}^{Be}$ and $\pi - \alpha_{41}^{Be}$, which are the same as those in the zero-thickness sheet, i.e.,

$$\alpha_{12}^{Be} = \alpha_{12}, \quad \alpha_{23}^{Be} = \alpha_{23}, \quad \pi - \alpha_{34}^{Be} = \alpha_{34}, \quad \pi - \alpha_{41}^{Be} = \alpha_{41}. \quad (4-3)$$

Adapting $\pi - \alpha_{34}^{Be}$ and $\pi - \alpha_{41}^{Be}$ for sector angles is required by the Denavit and Hartenberg notation.

For the thick panel, the fold lines connecting each adjacent panels are placed on either top or bottom surfaces of each panel, resulting in none zero distances between the axes of the neighbouring revolute joints. To enable rigid folding, this assembly must be a $4R$ Bennett linkage, the only known spatial $4R$ linkage.

The Bennett linkage is an overconstrained spatial linkage whose geometrical

parameters must satisfy Eqn. (1-7), i.e.,

$$a_{12}^{Be} = a_{34}^{Be}, \quad a_{23}^{Be} = a_{41}^{Be} \quad (4-4a)$$

$$\alpha_{12}^{Be} = \alpha_{34}^{Be}, \quad \alpha_{23}^{Be} = \alpha_{41}^{Be} \quad (4-4b)$$

$$\frac{a_{12}^{Be}}{a_{23}^{Be}} = \frac{\sin \alpha_{12}^{Be}}{\sin \alpha_{23}^{Be}} \quad (4-4c)$$

Referring to Eqn. (1-8), the closure equations for the Bennett linkage are

$$\theta_1^{Be} + \theta_3^{Be} = 2\pi, \quad (4-5a)$$

$$\theta_2^{Be} + \theta_4^{Be} = 2\pi, \quad (4-5b)$$

$$\tan \frac{\theta_1^{Be}}{2} \cdot \tan \frac{\theta_2^{Be}}{2} = \frac{\sin \frac{\alpha_{12}^{Be} + \alpha_{23}^{Be}}{2}}{\sin \frac{\alpha_{12}^{Be} - \alpha_{23}^{Be}}{2}} \quad (4-5c)$$

Hence, the thick rigid panel can be folded only with a set of fold lines arranged in such a way that meet the conditions given in Eqn. (4-4), whose motion can be illustrated by the closure equations given by Eqn. (4-5). Next, we shall prove that the motion of the thick panel is equivalent to that of the zero-thickness rigid sheet.

In origami, the dihedral angles are commonly used to describe the folding process. In the spherical 4R linkage, Fig. 4-1, the relationships between kinematic variables θ_i and dihedral angle φ_i are

$$\theta_1 = \varphi_1 + \pi, \quad \theta_2 = \pi - \varphi_2, \quad \theta_3 = \pi - \varphi_3, \quad \theta_4 = \pi - \varphi_4 \quad (4-6)$$

Substituting Eqn. (4-6) into the closure equations (4-2) of the spherical linkage yields

$$\varphi_1 = \varphi_3 \quad (4-7a)$$

$$\varphi_2 = \varphi_4 \quad (4-7b)$$

And

$$\frac{\tan \frac{\varphi_2}{2}}{\tan \frac{\varphi_1}{2}} = \frac{\sin \frac{\alpha_{23} - \alpha_{12}}{2}}{\sin \frac{\alpha_{12} + \alpha_{23}}{2}} \quad (4-7c)$$

Similarly for the Bennett linkage, Fig. 4-2, the relationships between kinematic

variables θ^{Be} and dihedral angle ϕ^{Be} are

$$\theta_1^{Be} = \varphi_1^{Be}, \theta_2^{Be} = \pi - \varphi_2^{Be}, \theta_3^{Be} = 2\pi - \varphi_3^{Be}, \theta_4^{Be} = \pi + \varphi_4^{Be} \quad (4-8)$$

and thus its closure equations (4-5) become

$$\varphi_1^{Be} = \varphi_3^{Be} \quad (4-9a)$$

$$\varphi_2^{Be} = \varphi_4^{Be} \quad (4-9b)$$

And

$$\frac{\tan \frac{\varphi_2^{Be}}{2}}{\tan \frac{\varphi_1^{Be}}{2}} = \frac{\sin \frac{\alpha_{23}^{Be} - \alpha_{12}^{Be}}{2}}{\sin \frac{\alpha_{12}^{Be} + \alpha_{23}^{Be}}{2}} \quad (4-9c)$$

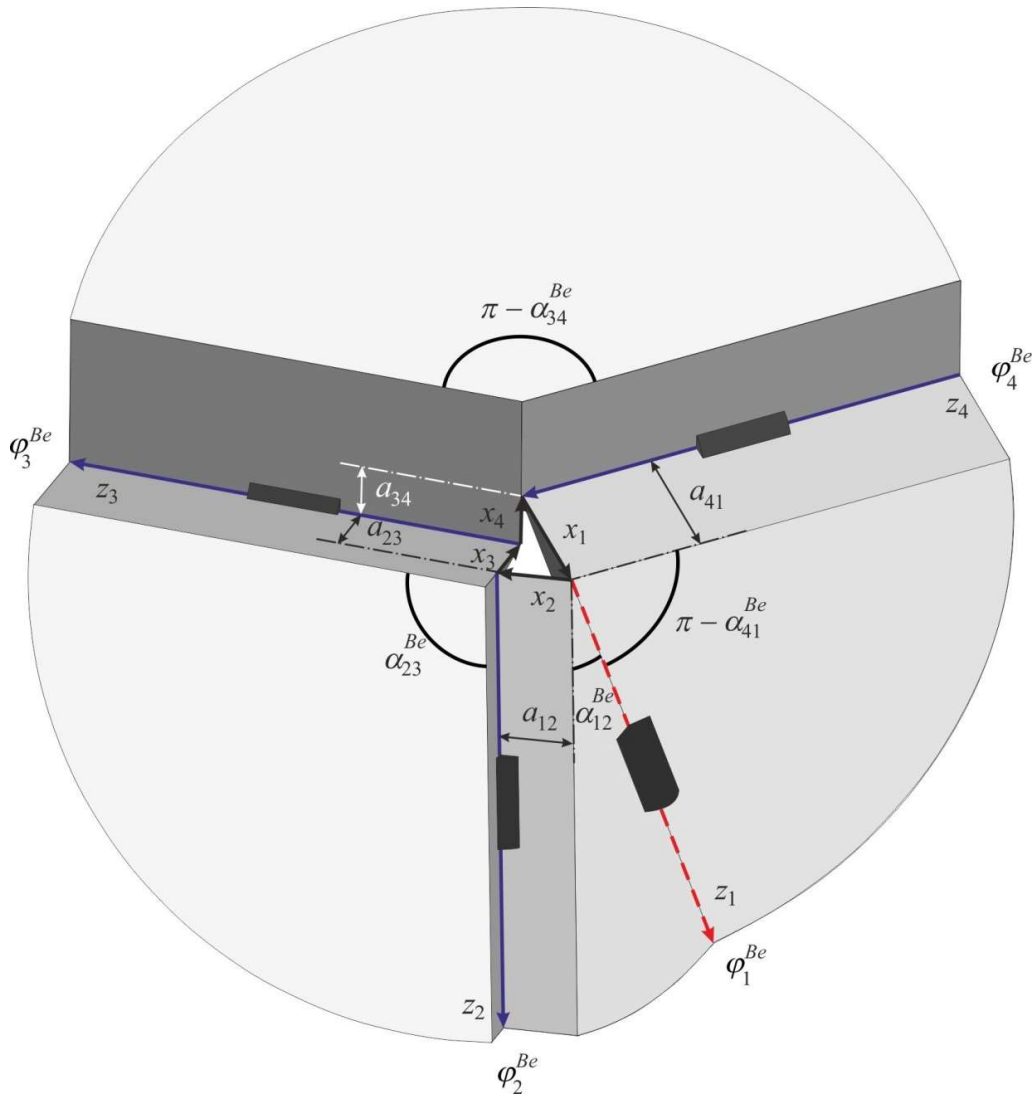


Figure 4-2 Thick origami model for four-crease origami vertex.

It is clear that Eqn. (4-9), the closure equations for the thick panel origami, match exactly Eqn. (4-7), the closure equations for the zero-thickness sheet should satisfy that the sheet is partitioned in the same way described by Eqn. (4-3). We therefore conclude that the two linkages are kinematically equivalent. The relationships between the dihedral angles of the panels φ_1^{Be} and φ_2^{Be} , is identical to that between the dihedral angles φ_1 and φ_2 of the spherical 4R linkage throughout the entire folding process, see Fig. 4-3. Curves a – c are relationships between dihedral angles φ_1 and φ_2 in zero-thickness rigid origami for three sets of sector angles, respectively. They overlap with those between φ_1^{Be} and φ_2^{Be} for their thick panel counterparts, respectively.

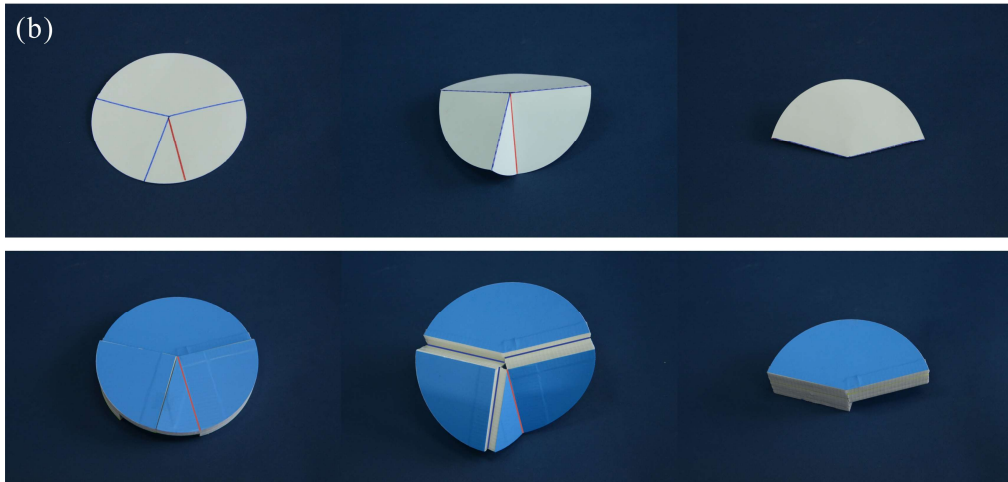
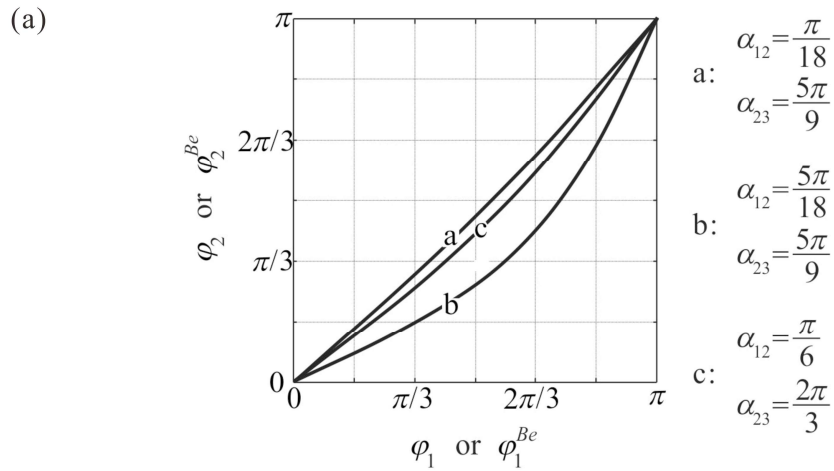


Figure 4-3 Kinematics of origami vertex and its thick panel model, (a) relationships between dihedral angles for four-crease single vertex origami, (b) zero-thickness model and its corresponding thick panel model.

The above method to syntheses single vertex four-crease thick panel origami can be extended to multiple vertex origami. Take the square-twist pattern as an example in Fig. 4-4. We apply the Bennett linkage to each of the “vertices” A, B, C and D,

preserving the section angle of each panel. The corresponding fold lines around each vertex are denoted by a's, b's, c's and d's. And then we merge the fold lines which are shared by two adjacent Bennett linkages. For instance, the fold line a_4 of linkage A and fold line b_1 of linkage B are combined into one fold line. This is possible because there is rotational symmetry in the square-twist pattern shown here, leading to the exact same amount of rotation for the combined fold lines. For other four crease multi-vertex patterns, one has to prove that this combination is possible for each of them.



Figure 4-4 Thick panel models of square twist pattern, (a) Solidworks model for the square-twist pattern with thick panels, (b) zero-thickness model of square twist pattern and its corresponding thick panel model.

4.3 Five-crease Origami Pattern and Its Thick Model

A specific single vertex of origami pattern of zero-thickness panel is shown in Fig. 4-5 in which

$$\alpha_{51} = \alpha_{12}, \alpha_{23} = \alpha_{45} = \frac{\pi}{2} \text{ and } \alpha_{34} = \pi - 2\alpha_{12} \quad (4-10)$$

The mountain and valley creases are denoted by solid and dash lines, respectively. The creases divide the sheet into five portions with sector angles α 's. z 's represent the axes of creases. φ 's are dihedral angles.

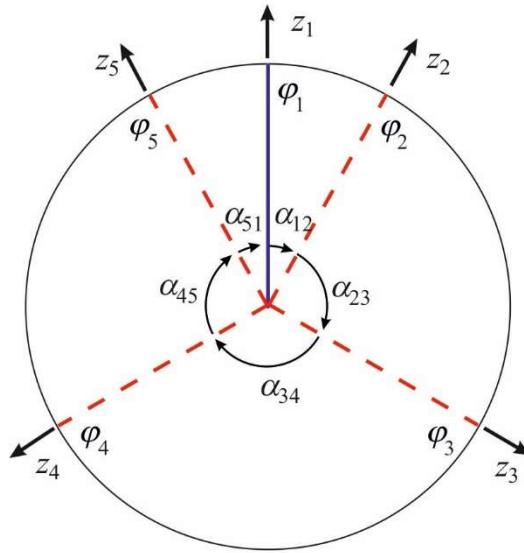


Figure 4-5 A specific symmetric single vertex five-crease origami pattern.

This is a $5R$ spherical linkage. In general it has two degrees of freedom. If the symmetry is preserved during folding, i.e.,

$$\theta_4 = \theta_3, \theta_5 = \theta_2 \quad (4-11)$$

Similar as (2-3), the closure equation of spherical $5R$ linkage can be written as

$$\mathbf{Q}_{12} \mathbf{Q}_{23} \mathbf{Q}_{34} = \mathbf{Q}_{15} \mathbf{Q}_{54} \quad (4-12)$$

We note it as

$$\begin{aligned} \mathbf{Q}_L^{55R} &= \mathbf{Q}_{12} \mathbf{Q}_{23} \mathbf{Q}_{34}, \\ \mathbf{Q}_R^{55R} &= \mathbf{Q}_{15} \mathbf{Q}_{54}, \end{aligned} \quad (4-13)$$

All elements of the matrices of Eqn. (4-12) are given in the Appendix. From $\mathbf{Q}_L^{SSR}(3,3) = \mathbf{Q}_R^{SSR}(3,3)$ and $\mathbf{Q}_L^{SSR}(2,1) = \mathbf{Q}_R^{SSR}(2,1)$, we can have

$$\begin{aligned} & \cos(2\alpha_{12}) \cdot \sin \alpha_{12} \cdot \cos \theta_2 - \sin(2\alpha_{12}) \cdot \cos \alpha_{12} \cdot \cos \theta_3 \\ & + \sin(2\alpha_{12}) \cdot \sin \alpha_{12} \cdot \sin \theta_2 \cdot \sin \theta_3 = -\sin \alpha_{12} \cdot \cos \theta_2 \end{aligned} \quad (4-14a)$$

$$\begin{aligned} & \cos \theta_3 \cdot (\cos \theta_2 \cdot \sin \theta_1 + \cos \alpha_{12} \cdot \cos \theta_1 \cdot \sin \theta_2) \\ & - \sin \alpha_{12} \cdot \cos \theta_1 \cdot \sin \theta_3 = -\cos \alpha_{12} \cdot \cos \theta_3 \cdot \sin \theta_2 + \sin \alpha_{12} \cdot \sin \theta_3 \end{aligned} \quad (4-14b)$$

Then, we use the following trigonometric transforms to simplify them,

$$t_1 = \tan \frac{\theta_1}{2}, t_2 = \tan \frac{\theta_2}{2}, t_3 = \tan \frac{\theta_3}{2}, \quad (4-15)$$

From Eqn. (4-14a), we can get

$$\frac{4 \cdot \sin \alpha \cdot \cos \alpha \cdot (-\cos \alpha \cdot (t_2)^2 + 2 \cdot \sin \alpha \cdot t_2 \cdot t_3 + \cos \alpha \cdot (t_3)^2)}{((t_2)^2 + 1) \cdot ((t_3)^2 + 1)} = 0 \quad (4-16)$$

By simplifying it, we have

$$\frac{t_3}{t_2} = \frac{-\sin \alpha \pm 1}{\cos \alpha} \quad (4-17)$$

As the creases corresponding to θ_2 and θ_3 are both valley, t_2 and t_3 have the same signs, we have

$$\frac{t_3}{t_2} = \frac{-\sin \alpha + 1}{\cos \alpha} \quad (4-18)$$

Substituting (4-15) and (4-18) into (4-14b), eliminate t_3^{SSR} , we have

$$\frac{H_1 \cdot H_2}{H_3} = 0, \quad (4-18)$$

In which

$$\begin{aligned} H_1 &= 2((t_2)^2 - 1), \\ H_2 &= 2t_2 \cdot \cos \alpha_{12} - 2t_1 \cdot (t_2)^2 + \cos^2 \alpha_{12} \cdot t_1 - 2 \cdot t_2 \cdot \sin \alpha_{12} \cdot \cos \alpha_{12} \\ & \quad + 2 \sin \alpha_{12} \cdot t_1 \cdot (t_2)^2 + t_1 \cdot (t_2)^2 \cdot \cos^2 \alpha_{12}, \\ H_3 &= ((t_1)^2 + 1) \cdot ((t_2)^2 + 1) \cdot (\sin \alpha_{12} - 1) \cdot (\sin \alpha_{12} - \sin \alpha_{12} \cdot (t_2)^2 + (t_2)^2 + 1)^2. \end{aligned}$$

From H_2 , we can have the relationship between t_1 and t_2 .

$$\begin{aligned}
 &2t_2 \cdot \cos \alpha_{12} - 2t_1 \cdot (t_2)^2 + \cos^2 \alpha_{12} \cdot t_1 - 2 \cdot t_2 \cdot \sin \alpha_{12} \cdot \cos \alpha_{12} \\
 &+ 2 \sin \alpha_{12} \cdot t_1 \cdot (t_2)^2 + t_1 \cdot (t_2)^2 \cdot \cos^2 \alpha_{12} = 0
 \end{aligned} \tag{4-19}$$

Which can be simplified as

$$(t_2)^2 - \frac{t_2}{2t_1} \cdot \frac{\cos \alpha_{12}}{1 - \sin \alpha_{12}} - \frac{1 + \sin \alpha_{12}}{1 - \sin \alpha_{12}} = 0 \tag{4-20}$$

Besides Eqn. (4-11), considering with (4-15), (4-18) and (4-20), the rest of the closure equations can be obtained, which are

$$\frac{\tan \frac{\theta_3}{2}}{\tan \frac{\theta_2}{2}} = \frac{1 - \sin \alpha_{12}}{\cos \alpha_{12}}, \tag{4-21a}$$

$$\tan^2 \frac{\theta_2}{2} - \frac{2 \tan \frac{\theta_2}{2}}{\tan \frac{\theta_1}{2}} \frac{\cos \alpha_{12}}{1 - \sin \alpha_{12}} - \frac{1 + \sin \alpha_{12}}{1 - \sin \alpha_{12}} = 0 \tag{4-21b}$$

The angular variables in the closure equations can be replaced by the corresponding dihedral angles commonly used in origami. Noting that

$$\theta_1 = \pi - \varphi_1, \theta_2 = \pi + \varphi_2, \theta_3 = \pi + \varphi_3, \theta_4 = \pi + \varphi_4, \theta_5 = \pi + \varphi_5 \tag{4-22}$$

Eqns. (4-11) and (4-21) become

$$\varphi_3 = \varphi_4, \varphi_2 = \varphi_5, \tag{4-23a}$$

$$\tan \frac{\varphi_2}{2} = \frac{1 - \sin \alpha_{12}}{\cos \alpha_{12}} \tan \frac{\varphi_3}{2} \tag{4-23b}$$

$$\frac{1}{\tan^2 \frac{\varphi_2}{2}} - \frac{2 \tan \frac{\varphi_1}{2}}{\tan \frac{\varphi_2}{2}} \frac{\cos \alpha_{12}}{1 - \sin \alpha_{12}} - \frac{1 + \sin \alpha_{12}}{1 - \sin \alpha_{12}} = 0 \tag{4-23c}$$

Now we consider folding a single vertex five crease sheet with finite thickness. When it is divided into five panels using the same sector angles as those for zero-thickness rigid sheet, i.e.,

$$\pi - \alpha_{12}^{My} = \alpha_{12}, \pi - \alpha_{23}^{My} = \alpha_{23}, 2\pi - \alpha_{34}^{My} = \alpha_{34}, \alpha_{45}^{My} = \alpha_{45}, \alpha_{51}^{My} = \alpha_{51}. \tag{4-24}$$

but the fold lines are placed either on top of or at the bottom of the thick panels, we obtain a spatial $5R$ assembly, Fig. 4-6. Thick origami model with five fold lines that do

not meet at a point. The dihedral angles are marked along each joint axis.

Not all the 5R assemblies can have a degree of freedom. The creases arranged using Eqn. (4-24) makes it likely to be a Myard linkage. However, unlike the spherical 5R linkage, the Myard linkage is overconstrained, meaning that a set of additional specific geometrical conditions have to be met to produce a degree of freedom. These conditions are

$$\alpha_{23}^{My} = \frac{\pi}{2}, \alpha_{34}^{My} = 2\alpha_{12}^{My} - \pi, \alpha_{45}^{My} = \frac{\pi}{2}, \alpha_{51}^{My} = \pi - \alpha_{12}^{My} \quad (4-25a)$$

$$a_{12}^{My} = a_{51}^{My}, a_{23}^{My} = a_{45}^{My}, a_{34}^{My} = 0 \quad (4-25a)$$

and

$$\frac{\sin \alpha_{12}^{My}}{a_{12}^{My}} = \frac{\sin \alpha_{23}^{My}}{a_{23}^{My}} \quad (4-25a)$$

Eqns. (4-25b) and (4-25c) concern with the distances between the neighbouring fold lines.

If all the conditions given in Eqn. (4-25) are met, the linkage is the Myard linkage and it can be folded. The closure equations of this Myard linkage are [30]

$$\theta_3^{My} = \pi + \theta_4^{My}, \theta_2^{My} + \theta_5^{My} = 2\pi \quad (4-26a)$$

$$\tan \frac{\theta_3^{My}}{2} = -\frac{1 - \sin \alpha_{12}^{My}}{\cos \alpha_{12}^{My}} \tan \frac{\theta_2^{My}}{2} \quad (4-26b)$$

$$\tan^2 \frac{\theta_2^{My}}{2} - \frac{2 \cos \alpha_{12}^{My}}{1 - \sin \alpha_{12}^{My}} \tan \frac{\theta_1^{My}}{2} \cdot \tan \frac{\theta_2^{My}}{2} - \frac{1 + \sin \alpha_{12}^{My}}{1 - \sin \alpha_{12}^{My}} = 0 \quad (4-26c)$$

The relationships between the kinematic variables and their respective dihedral angles are

$$\theta_1^{My} = 2\pi - \varphi_1^{My}, \theta_2^{My} = \pi - \varphi_2^{My}, \theta_3^{My} = \pi + \varphi_3^{My}, \theta_4^{My} = \varphi_4^{My}, \theta_5^{My} = \pi + \varphi_5^{My} \quad (4-27)$$

Substituting them into Eqns. (4-26a to c), a set of equations are obtained

$$\varphi_3^{My} = \varphi_4^{My}, \varphi_2^{My} = \varphi_5^{My}, \quad (4-28a)$$

$$\tan \frac{\varphi_2^{My}}{2} = \frac{1 - \sin \alpha_{12}}{\cos \alpha_{12}} \tan \frac{\varphi_3^{My}}{2} \quad (4-28b)$$

$$\frac{1}{\tan^2 \frac{\varphi_2^{My}}{2}} - \frac{2 \tan \frac{\varphi_1^{My}}{2}}{\tan \frac{\varphi_2^{My}}{2}} \frac{\cos \alpha_{12}}{1 - \sin \alpha_{12}} - \frac{1 + \sin \alpha_{12}}{1 - \sin \alpha_{12}} = 0 \quad (4-28c)$$

Eqns. (4-23) and (4-28) have the same forms except that α^{My} 's and φ^{My} 's take the places of α 's and φ 's, respectively. Fig. 4-7 presents the relationships between a pair of dihedral angles with different geometric parameter α_{12} 's, and show the spherical 5R linkage and Myard linkage are kinematically equivalent.

Hence, the spherical 5R linkage and the Myard linkage are kinematically equivalent.

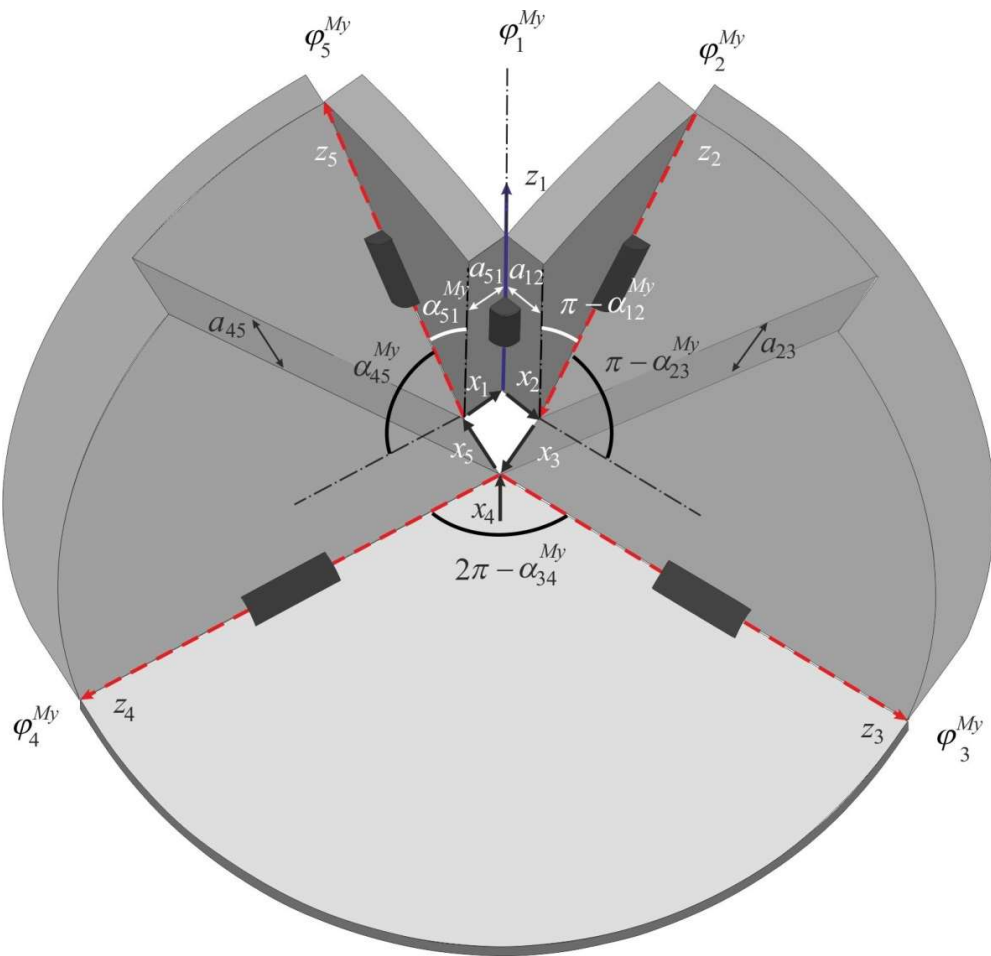


Figure 4-6 Thick origami model for four-crease origami vertex.

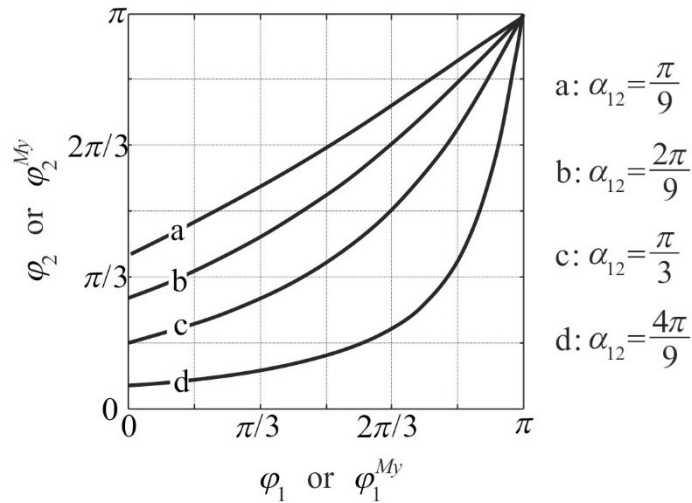


Figure 4-7 Dihedral angles φ_1 vs. φ_2 (or φ_1^{My} vs. φ_2^{My}) with different α_{12}

The thick panel assembly will have one DOF if the arrangement of fold lines satisfies Eqn. (4-25) because it is now a Myrd linkage. Furthermore, the proof in the Supplementary Text shows that the motion of this linkage is identical to that of the spherical $5R$ linkage when Eqn. (4-11) is imposed. This folding scheme has been used to fold a box. Fig. 4-8 shows the folding sequence of a zero-thickness rigid origami with five-crease vertices and its thick panel counterpart based on the Myrd linkage. The pattern has six five-crease vertices arranged in rotational symmetry. The sector angles at each vertex are $\pi/6$, $\pi/2$, $2\pi/3$, $\pi/2$ and $\pi/6$.

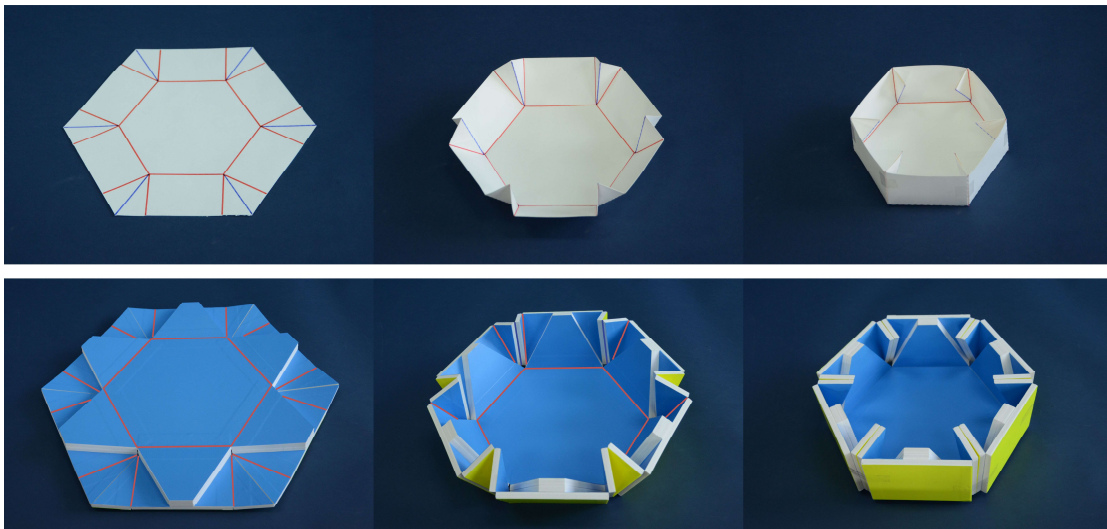


Figure 4-8 Multiple five-crease vertex origami zero-thickness model and its corresponding thick panel model.

4.4 Six-crease Origami Pattern and Its Thick Model

There are two kinds of six-crease origami patterns introduced in this section, the diamond pattern and waterbomb pattern. Only one kind of vertex exists in diamond pattern, two kinds of vertices exist in waterbomb pattern.

4.4.1 Diamond Pattern

The diamond pattern has a single vertex where six creases meet, Fig. 4-9. The angles between adjacent creases satisfy

$$\begin{aligned}\alpha_{12} &= \alpha_{34} = \alpha_{45} = \alpha_{61}, \\ \alpha_{23} &= \alpha_{56} = \pi - 2\alpha_{12}.\end{aligned}\quad (4-29)$$

in which $0 < \alpha_{12} \leq \frac{\pi}{4}$. This also ensures that the pattern has flat foldability. The closure conditions for this spherical $6R$ linkage in line and plane symmetry are

$$\begin{aligned}\theta_1 &= \theta_4, \\ \theta_2 &= \theta_3 = \theta_5 = \theta_6\end{aligned}\quad (4-30)$$

Similar as (2-3), the closure equation of spherical $6R$ linkage can be written as

$$\mathbf{Q}_{12}\mathbf{Q}_{23}\mathbf{Q}_{34} = \mathbf{Q}_{16}\mathbf{Q}_{65}\mathbf{Q}_{54}\quad (4-31)$$

We note it as

$$\begin{aligned}\mathbf{Q}_L^{S6R} &= \mathbf{Q}_{12}\mathbf{Q}_{23}\mathbf{Q}_{34}, \\ \mathbf{Q}_R^{S6R} &= \mathbf{Q}_{16}\mathbf{Q}_{65}\mathbf{Q}_{54},\end{aligned}\quad (4-32)$$

All elements of the matrices of Eqn. (4-32) are given in the Appendix. From $\mathbf{Q}_L^{S6R}(1,3) = \mathbf{Q}_R^{S6R}(1,3)$, we can have

$$\begin{aligned}&2 \cdot \sin \alpha_{12} \cdot (\cos^2 \alpha_{12} + \cos \theta_2 - \cos^2 \alpha_{12} \cdot \cos \theta_2) \\ &\cdot (-\cos \alpha_{12} \cdot \sin \theta_1 + \cos \theta_1 \cdot \sin \theta_2 + \cos \alpha_{12} \cdot \cos \theta_2 \cdot \sin \theta_1) \\ &= 2 \cdot \sin \alpha_{12} \cdot \sin \theta_2 \cdot (\cos^2 \alpha_{12} + \cos \theta_2 - \cos^2 \alpha_{12} \cdot \cos \theta_2)\end{aligned}\quad (4-33)$$

Then, we use the following trigonometric transforms to simplify them,

$$t_1 = \tan \frac{\theta_1}{2}, t_2 = \tan \frac{\theta_2}{2},\quad (4-34)$$

From Eqn. (4-33), we can get

$$\frac{8 \cdot \sin \alpha_{12} \cdot t_1 \cdot t_2 \cdot (t_1 + t_2 \cdot \cos \alpha_{12}) \cdot ((t_2)^2 \cdot \cos 2\alpha_{12} + 1)}{((t_1)^2 + 1) \cdot ((t_2)^2 + 1)^2} = 0\quad (4-35)$$

By simplifying it, we have

$$t_1 = -\cos \alpha_{12} \cdot t_2 \quad (4-36)$$

Besides Eqn. (4-30), considering with (4-34) and (4-36), the rest of the closure equations can be obtained, which are

$$\tan \frac{\theta_1}{2} + \cos \alpha_{12} \tan \frac{\theta_2}{2} = 0 \quad (4-37)$$

The angular variables to the corresponding dihedral angles are related by

$$\begin{aligned} \theta_1 &= \pi - \varphi_1, \quad \theta_2 = \pi + \varphi_2, \quad \theta_3 = \pi + \varphi_3, \\ \theta_4 &= \pi - \varphi_4, \quad \theta_5 = \pi + \varphi_5, \quad \theta_6 = \pi + \varphi_6, \end{aligned} \quad (4-38)$$

Substituting them into Eqns. (4-30) and (4-37) yields

$$\begin{aligned} \varphi_1 &= \varphi_4, \\ \varphi_2 &= \varphi_3 = \varphi_5 = \varphi_6, \end{aligned} \quad (4-39a)$$

$$\tan \frac{\varphi_2}{2} = \cos \alpha_{12} \cdot \tan \frac{\varphi_1}{2}. \quad (4-39b)$$

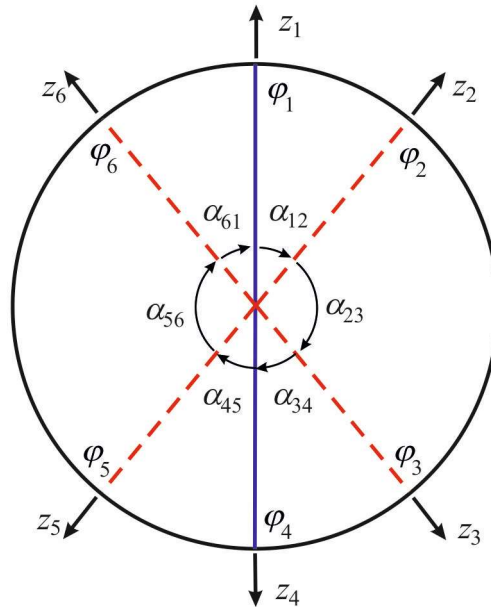


Figure 4-9 A specific symmetric single vertex six-crease origami pattern.

Apply the same partition angles to divide the thick sheet into six panels, i.e.,

$$\begin{aligned} 2\pi - \alpha_{12}^{Br} &= \alpha_{12}, \quad \alpha_{23}^{Br} = \alpha_{23}, \quad \alpha_{34}^{Br} = \alpha_{34}, \\ 2\pi - \alpha_{45}^{Br} &= \alpha_{45}, \quad 2\pi - \alpha_{56}^{Br} = \alpha_{56}, \quad \alpha_{61}^{Br} = \alpha_{61}. \end{aligned} \quad (4-40)$$

and then place revolute joints in-between each adjacent panels, we obtain a 6R assembly in Fig. 4-10. Thick origami model with six fold lines that do not meet at a point. The dihedral angles are marked along each joint axis.

To enable the motion of this 6R assembly, it must be a plane symmetric Bricard linkage. The geometrical conditions for the Bricard linkage are

$$\begin{aligned} \alpha_{12}^{Br} &= 2\pi - \alpha_{34}^{Br}, \quad \alpha_{23}^{Br} = \pi - 2\alpha_{34}^{Br}, \\ \alpha_{12}^{Br} + \alpha_{61}^{Br} &= 2\pi, \quad \alpha_{23}^{Br} + \alpha_{56}^{Br} = 2\pi, \quad \alpha_{34}^{Br} + \alpha_{45}^{Br} = 2\pi, \end{aligned} \quad (4-41a)$$

$$a_{12}^{Br} = a_{61}^{Br}, \quad a_{23}^{Br} = a_{56}^{Br}, \quad a_{34}^{Br} = a_{45}^{Br} \quad (4-41b)$$

Moreover, to achieve compact folding, there must be

$$a_{12}^{Br} + a_{23}^{Br} = a_{34}^{Br}. \quad (4-41c)$$

which is obvious by considering the complete packaged configuration.

According to the symmetric condition, we have

$$\begin{aligned} \theta_2^{Br} &= \theta_6^{Br}, \\ \theta_3^{Br} &= \theta_5^{Br}, \\ \theta_3^{Br} &= \pi + \theta_2^{Br}. \end{aligned} \quad (4-42)$$

Referring to Eqn. (1-1), the closure equation of Bricard 6R linkage can be written as

$$\mathbf{T}_{12} \mathbf{T}_{23} \mathbf{T}_{34} = \mathbf{T}_{16} \mathbf{T}_{65} \mathbf{T}_{54} \quad (4-43)$$

We note it as

$$\begin{aligned} \mathbf{T}_L^{Br} &= \mathbf{T}_{12} \mathbf{T}_{23} \mathbf{T}_{34}, \\ \mathbf{T}_R^{Br} &= \mathbf{T}_{16} \mathbf{T}_{65} \mathbf{T}_{54}, \end{aligned} \quad (4-44)$$

All elements of the matrices of Eqn. (4-44) are given in the Appendix. From $\mathbf{T}_L^{Br}(1,1) = \mathbf{T}_R^{Br}(1,1)$, $\mathbf{T}_L^{Br}(1,3) = \mathbf{T}_R^{Br}(1,3)$ and $\mathbf{T}_L^{Br}(1,4) = \mathbf{T}_R^{Br}(1,4)$, we can have

$$\begin{aligned} &-\sin \theta_2^{Br} \cdot (\cos 2\alpha_{12}^{Br} \cdot \cos \theta_1^{Br} \cdot \sin \theta_2^{Br} - \sin 2\alpha_{12}^{Br} \cdot \sin \alpha_{12}^{Br} \cdot \sin \theta_1^{Br} \\ &+ \cos 2\alpha_{12}^{Br} \cdot \cos \alpha_{12}^{Br} \cdot \cos \theta_2^{Br} \cdot \sin \theta_1^{Br}) \\ &-\cos \theta_2^{Br} \cdot (\cos \theta_1^{Br} \cdot \cos \theta_2^{Br} - \cos \alpha_{12}^{Br} \cdot \sin \theta_1^{Br} \cdot \sin \theta_2^{Br}) \\ &= \sin 2\alpha_{12}^{Br} \cdot \sin \alpha_{12}^{Br} \cdot \sin \theta_2^{Br} \cdot \sin \theta_4^{Br} \\ &-\cos \theta_4^{Br} \cdot (\cos^2 \theta_2^{Br} + \cos 2\alpha_{12}^{Br} \cdot \sin^2 \theta_2^{Br}) \\ &+ 2 \cdot \cos \alpha_{12}^{Br} \cdot \cos \theta_2^{Br} \cdot \sin \theta_2^{Br} \cdot \sin \theta_4^{Br} \cdot \sin^2 \alpha_{12}^{Br} \end{aligned} \quad (4-45a)$$

$$\begin{aligned}
 & 2 \cdot \sin \alpha_{12}^{Br} \cdot (\cos^2 \alpha_{12}^{Br} - \cos \theta_2^{Br} + \cos^2 \alpha_{12}^{Br} \cdot \cos \theta_2^{Br}) \cdot (\cos \alpha_{12}^{Br} \cdot \sin \theta_1^{Br} \\
 & + \cos \theta_1^{Br} \cdot \sin \theta_2^{Br} + \cos \alpha_{12}^{Br} \cdot \cos \theta_2^{Br} \cdot \sin \theta_1^{Br}) = \\
 & -2 \cdot \sin \alpha_{12}^{Br} \cdot \sin \theta_2^{Br} \cdot (\cos^2 \alpha_{12}^{Br} - \cos \theta_2^{Br} + \cos^2 \alpha_{12}^{Br} \cdot \cos \theta_2^{Br})
 \end{aligned} \tag{4-45b}$$

$$\begin{aligned}
 & a_{12}^{Br} \cdot \cos \theta_1^{Br} + a_{23}^{Br} \cdot \cos \theta_1^{Br} \cdot \cos \theta_2^{Br} \\
 & - \sin \theta_2^{Br} \cdot (a_{12}^{Br} + a_{23}^{Br}) \cdot (\cos 2\alpha_{12}^{Br} \cdot \cos \theta_1^{Br} \cdot \sin \theta_2^{Br} - \sin 2\alpha_{12}^{Br} \cdot \sin \alpha_{12}^{Br} \cdot \sin \theta_1^{Br} \\
 & + \cos 2\alpha_{12}^{Br} \cdot \cos \alpha_{12}^{Br} \cdot \cos \theta_2^{Br} \cdot \sin \theta_1^{Br}) \\
 & - \cos \theta_2^{Br} \cdot (a_{12}^{Br} + a_{23}^{Br}) \cdot (\cos \theta_1^{Br} \cdot \cos \theta_2^{Br} - \cos \alpha_{12}^{Br} \cdot \sin \theta_1^{Br} \cdot \sin \theta_2^{Br}) \\
 & - a_{23}^{Br} \cdot \cos \alpha_{12}^{Br} \cdot \sin \theta_1^{Br} \cdot \sin \theta_2^{Br} \\
 & = (a_{12}^{Br} + a_{23}^{Br}) \cdot (\cos^2 \theta_2^{Br} + \cos 2\alpha_{12}^{Br} \cdot \sin^2 \theta_2^{Br}) - a_{23}^{Br} \cdot \cos \theta_2^{Br} - a_{12}^{Br}
 \end{aligned} \tag{4-45c}$$

Then, we use the following trigonometric transforms to simplify them,

$$t_1^{Br} = \tan \frac{\theta_1^{Br}}{2}, t_2^{Br} = \tan \frac{\theta_2^{Br}}{2}, t_3^{Br} = \tan \frac{\theta_3^{Br}}{2}, t_4^{Br} = \tan \frac{\theta_4^{Br}}{2}, \tag{4-46}$$

Substituting (4-46) into (4-45) gives

$$t_1^{Br} = t_4^{Br} \tag{4-47a}$$

$$t_2^{Br} = -\cos \alpha^{Br} \cdot t_1^{Br} \tag{4-47b}$$

Besides Eqn. (4-42), considering with (4-46) and (4-47), the rest of the closure equations can be obtained, which are

$$\theta_1^{Br} = \theta_4^{Br}, \tag{4-48a}$$

$$\cos \alpha_{34}^{Br} \tan \frac{\theta_1^{Br}}{2} + \tan \frac{\theta_2^{Br}}{2} = 0. \tag{4-48b}$$

Note that the relationships between the angular variables and the corresponding dihedral angles of the Bricard linkage are

$$\begin{aligned}
 \theta_1^{Br} &= 2\pi - \varphi_1^{Br}, \theta_2^{Br} = \varphi_2^{Br}, \theta_3^{Br} = \pi + \varphi_3^{Br}, \\
 \theta_4^{Br} &= 2\pi - \varphi_4^{Br}, \theta_5^{Br} = \pi + \varphi_5^{Br}, \theta_6^{Br} = \varphi_6^{Br}.
 \end{aligned} \tag{4-49}$$

Substituting them into Eqns. (4-42) and (4-48),

$$\begin{aligned}
 \varphi_1^{Br} &= \varphi_4^{Br}, \\
 \varphi_2^{Br} &= \varphi_3^{Br} = \varphi_5^{Br} = \varphi_6^{Br},
 \end{aligned} \tag{4-50a}$$

$$\tan \frac{\varphi_2^{Br}}{2} = \cos \alpha_{12}^{Br} \cdot \tan \frac{\varphi_1^{Br}}{2}. \tag{4-50b}$$

Eqns. (4-39) and (4-50) are identical except that α^{Br} 's and φ^{Br} 's take the places of α 's and φ 's, respectively. The Bricard linkage is therefore kinematically equivalent to the spherical linkage. The relationships between a pair of dihedral angles are plotted in Fig. 4-11. Curves a and b are relationships between dihedral angles φ_1 and φ_2 in zero-thickness rigid origami for three sets of sector angles, respectively. They overlap with those between φ_1^{Br} and φ_2^{Br} for their thick panel counterparts, respectively.

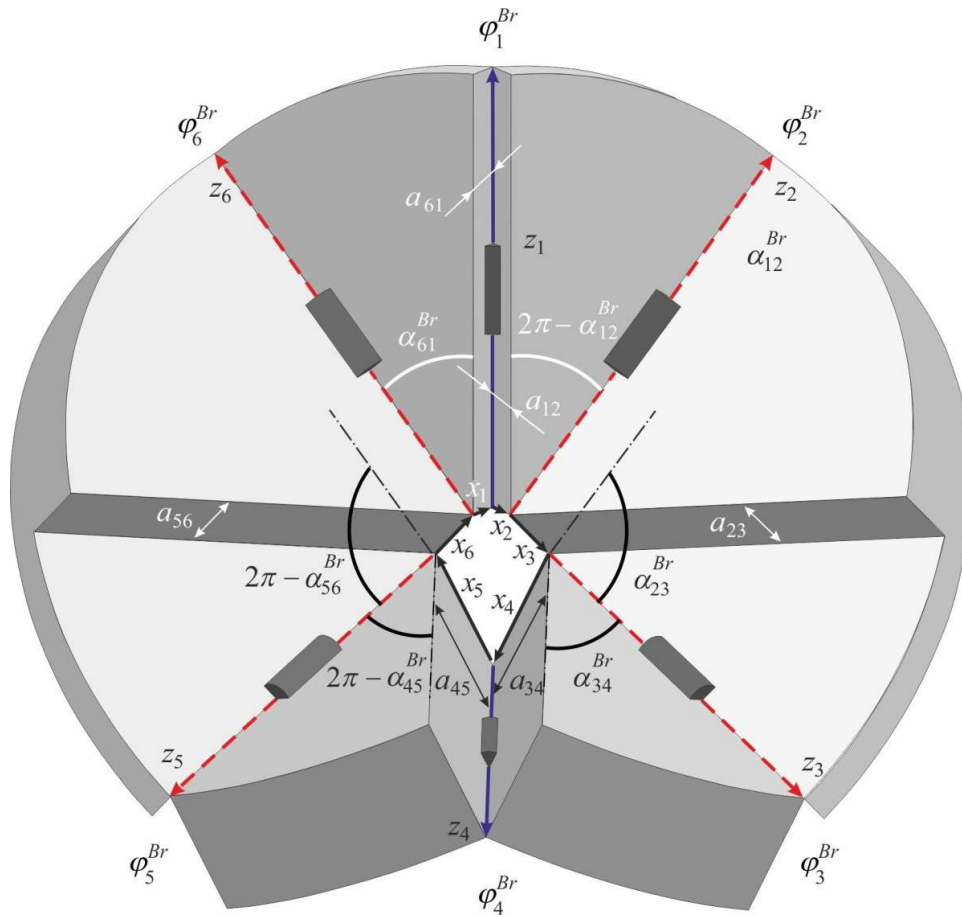


Figure 4-10 Thick origami model for six-crease origami vertex.

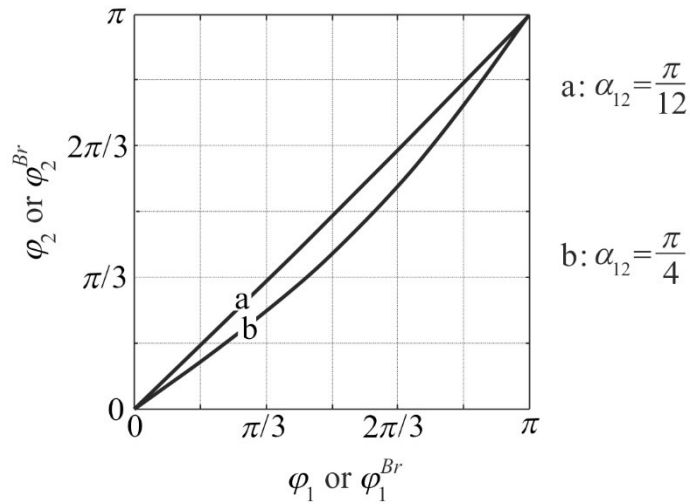


Figure 4-11 Relationships between dihedral angles for six-crease single vertex origami.

The kinematic motion of this Bricard linkage again matches that of the spherical $6R$ linkage of the zero-thickness model. This enables us to make a thick panel origami arch using the diamond pattern. The folding sequence of both zero and non-zero thickness models are shown in Fig. 4-12.

Folding sequence of a zero-thickness origami model of the diamond pattern and its thick panel counterpart based on the plane-symmetric Bricard linkage. All the vertices are identical. The sector angles around each vertex are $\pi/6, 2\pi/3, \pi/6, \pi/6, 2\pi/3$ and $\pi/6$.

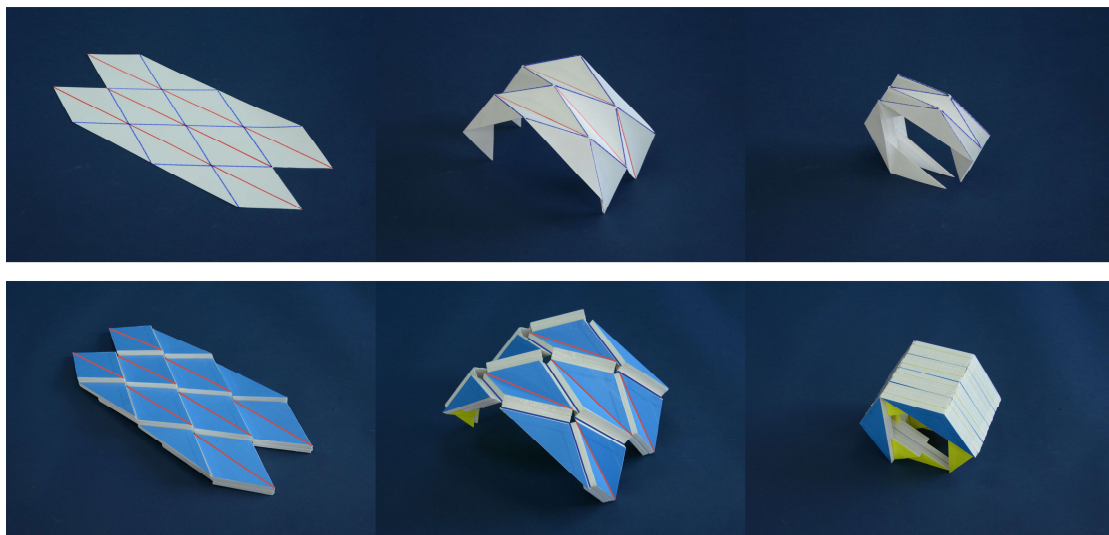


Figure 4-12 Zero-thickness model of Diamond pattern and its corresponding thick panel model.

4.4.2 Waterbomb Pattern

The waterbomb pattern has two types of six-crease vertices: **D** and **W** as shown in Fig. 4-13.

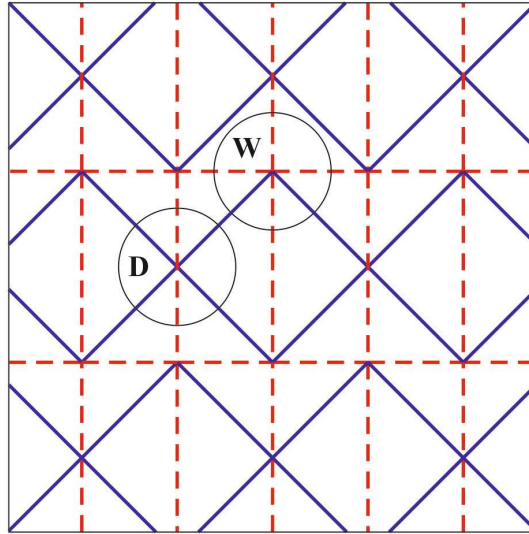


Figure 4-13 Waterbomb pattern.

Vertex **D** is a special case of the diamond pattern. Vertex **W** is enlarged in Figure S11. The sector angles between adjacent creases of vertex **W** satisfy

$$\alpha_{12} = \alpha_{61} = \frac{\pi}{2}, \alpha_{23} = \alpha_{34} = \alpha_{45} = \alpha_{56} = \frac{\pi}{4}. \quad (4-51)$$

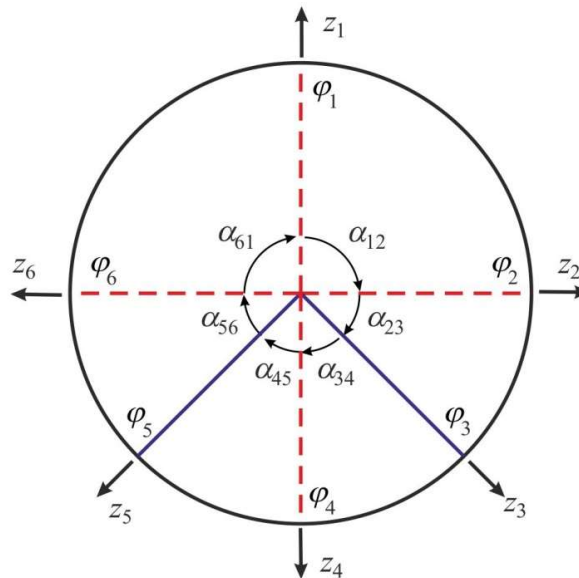


Figure 4-14 Vertex **W** of the waterbomb pattern.

The spherical $6R$ linkage has, in general, mobility three. To reduce it to mobility one, the following constraints are imposed. First, plane symmetry is maintained, so,

$$\theta_2 = \theta_6, \theta_3 = \theta_5, \quad (4-52a)$$

Moreover, considering it is connected to the neighbouring vertices \mathbf{D} 's, the kinematic relationship between θ_1 and θ_3 (or θ_5) of vertex \mathbf{W} must identical to that between θ_1 and θ_2 of vertex \mathbf{D} . The latter is given by Eqn. (4-37). Replacing θ_1 and θ_2 in Eqn. (4-37) with θ_1 and θ_3 , respectively, yields

$$\tan \frac{\theta_1}{2} + \frac{\sqrt{2}}{2} \tan \frac{\theta_3}{2} = 0 \quad (4-52b)$$

noting that $\alpha_{12} = \frac{\pi}{2}$ for vertex \mathbf{W} .

With constraints of Eqn. (4-52), the mobility of this spherical $6R$ linkage becomes one. Using Eqn. (4-31), we found two remaining equations governing the motion of this linkage, which are

$$\tan \frac{\theta_2}{2} = 2 \tan \frac{\theta_1}{2} \quad (4-52c)$$

$$\tan \frac{\theta_4}{2} = 4 \tan^3 \frac{\theta_1}{2} + 3 \tan \frac{\theta_1}{2} \quad (4-52d)$$

Eqn. (4-52) are the complete set of closure equations of the spherical $6R$ linkage in vertex \mathbf{W} .

The relationships between the angular variables and their respective dihedral angles are

$$\begin{aligned} \theta_1 &= \pi + \varphi_1, \quad \theta_2 = \pi + \varphi_2, \quad \theta_3 = \pi - \varphi_3, \\ \theta_4 &= \pi + \varphi_4, \quad \theta_5 = \pi - \varphi_5, \quad \theta_6 = \pi + \varphi_6. \end{aligned} \quad (4-53)$$

Substituting them into Eqn. (4-52) gives

$$\varphi_5 = \varphi_3, \quad \varphi_6 = \varphi_2. \quad (4-54a)$$

$$\tan \frac{\varphi_2}{2} = \frac{1}{2} \tan \frac{\varphi_1}{2} \quad (4-54b)$$

$$\tan \frac{\varphi_3}{2} = \frac{\sqrt{2}}{2} \tan \frac{\varphi_1}{2} \quad (4-54c)$$

$$\tan \frac{\varphi_4}{2} = \frac{\tan^3 \frac{\varphi_1}{2}}{4 + 3 \tan^2 \frac{\varphi_1}{2}} \quad (4-54d)$$

Now apply the same partition angles to divide the thick panel into six subpanels by letting

$$\begin{aligned} \alpha_{12}^{Br} &= \alpha_{12}, \quad \alpha_{23}^{Br} = \alpha_{23}, \quad \alpha_{34}^{Br} = 2\pi - \alpha_{34}, \\ \alpha_{45}^{Br} &= \alpha_{45}, \quad \alpha_{56}^{Br} = 2\pi - \alpha_{56}, \quad \alpha_{61}^{Br} = 2\pi - \alpha_{61} \end{aligned} \quad (4-55)$$

and then place revolute joints in-between each adjacent panels, a $6R$ assembly is obtained, Fig. 4-15. Thick origami model with six fold lines that do not meet at a point. The dihedral angles are marked along each joint axis.

This $6R$ assembly must be a plane symmetric Bricard linkage to acquire mobility, which requires the thicknesses of the subpanels satisfy

$$a_{56}^{Br} = a_{23}^{Br}, \quad a_{12}^{Br} = a_{61}^{Br}, \quad a_{34}^{Br} = a_{45}^{Br} \quad (4-56)$$

In order to achieve compact folding, the above equations have to be modified to

$$a_{56}^{Br} = a_{23}^{Br}, \quad a_{12}^{Br} = a_{61}^{Br} = (1 + \mu)a_{23}^{Br}, \quad a_{34}^{Br} = a_{45}^{Br} = \mu a_{23}^{Br} \quad (4-57)$$

in which μ is a constant yet to be determined.

Similar to what we have done with the Bennett and Myard linkages, the closure equations for this Bricard linkage can be obtained, which are

$$\theta_5^{Br} = \theta_3^{Br}, \quad \theta_6^{Br} = \theta_2^{Br} \quad (4-58a)$$

$$\tan \frac{\theta_1^{Br}}{2} = -\frac{\mu(\mu+1) \cdot \tan^2 \frac{\theta_2^{Br}}{2} + \mu + 1}{\mu^2 \cdot \tan \frac{\theta_2^{Br}}{2} \cdot (\tan^2 \frac{\theta_2^{Br}}{2} + 1)} \quad (4-58b)$$

$$\tan \frac{\theta_3^{Br}}{2} = \frac{\sqrt{2}(\mu+1)}{2\mu} / \tan \frac{\theta_2^{Br}}{2} \quad (4-58c)$$

$$\tan \frac{\theta_4^{Br}}{2} = \frac{\mu(\mu-1) \cdot \tan^2 \frac{\theta_2^{Br}}{2} - \mu - 1}{\mu \cdot \tan \frac{\theta_2^{Br}}{2} \cdot (\mu \cdot \tan^2 \frac{\theta_2^{Br}}{2} + \mu + 2)} \quad (4-58d)$$

These equations can be written in terms of dihedral angles considering that the relationships between the angular variables and their respective dihedral angles are

$$\begin{aligned}\theta_1^{Br} &= \varphi_1^{Br}, \theta_2^{Br} = \pi + \varphi_2^{Br}, \theta_3^{Br} = 2\pi - \varphi_3^{Br}, \\ \theta_4^{Br} &= \varphi_4^{Br}, \theta_5^{Br} = 2\pi - \varphi_5^{Br}, \theta_6^{Br} = \pi + \varphi_6^{Br}\end{aligned}\quad (4-59)$$

It can be show that, if

$$\mu = 1 \quad (4-60)$$

the resultant equations are identical to those of the spherical 6R linkage given by Eqn.(4-54) except that α^{Br} 's and φ^{Br} 's take the places of α 's and φ 's, respectively.

Substituting Equation (4-60) into Equation (4-57), the thickness of subpanels must satisfy

$$a_{23}^{Br} = a_{34}^{Br} = a_{45}^{Br} = a_{56}^{Br}, a_{12}^{Br} = a_{61}^{Br} = 2a_{23}^{Br} \quad (4-61)$$

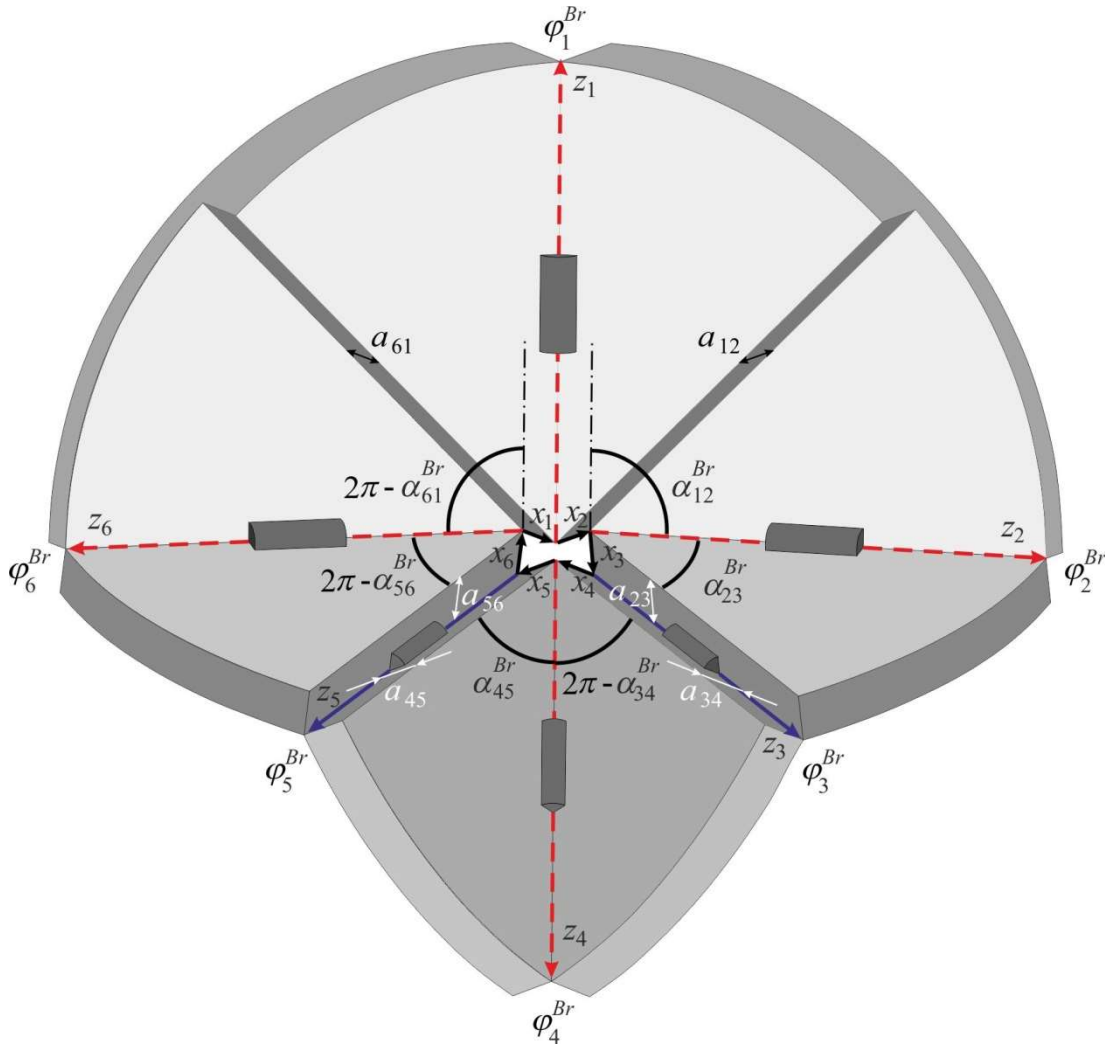


Figure 4-15 Thick origami model for origami vertex W.

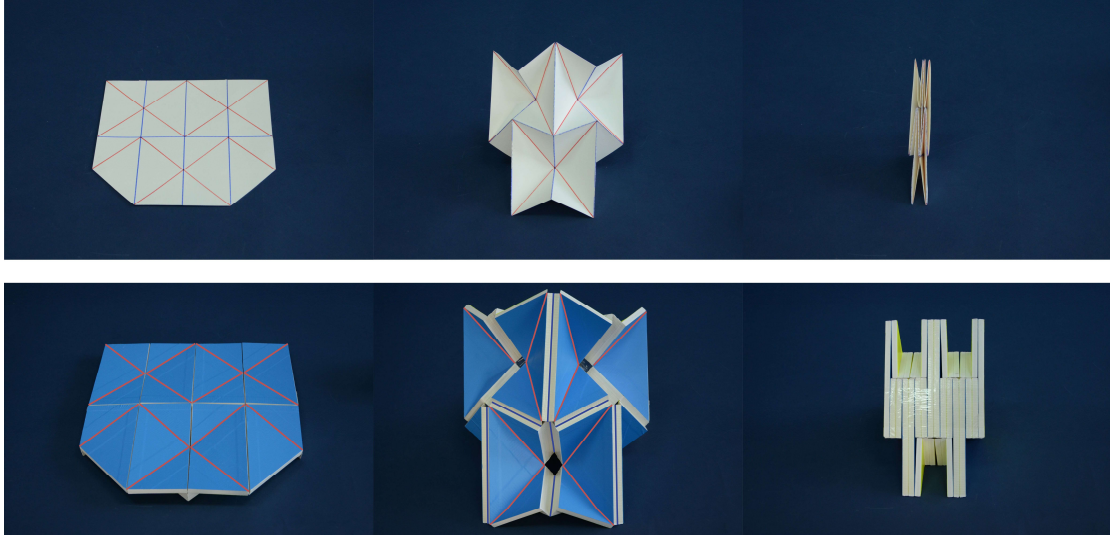


Figure 4-16 Zero-thickness model of Waterbomb pattern and its corresponding thick panel model.

When $\mu \neq 1$, the thick panel origami of vertex **W** in the traditional waterbomb pattern can still be flat foldable. This is evident by curve **c** in Fig. 4-17 where $\mu = \frac{1}{2}$. Curve **a** is the relationships between dihedral angles φ_1 and φ_2 in zero-thickness six-crease rigid origami for vertex **W**. Curves **b** and **c** are the relationships between dihedral angles φ_1^{Br} and φ_2^{Br} for the thick panel counterparts based on the Bricard linkage with different panel thicknesses. Note that curve **b** overlaps with curve **a**, demonstrating that the kinematical equivalence of the spherical linkage and the Bricard linkage. However in such circumstance, the motion of vertices **D** and **W** are not compatible any more, i.e., the changes in dihedral angle about fold lines shared by linkages around **D** and **W** differ during folding process. As a result, the mobility is lost.

In addition, it should be pointed out that the bifurcation does exist in both zero-thickness and thick panel origami of the traditional waterbomb patterns due to the fact that axes z_2 and z_6 in both Fig. 4-14 and Fig. 4-15 are co-linear initially when the sheet or panel is completely flat. This can be avoid in making $\alpha_{12} = \alpha_{61} \neq \frac{\pi}{2}$, but it is beyond the scope of this article.

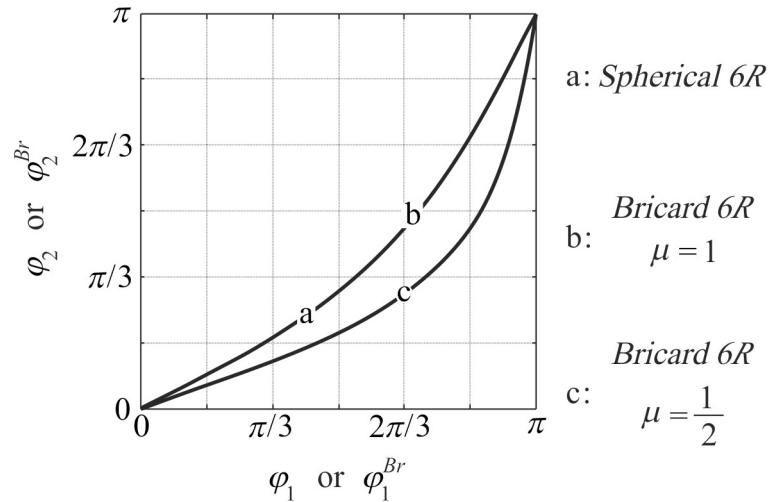


Figure 4-17 Relationships between dihedral angles for vertex W in the waterbomb origami pattern.

4.5 Conclusion

We have developed a comprehensive kinematic model for rigid origami of panels with non-zero thickness. This is done by identifying a spatial linkage model that is kinematically equivalent to the rigid origami of a zero-thickness sheet. In other words, the motion of the spatial linkage mimics that of the spherical linkage commonly used to model rigid origami. To achieve this, we identify a spatial linkage that has the angular conditions for arrangement of fold lines identical to that of the spherical linkage, and then prove analytically that their motions are precisely alike.

The thick panel counterparts to four-, five- and six-crease vertex origami patterns are overconstrained spatial linkages. The number of such linkages is rather limited. It is relatively straightforward for four-crease origami patterns as only one spatial $4R$ linkage exists. However, five- and six-crease single vertex patterns commonly comprise two or three degrees of freedom, whereas their corresponding spatial overconstrained linkages have only one mobility degree of freedom. In these cases, equivalence can only be accomplished through reducing the degrees of freedom of the former by symmetry or other means. This may be beneficial for practical applications as the folding of thick panels can be more easily controlled due to their single degree of freedom. Moreover, the synthesis can also be used for origami patterns consisting of a mixture of vertices with various creases. Fig. 4-18 shows the folding sequence of a thick panel origami based on a pattern with both four- and six-crease vertices.

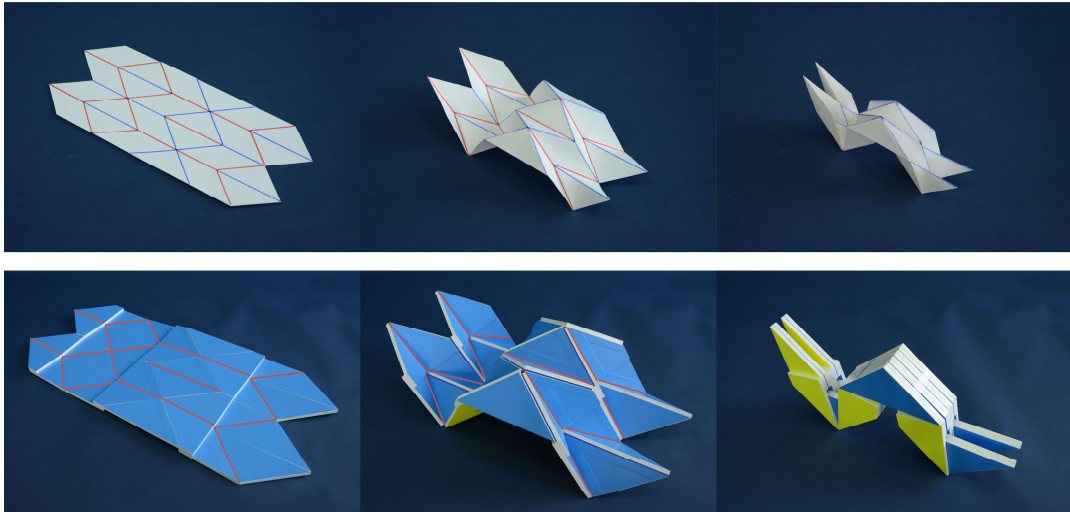


Figure 4-18 A thick panel origami based on a pattern with both four- and six-crease vertices.

Chapter 5 Conclusion and Future Works

5.1 Conclusion

This thesis presents our work on constructing mobile networks of spherical $4R$ linkages and design rigid origami patterns. Then the kinematic theory is used to judge the rigidity of origami patterns and the effect of mountain-valley fold assignments on the rigidity is presented. Negative Poisson's ratio metamaterials based on rigid origami patterns are also proposed in this thesis. A novel kinematic synthesis for rigid origami of thick panels is established for real engineering applications. In this chapter, we have a whole conclusion for the whole thesis.

(1) Network of four spherical $4R$ linkages

Based on the analysis of kinematics of spherical $4R$ linkage, we propose sixteen alternative input-output relationships between the kinematic variables. Then we build three types of assemblies of four identical spherical $4R$ linkages. The topology structures of these three types are respectively rotational symmetric, plane symmetric and two-fold symmetric. The symmetrical characters make these assemblies compatible and mobile.

Then, the symmetrical compatible conditions are equivalent to the kinematic transmission loops, i.e., the geometrical conditions are presented by the kinematic theories. We use the sixteen alternative relationships to modify the transmission loops and keep closed. According to the new modified transmission loops, the mobile assemblies of four different spherical $4R$ linkages are derived while the kinematic compatibility is always kept.

With the paper treated as links and the creases as joints, new rigid origami patterns are obtained by referring to mobile assemblies of spherical $4R$ linkages with the paper flat geometric condition. The theory proposed in this thesis not only provides the solutions for the mobile assemblies of spherical $4R$ linkages, but also shows the feasibility to design rigid origami patterns by studying the kinematic compatibility condition of spherical $4R$ linkage assemblies.

(2) Mountain-valley folds of origami patterns

The rigid origami patterns should satisfy strict geometrical conditions, e.g., paper facets in the double corrugated pattern are all parallelograms. The types of creases, mountain fold and valley fold, also have important role in the rigid foldability of origami patterns. According to the relationship between spherical linkages and rigid origami, the effect of mountain-valley fold assignments on the rigidity of flat foldable origami patterns are analysed with a kinematic method. The analysis result gives multiple kinds of rigid double corrugated pattern with different mountain-valley fold

assignments.

Metamaterials from the stacks of double corrugated patterns have been proposed with many varieties when changing the mountain-valley assignments. Following the folding of the rigid origami patterns, the metamaterials exhibit negative Poisson's ratio and different mountain-valley assignments can affect the deformation property of origami metamaterials largely. The square-twist pattern and its metamaterials with negative Poisson's ratio are also discussed to show the generalization of this method.

(3) Origami of thick panels

The traditional kinematic model for rigid origami is based on spherical linkages, but the material thickness can not be accommodated. By shifting hinges out of plane of the origami pattern, this problem will be solved. This new comprehensive kinematic model for rigid origami of panels with non-zero thickness is based on the spatial linkages.

The number of such linkages is rather limited. It is relatively straightforward for four-crease origami patterns as only one spatial $4R$ linkage exists. However, five-crease and six-crease single vertex patterns commonly comprise two or three degrees of freedom, whereas their corresponding spatial overconstrained linkages have only one mobility degree of freedom.

The construction process of thick panel origami models for four-crease origami vertex is using Bennett linkage, five-crease origami vertex by using Myard linkage, and six-crease origami vertex by using Bricard linkage. This is done by identifying a spatial linkage model that is kinematically equivalent to the rigid origami of a zero-thickness sheet, i.e., the motion of the spatial linkage mimics that of the spherical linkage commonly used to model rigid origami.

Thick panel models for multi-vertex patterns by this technique is also presented in this thesis. Moreover, the synthesis can also be used for origami patterns consisting of a mixture of vertices with various creases. A thick panel origami based on a pattern with both four- and six-crease vertices are also shown in this thesis.

5.2 Future Works

This thesis systemically presents the theories of using the network of spherical $4R$ linkages and rigid origami for constructing deployable structures and metamaterials. In order to improve the performance of the deployable structure, a number of potential research areas are outlined as follows.

(1) The mobile assemblies of spherical $4R$ linkages are based on the topological symmetric. More general method of constructing mobile network of spherical $4R$ linkages will be explored in the future.

(2) Referring to the assemblies proposed by our method, a lot of rigid origami

patterns with 3×3 quadrilateral mesh can be designed. In the further research, we will extend the unit patterns unlimitedly to get large-scale rigid origami patterns by tessellation method.

(3) The mechanical property of the metamaterials will be analysed in the future and find suitable engineering application fields of these metamaterials.

(4) Use the thick origami technique to design new solar arrays, antenna of satellites, and other deployable structures in the space engineering.

(5) Finish the force analysis of the origami-inspiration deployable structures and optimize the design parameter to achieve better performance, such as larger deploy-fold ratios, easier to actuate the structure and better controllable deploying motion.

Reference

- [1] 邓宗全. 空间折展机构设计 [M]. 哈尔滨: 哈尔滨工业大学出版社, 2013.
- [2] Hunt K H. Kinematic geometry of mechanisms [M]. Clarendon Press Oxford, 1978.
- [3] McCarthy J M. Introduction to theoretical kinematics [M]. MIT press, 1990.
- [4] You Z, Chen Y. Motion structures [M]. Taylor and Francis, 2011.
- [5] Baker J E. The Bennett, Goldberg and Myard linkages—in perspective [J]. Mechanism and Machine Theory, 1979, 14(4): 239-253.
- [6] Gogu G. Mobility of mechanisms: a critical review [J]. Mechanism and Machine Theory, 2005, 40(9): 1068-1097.
- [7] Huang H, Deng Z, Bing L. Mobile assemblies of large deployable mechanisms [J]. Journal of Space Engineering, 2012, 5(1): 1-14.
- [8] Kiper G, Soylemez E. Deployable space structures; proceedings of the Recent Advances in Space Technologies, 2009 RAST'09 4th International Conference on, F, 2009 [C]. IEEE.
- [9] Tibert A G, Pellegrino S. Deployable tensegrity reflectors for small satellites [J]. Journal of Spacecraft and Rockets, 2002, 39(5): 701-709.
- [10] Schenk M, Viquerat A D, Seffen K A, et al. Review of inflatable booms for deployable space structures: packing and rigidization [J]. Journal of Spacecraft and Rockets, 2014, 51(3): 762-778.
- [11] Luo Y, Mao D, You Z. On a type of radially retractable plate structures [J]. International Journal of Solids and Structures, 2007, 44(10): 3452-3467.
- [12] Buhl T, Jensen F V, Pellegrino S. Shape optimization of cover plates for retractable roof structures [J]. Computers & Structures, 2004, 82(15): 1227-1236.
- [13] Mao D, Luo Y. Analysis and design of a type of retractable roof structure [J]. Advances in Structural Engineering, 2008, 11(4): 343-354.
- [14] You Z, Pellegrino S. Foldable bar structures [J]. International Journal of Solids and Structures, 1997, 34(15): 1825-1847.
- [15] Mao D, Luo Y, You Z. Planar closed loop double chain linkages [J]. Mechanism and Machine Theory, 2009, 44(4): 850-859.
- [16] Kassabian P, You Z, Pellegrino S. Retractable roof structures [J]. Proceedings of the Institution of Civil Engineers-Structures and Buildings, 1999, 134(1): 45-56.
- [17] Jensen F, Pellegrino S. Expandable 'blob' structures [J]. An Anthology of Structural Morphology, 2009, 189.
- [18] You Z. Deployable structure of curved profile for space antennas [J]. Journal of Aerospace Engineering, 2000, 13(4): 139-143.
- [19] Chiang C H. Kinematics of spherical mechanisms [M]. Cambridge University Press Cambridge, 1988.
- [20] Bennett G. A new mechanism [J]. Engineering, 1903, 76(12): 777-8.
- [21] Chen Y, Baker J. Using a Bennett linkage as a connector between other Bennett loops [J]. Proceedings of the Institution of Mechanical Engineers, Part K: Journal of Multi-body Dynamics, 2005, 219(2): 177-185.

- [22] Baker J E. A collapsible network of similar pairs of nested Bennett linkages [J]. *Mechanism and Machine Theory*, 2013, 59(4):119-24.
- [23] Chen Y, You Z. Mobile assemblies based on the Bennett linkage [J]. *Proceedings of the Royal Society A: Mathematical, Physical and Engineering Science*, 2005, 461(2056): 1229-45.
- [24] Chen Y, You Z. On mobile assemblies of Bennett linkages [J]. *Proceedings of the Royal Society A: Mathematical, Physical and Engineering Science*, 2008, 464(2093): 1275-93.
- [25] Yu Y, Luo Y, Li L. Deployable membrane structure based on the Bennett linkage [J]. *Proceedings of the Institution of Mechanical Engineers, Part G: Journal of Aerospace Engineering*, 2007, 221(5): 775-83.
- [26] Kiper G, Soylemez E. Regular polygonal and regular spherical polyhedral linkages comprising bennett loops [M]. *Computational Kinematics*. Springer. 2009: 249-56.
- [27] Marras A E, Zhou L, Su H, et al. Programmable motion of DNA origami mechanisms [J]. *Proceedings of the National Academy of Sciences*, 2015, 112(3): 713-718.
- [28] Goldberg M. New five-bar and six-bar linkages in three dimensions [J]. *Transactions of the ASME*, 1943, 65(1): 649-663.
- [29] Myard F. Contribution à la géométrie des systèmes articulés [J]. *Bulletin de la Société Mathématique de France*, 1931, 59:183-210.
- [30] Chen Y, You Z. An extended Myard linkage and its derived 6R linkage [J]. *Journal of Mechanical Design*, 2008, 130(5): 052301.
- [31] Liu S, Chen Y. Myard linkage and its mobile assemblies [J]. *Mechanism and Machine Theory*, 2009, 44(10): 1950-63.
- [32] Qi X Z, Deng Z Q, Ma B Y, et al. Design of Large Deployable Networks Constructed by Myard Linkages[J]. *Key Engineering Materials*, 2011, 486:291-296.
- [33] Wei G, Dai J S. A Spatial Eight-Bar Linkage and Its Association With the Deployable Platonic Mechanisms[J]. *Journal of Mechanisms and Robotics*, 2014, 6(2).
- [34] Bennett G T. LXXVII. The parallel motion of Sarrut and some allied mechanisms [J]. *The London, Edinburgh, and Dublin Philosophical Magazine and Journal of Science*, 1905, 9(54): 803-810.
- [35] Bricard R. *Leçons de cinématique* [M]. Gauthier-Villars, 1926.
- [36] Goldberg M. Polyhedral linkages [J]. *National Mathematics Magazine*, 1942, 16(7): 323-332.
- [37] Baker J. On the skew network corresponding to Bricard's doubly collapsible octahedron [J]. *Proceedings of the Institution of Mechanical Engineers, Part C: Journal of Mechanical Engineering Science*, 2009, 223(5): 1213-1221.
- [38] Lee C, Dai J. Configuration analysis of the Schatz linkage [J]. *Proceedings of the Institution of Mechanical Engineers, Part C: Journal of Mechanical Engineering Science*, 2003, 217(7): 779-786.
- [39] Chen Y, You Z. Deployable structures based on the Bricard linkages[C]. *Proceedings of the 45th AIAA/ASME/ASCE/AHS/ASC Structures, Structural Dynamics & Materials Conference*, 2004.
- [40] Kong X, Huang C. Type synthesis of single-DOF single-loop mechanisms with

- two operation modes[C]. ASME/IFTOMM International Conference on Reconfigurable Mechanisms and Robots. IEEE, 2009:136-141.
- [41] Dai J S, Caldwell D. Origami-based robotic paper-and-board packaging for food industry [J]. *Trends in Food Science & Technology*, 2010, 21(3): 153-157.
- [42] Hawkes E, An B, Benbernou N, et al. Programmable matter by folding [J]. *Proceedings of the National Academy of Sciences*, 2010, 107(28): 12441-12445.
- [43] Kuribayashi K, Onoe H, Takeuchi S. Cell origami: self-folding of three-dimensional cell-laden microstructures driven by cell traction force [J]. *PloS One*, 2012, 7(12): e51085.
- [44] Hagiwara I. Current trends and issues of origami engineering [M]. *System Simulation and Scientific Computing*. Springer. 2012: 259-268.
- [45] Peraza E A, Hartl D J, Malak R J, et al. Origami-inspired active structures: a synthesis and review [J]. *Smart Materials and Structures*, 2014, 23(9): 094001.
- [46] Turner N, Goodwine B, Sen M. A review of origami applications in mechanical engineering [J]. *Proceedings of the Institution of Mechanical Engineers, Part C: Journal of Mechanical Engineering Science*, 2016, 230(14): 2345-2362.
- [47] Tang R, Huang H, Tu H, et al. Origami-enabled deformable silicon solar cells [J]. *Applied Physics Letters*, 2014, 104(8): 083501.
- [48] Ma J, You Z. Energy absorption of thin-walled square tubes with a prefolded origami pattern—part I: geometry and numerical simulation [J]. *Journal of Applied Mechanics*, 2014, 81(1): 011003.
- [49] Ma J, You Z. Energy absorption of thin-walled beams with a pre-folded origami pattern [J]. *Thin-Walled Structures*, 2013, 56(4):569-574.
- [50] Gattas J M, You Z. Geometric assembly of rigid-foldable morphing sandwich structures [J]. *Engineering structures*, 2015, 94:149-159.
- [51] Thrall A, Quaglia C. Accordion shelters: A historical review of origami-like deployable shelters developed by the US military [J]. *Engineering structures*, 2014, 59:686-92.
- [52] Lee T, Gattas J M. Geometric design and construction of structurally stabilized accordion shelters [J]. *Journal of Mechanisms and Robotics*, 2016, 8(3): 031009.
- [53] Mousanezhad D, Kamrava S, Vaziri A. Origami-based Building Blocks for Modular Construction of Foldable Structures [J]. *Scientific Reports*, 2017, 7(1).
- [54] Wilson L, Pellegrino S, Danner R. Origami sunshield concepts for space telescopes[C]. *Proceedings of the 54th AIAA/ASME/ASCE/AHS/ASC Structures, Structural Dynamics, and Materials Conference*, 2013.
- [55] Miura K. A note on intrinsic geometry of origami [J]. *Research of Pattern Formation*, KTK Scientific Publishers, Tokyo, Japan, 1989, 91-102.
- [56] Hull T. *Project origami: activities for exploring mathematics* [M]. CRC Press, 2012.
- [57] Kobayashi H, Kresling B, Vincent J F. The geometry of unfolding tree leaves [J]. *Proceedings of the Royal Society of London B: Biological Sciences*, 1998, 265(1391): 147-154.
- [58] Watanabe N, Kawaguchi K. The method for judging rigid foldability [J]. *Origami*, 2009, 4:165-174.
- [59] Huffman D A. Curvature and Creases: A Primer on Paper[J]. *IEEE Transactions on Computers*, 1976, C-25(10):1010-1019.

- [60] Wu W, You Z. Modelling rigid origami with quaternions and dual quaternions[J]. Proceedings Mathematical Physical & Engineering Sciences, 2010, 466(2119):2155-2174.
- [61] Dai J S, Jones J R. Mobility in Metamorphic Mechanisms of Foldable/Erectable Kinds[J]. Journal of Mechanical Design, 1999, 121(3):375-382.
- [62] Stachel H. A kinematic approach to Kokotsakis meshes [J]. Computer Aided Geometric Design, 2010, 27(6): 428-437.
- [63] Filipov E T, Liu K, Tachi T, et al. Bar and hinge models for scalable analysis of origami [J]. International Journal of Solids & Structures, 2017,
- [64] Nojima T. Modelling of folding patterns in flat membranes and cylinders by origami [J]. JSME International Journal, 2002, 45(1): 364-370.
- [65] Wang K, Chen Y. Folding a patterned cylinder by rigid origami [J]. Origami, 2011, 5:265-276.
- [66] Pellegrino S. The folding of triangulated cylinders, part I: geometric considerations [J]. Journal of Applied Mechanics, 1994, 61(4).
- [67] Martinez R V, Fish C R, Chen X, et al. Elastomeric origami: programmable paper elastomer composites as pneumatic actuators [J]. Advanced Functional Materials, 2012, 22(7): 1376-1384.
- [68] Kuribayashi K, Tsuchiya K, You Z, et al. Self-deployable origami stent grafts as a biomedical application of Ni-rich TiNi shape memory alloy foil [J]. Materials Science and Engineering: A, 2006, 419(1): 131-137.
- [69] Tachi T. One-DOF cylindrical deployable structures with rigid quadrilateral panels[J]. Symposium of the International Association for Shell and Spatial Structures (50th. 2009. Valencia). Evolution and Trends in Design, Analysis and Construction of Shell and Spatial Structures : Proceedings, 2010.
- [70] Aleksandrov V A. A new example of a flexible polyhedron [J]. Siberian Mathematical Journal, 1995, 36(6): 1049-1057.
- [71] Liu S, Weilin L V, Chen Y, et al. Deployable Prismatic Structures with Rigid Origami Patterns[J]. Journal of Mechanisms & Robotics, 2015, 8(3):V05BT08A037.
- [72] MIURA K, TACHI T. Synthesis of rigid-foldable cylindrical polyhedral [J]. Symmetry: Art and Science, International Society for the Interdisciplinary Study of Symmetry, Gmuend, 2010.
- [73] Yasuda H, Yein T, Tachi T, et al. Folding behaviour of Tachi-Miura polyhedron bellows[J]. Proc Math Phys Eng Sci, 2016, 469(2159):20130351.
- [74] TACHI T. Rigid-foldable thick origami [J]. Origami, 2011, 5:253-264.
- [75] Edmondson B J, Lang R J, Morgan M R, et al. Thick rigidly foldable structures realized by an offset panel technique [M] Origami 6. 2015.
- [76] Ku J S, Demaine E D. Folding flat crease patterns with thick materials [J]. Journal of Mechanisms and Robotics, 2016, 8(3): 031003.
- [77] Hoberman C S. Reversibly expandable three-dimensional structure: US, US4780344[P]. 1988.
- [78] Temmerman D, Niels I A, Mollaert, et al. Design and Analysis of a Foldable Mobile Shelter System[J]. International Journal of Space Structures, 2009, 22(22):161-168.
- [79] Wang Z, Jing L, Yao K, et al. Origami based reconfigurable metamaterials for

- tunable chirality [J]. *Advanced Materials*, 2017, 29(27).
- [80] Zhai Z, Wang Y, Jiang H. Origami-inspired, on-demand deployable and collapsible mechanical metamaterials with tunable stiffness [J]. *Proceedings of the National Academy of Sciences*, 2018, 115(9): 2032-2037.
- [81] Boatti E, Vasios N, Bertoldi K. Origami metamaterials for tunable thermal expansion [J]. *Advanced Materials*, 2017, 29(26).
- [82] Miura K. Method of Packaging and Deployment of Large Membranes in Space[J]. *Institute of Space & Astronautical Science Report*, 1985, 618:1-9.
- [83] Natori M C, Katsumata N, Yamakawa H, et al. Conceptual model study using origami for membrane space structures[C]. *ASME 2013 International Design Engineering Technical Conferences and Computers and Information in Engineering Conference*. 2013:V06BT07A047.
- [84] Zirbel S A, Lang R J, Thomson M W, et al. Accommodating thickness in origami-based deployable arrays [J]. *Journal of Mechanical Design*, 2013, 135(11): 111005.
- [85] Felton S, Tolley M, Demaine E, et al. A method for building self-folding machines [J]. *Science*, 2014, 345(6197): 644-646.
- [86] Miyashita S, Guitron S, Ludersdorfer M, et al. An untethered miniature origami robot that self-folds, walks, swims, and degrades[C]. *International Conference on Robotics and Automation*, 2015: 1490-1496..
- [87] Zhang K, Fang Y, Fang H, et al. Geometry and constraint analysis of the three-spherical kinematic chain based parallel mechanism [J]. *Journal of Mechanisms and Robotics*, 2010, 2(3): 031014.
- [88] Onal C D, Wood R J, Rus D. An origami-inspired approach to worm robots [J]. *IEEE/ASME Transactions on Mechatronics*, 2013, 18(2): 430-438.
- [89] Li S, Vogt D M, Rus D, et al. Fluid-driven origami-inspired artificial muscles [J]. *Proceedings of the National Academy of Sciences of the United States of America*, 2017, 114(50): 13132.
- [90] Le P, Molina J, Hirai S. Application of Japanese origami ball for floating multirotor aerial robot [J]. *World Academy of Science, Engineering and Technology, International Journal of Mechanical, Aerospace, Industrial, Mechatronic and Manufacturing Engineering*, 2014, 8(10): 1747-1750.
- [91] Lee D Y, Kim J S, Kim S R, et al. The deformable wheel robot using magic-ball origami structure[C]. *ASME 2013 International Design Engineering Technical Conferences and Computers and Information in Engineering Conference*. 2013:V06BT07A040..
- [92] Schenk M, Guest S D. Geometry of Miura-folded metamaterials [J]. *Proceedings of the National Academy of Sciences*, 2013, 110(9): 3276-3281.
- [93] Schenk M, Guest S, Mcshane G. Novel stacked folded cores for blast-resistant sandwich beams [J]. *International Journal of Solids and Structures*, 2014, 51(25): 4196-4214.
- [94] Wei Z Y, Guo Z V, Dudte L, et al. Geometric mechanics of periodic pleated origami [J]. *Physical Review Letters*, 2013, 110(21): 215501.
- [95] Silverberg J L, Evans A A, Mcleod L, et al. Using origami design principles to fold reprogrammable mechanical metamaterials [J]. *Science*, 2014, 345(6197): 647-650.
- [96] Lv C, Krishnaraju D, Konjevod G, et al. Origami based mechanical

- metamaterials [J]. *Scientific Reports*, 2014, 4:5979.
- [97] Cheung K C, Tachi T, Calisch S, et al. Origami interleaved tube cellular materials [J]. *Smart Materials and Structures*, 2014, 23(9): 094012.
- [98] Filipov E T, Tachi T, Paulino G H. Origami tubes assembled into stiff, yet reconfigurable structures and metamaterials [J]. *Proceedings of the National Academy of Sciences*, 2015, 112(40): 12321-12326.
- [99] Yasuda H, Yang J. Reentrant origami-based metamaterials with negative Poisson's ratio and bistability [J]. *Physical Review Letters*, 2015, 114(18): 185502.
- [100] Silverberg J L, Na J, Evans A A, et al. Origami structures with a critical transition to bistability arising from hidden degrees of freedom [J]. *Nature Materials*, 2015, 14(4): 389-393.
- [101] Waitukaitis S, Menaut R, Chen B G, et al. Origami multistability: From single vertices to metasheets [J]. *Physical Review Letters*, 2015, 114(5): 055503.
- [102] Hanna B H, Lund J M, Lang R J, et al. Waterbomb base: a symmetric single-vertex bistable origami mechanism [J]. *Smart Materials and Structures*, 2014, 23(9): 094009.
- [103] Mills A. Robert Hooke's 'universal joint' and its application to sundials and the sundial-clock [J]. *Notes and Records*, 2007, 61(2): 219-36.
- [104] Arkin E M, Bender M A, Demaine E D, et al. When can you fold a map? [J]. *Computational Geometry*, 2004, 29(1): 23-46.
- [105] Huffman D A. *Curvature and Creases: A Primer on Paper*[J]. *IEEE Transactions on Computers*, 1976, C-25(10):1010-1019..
- [106] Li W, Mcadams D A. Novel pixelated multicellular representation for origami structures that innovates computational design and control[C]. *ASME 2013 International Design Engineering Technical Conferences and Computers and Information in Engineering Conference*. 2013:V06BT07A041..
- [107] Saito K, Tsukahara A, Okabe Y. New deployable structures based on an elastic origami model [J]. *Journal of Mechanical Design*, 2015, 137(2): 021402.
- [108] Hull T. On the mathematics of flat origamis [J]. *Congressus Numerantium*, 1994, 215-224.
- [109] Evans T A, Lang R J, Magleby S P, et al. Rigidly foldable origami twists [J]. *Origami*, 2015, 6:119-130.

Table A4. Geometrical conditions of rotation assemblies for Kokotsakis meshes (continued)

Rotation case	
<i>R3R13R12</i>	<i>R4R11R5</i>
$\alpha_{12}^a = \alpha_{12}, \alpha_{12}^b = \alpha_{12}, \alpha_{12}^c = \pi - \alpha_{12}, \alpha_{12}^d = \alpha_{12},$ $\alpha_{23}^a = \pi - \alpha_{23}, \alpha_{23}^b = \pi - \alpha_{23}, \alpha_{23}^c = \pi - \alpha_{23}, \alpha_{23}^d = \alpha_{23}$ $\alpha_{34}^a = \pi - \alpha_{34}, \alpha_{34}^b = \pi - \alpha_{34}, \alpha_{34}^c = \pi - \alpha_{34}, \alpha_{34}^d = \alpha_{34}$ $\alpha_{41}^a = \alpha_{41}, \alpha_{41}^b = \alpha_{41}, \alpha_{41}^c = \pi - \alpha_{41}, \alpha_{41}^d = \alpha_{41}.$ $\alpha_{12} + \alpha_{41} = \alpha_{23} + \alpha_{34} = \pi$	$\alpha_{12}^a = \pi - \alpha_{12}, \alpha_{12}^b = \alpha_{12}, \alpha_{12}^c = \alpha_{12}, \alpha_{12}^d = \alpha_{12},$ $\alpha_{23}^a = \pi - \alpha_{23}, \alpha_{23}^b = \alpha_{23}, \alpha_{23}^c = \alpha_{23}, \alpha_{23}^d = \alpha_{23},$ $\alpha_{34}^a = \pi - \alpha_{34}, \alpha_{34}^b = \pi - \alpha_{34}, \alpha_{34}^c = \pi - \alpha_{34}, \alpha_{34}^d = \alpha_{34}$ $\alpha_{41}^a = \pi - \alpha_{41}, \alpha_{41}^b = \pi - \alpha_{41}, \alpha_{41}^c = \pi - \alpha_{41}, \alpha_{41}^d = \alpha_{41}.$ $\alpha_{12} + \alpha_{34} = \alpha_{23} + \alpha_{41} = \pi$
<i>R4R10R16</i>	<i>R4R9R12</i>
$\alpha_{12}^a = \pi - \alpha_{12}, \alpha_{12}^b = \pi - \alpha_{12}, \alpha_{12}^c = \pi - \alpha_{12}, \alpha_{12}^d = \alpha_{12}$ $\alpha_{23}^a = \pi - \alpha_{23}, \alpha_{23}^b = \pi - \alpha_{23}, \alpha_{23}^c = \pi - \alpha_{23}, \alpha_{23}^d = \alpha_{23}.$ $\alpha_{34}^a = \pi - \alpha_{34}, \alpha_{34}^b = \alpha_{34}, \alpha_{34}^c = \alpha_{34}, \alpha_{34}^d = \alpha_{34},$ $\alpha_{41}^a = \pi - \alpha_{41}, \alpha_{41}^b = \alpha_{41}, \alpha_{41}^c = \alpha_{41}, \alpha_{41}^d = \alpha_{41}.$ $\alpha_{12} + \alpha_{23} = \alpha_{34} + \alpha_{41} = \pi$	$\alpha_{12}^a = \pi - \alpha_{12}, \alpha_{12}^b = \alpha_{12}, \alpha_{12}^c = \pi - \alpha_{12}, \alpha_{12}^d = \alpha_{12},$ $\alpha_{23}^a = \pi - \alpha_{23}, \alpha_{23}^b = \alpha_{23}, \alpha_{23}^c = \pi - \alpha_{23}, \alpha_{23}^d = \alpha_{23},$ $\alpha_{34}^a = \pi - \alpha_{34}, \alpha_{34}^b = \alpha_{34}, \alpha_{34}^c = \pi - \alpha_{34}, \alpha_{34}^d = \alpha_{34},$ $\alpha_{41}^a = \pi - \alpha_{41}, \alpha_{41}^b = \alpha_{41}, \alpha_{41}^c = \pi - \alpha_{41}, \alpha_{41}^d = \alpha_{41}.$ $\alpha_{12} + \alpha_{34} = \alpha_{23} + \alpha_{41} = \pi$

The results the compatible equation of spherical 4R linkage are

$$\begin{aligned}
 Q_L^{S4R}(1,1) &= \cos \theta_1^{S4R} \cdot \cos \theta_2^{S4R} - \cos \alpha_{12}^{S4R} \cdot \sin \theta_1^{S4R} \cdot \sin \theta_2^{S4R} \\
 Q_L^{S4R}(1,2) &= \sin \alpha_{12}^{S4R} \cdot \sin \alpha_{23}^{S4R} \cdot \sin \theta_1^{S4R} - \cos \alpha_{23}^{S4R} \cdot \cos \theta_1^{S4R} \cdot \sin \theta_2^{S4R} \\
 &\quad - \cos \alpha_{12}^{S4R} \cdot \cos \alpha_{23}^{S4R} \cdot \cos \theta_2^{S4R} \cdot \sin \theta_1^{S4R} \\
 Q_L^{S4R}(1,3) &= \cos \alpha_{23}^{S4R} \cdot \sin \alpha_{12}^{S4R} \cdot \sin \theta_1^{S4R} + \sin \alpha_{23}^{S4R} \cdot \cos \theta_1^{S4R} \cdot \sin \theta_2^{S4R} \\
 &\quad + \cos \alpha_{12}^{S4R} \cdot \sin \alpha_{23}^{S4R} \cdot \cos \theta_2^{S4R} \cdot \sin \theta_1^{S4R} \\
 Q_L^{S4R}(2,1) &= \cos \theta_2^{S4R} \cdot \sin \theta_1^{S4R} + \cos \alpha_{12}^{S4R} \cdot \cos \theta_1^{S4R} \cdot \sin \theta_2^{S4R} \\
 Q_L^{S4R}(2,2) &= \cos \alpha_{12}^{S4R} \cdot \cos \alpha_{23}^{S4R} \cdot \cos \theta_1^{S4R} \cdot \cos \theta_2^{S4R} - \cos \alpha_{23}^{S4R} \cdot \sin \theta_1^{S4R} \cdot \sin \theta_2^{S4R} \\
 &\quad - \sin \alpha_{12}^{S4R} \cdot \sin \alpha_{23}^{S4R} \cdot \cos \theta_1^{S4R} \\
 Q_L^{S4R}(2,3) &= \sin \alpha_{12}^{S4R} \cdot \sin \theta_1^{S4R} \cdot \sin \theta_2^{S4R} - \cos \alpha_{23}^{S4R} \cdot \sin \alpha_{12}^{S4R} \cdot \cos \theta_1^{S4R} \\
 &\quad - \cos \alpha_{12}^{S4R} \cdot \sin \alpha_{23}^{S4R} \cdot \cos \theta_1^{S4R} \cdot \cos \theta_2^{S4R} \\
 Q_L^{S4R}(3,1) &= \sin \alpha_{12}^{S4R} \cdot \sin \theta_2^{S4R} \\
 Q_L^{S4R}(3,2) &= \cos \alpha_{12}^{S4R} \cdot \sin \alpha_{23}^{S4R} + \cos \alpha_{23}^{S4R} \cdot \sin \alpha_{12}^{S4R} \cdot \cos \theta_2^{S4R} \\
 Q_L^{S4R}(3,3) &= \cos \alpha_{12}^{S4R} \cdot \cos \alpha_{23}^{S4R} - \sin \alpha_{12}^{S4R} \cdot \sin \alpha_{23}^{S4R} \cdot \cos \theta_2^{S4R} \\
 \\
 Q_R^{S4R}(1,1) &= \cos \theta_3^{S4R} \cdot \cos \theta_4^{S4R} + \cos \alpha_{12}^{S4R} \cdot \sin \theta_3^{S4R} \cdot \sin \theta_4^{S4R} \\
 Q_R^{S4R}(1,2) &= \cos \theta_4^{S4R} \cdot \sin \theta_3^{S4R} - \cos \alpha_{12}^{S4R} \cdot \cos \theta_3^{S4R} \cdot \sin \theta_4^{S4R} \\
 Q_R^{S4R}(1,3) &= \sin \alpha_{12}^{S4R} \cdot \sin \theta_4^{S4R} \\
 Q_R^{S4R}(2,1) &= \sin \alpha_{12}^{S4R} \cdot \sin \alpha_{23}^{S4R} \cdot \sin \theta_3^{S4R} + \cos \alpha_{23}^{S4R} \cdot \cos \theta_3^{S4R} \cdot \sin \theta_4^{S4R} \\
 &\quad - \cos \alpha_{12}^{S4R} \cdot \cos \alpha_{23}^{S4R} \cdot \cos \theta_4^{S4R} \cdot \sin \theta_3^{S4R} \\
 Q_R^{S4R}(2,2) &= \cos \alpha_{12}^{S4R} \cdot \cos \alpha_{23}^{S4R} \cdot \cos \theta_3^{S4R} \cdot \cos \theta_4^{S4R} + \cos \alpha_{23}^{S4R} \cdot \sin \theta_3^{S4R} \cdot \sin \theta_4^{S4R} \\
 &\quad - \sin \alpha_{12}^{S4R} \cdot \sin \alpha_{23}^{S4R} \cdot \cos \theta_3^{S4R} \\
 Q_R^{S4R}(2,3) &= -\cos \alpha_{12}^{S4R} \cdot \sin \alpha_{23}^{S4R} - \cos \alpha_{23}^{S4R} \cdot \sin \alpha_{12}^{S4R} \cdot \cos \theta_4^{S4R} \\
 Q_R^{S4R}(3,1) &= \cos \alpha_{23}^{S4R} \cdot \sin \alpha_{12}^{S4R} \cdot \sin \theta_3^{S4R} - \sin \alpha_{23}^{S4R} \cdot \cos \theta_3^{S4R} \cdot \sin \theta_4^{S4R} \\
 &\quad - \cos \alpha_{12}^{S4R} \cdot \sin \alpha_{23}^{S4R} \cdot \cos \theta_4^{S4R} \cdot \sin \theta_3^{S4R} \\
 Q_R^{S4R}(3,2) &= \sin \alpha_{23}^{S4R} \cdot \sin \theta_3^{S4R} \cdot \sin \theta_4^{S4R} + \cos \alpha_{23}^{S4R} \cdot \sin \alpha_{12}^{S4R} \cdot \cos \theta_3^{S4R} \\
 &\quad + \cos \alpha_{12}^{S4R} \cdot \sin \alpha_{23}^{S4R} \cdot \cos \theta_3^{S4R} \cdot \cos \theta_4^{S4R} \\
 Q_R^{S4R}(3,3) &= \cos \alpha_{12}^{S4R} \cdot \cos \alpha_{23}^{S4R} - \sin \alpha_{12}^{S4R} \cdot \sin \alpha_{23}^{S4R} \cdot \cos \theta_4^{S4R}
 \end{aligned}$$

The results the compatible equation of spherical 5R linkage are

$$Q_L^{S5R}(1,1) = \cos \theta_3^{S5R} \cdot (\cos \theta_1^{S5R} \cdot \cos \theta_2^{S5R} - \cos \alpha^{S5R} \cdot \sin \theta_1^{S5R} \cdot \sin \theta_2^{S5R}) \\ + \sin \alpha^{S5R} \cdot \sin \theta_1^{S5R} \cdot \theta_3^{S5R}$$

$$Q_L^{S5R}(1,2) = \sin(2\alpha^{S5R}) \cdot (\cos \theta_1^{S5R} \cdot \sin \theta_2^{S5R} + \cos \alpha^{S5R} \cdot \cos \theta_2^{S5R} \cdot \sin \theta_1^{S5R}) \\ + \cos(2\alpha^{S5R}) \cdot \sin \theta_3^{S5R} (\cos \theta_1^{S5R} \cdot \cos \theta_2^{S5R} - \cos \alpha^{S5R} \cdot \sin \theta_1^{S5R} \cdot \sin \theta_2^{S5R}) \\ - \cos(2\alpha^{S5R}) \cdot \sin \alpha^{S5R} \cdot \cos \theta_3^{S5R} \cdot \sin \theta_1^{S5R}$$

$$Q_L^{S5R}(1,3) = \sin(2\alpha^{S5R}) \cdot \sin \theta_3^{S5R} \cdot (\cos \theta_1^{S5R} \cdot \cos \theta_2^{S5R} - \cos \alpha^{S5R} \cdot \sin \theta_1^{S5R} \cdot \sin \theta_2^{S5R}) \\ - \cos(2\alpha^{S5R}) \cdot (\cos \theta_1^{S5R} \cdot \sin \theta_2^{S5R} + \cos \alpha^{S5R} \cdot \cos \theta_2^{S5R} \cdot \sin \theta_1^{S5R}) \\ - \sin(2\alpha^{S5R}) \cdot \sin \alpha^{S5R} \cdot \cos \theta_3^{S5R} \cdot \sin \theta_1^{S5R}$$

$$Q_L^{S5R}(2,1) = \cos \theta_3^{S5R} \cdot (\cos \theta_2^{S5R} \cdot \sin \theta_1^{S5R} + \cos \alpha^{S5R} \cdot \cos \theta_1^{S5R} \cdot \sin \theta_2^{S5R}) \\ - \sin \alpha^{S5R} \cdot \cos \theta_1^{S5R} \cdot \sin \theta_3^{S5R}$$

$$Q_L^{S5R}(2,2) = \sin(2\alpha^{S5R}) \cdot (\sin \theta_1 \cdot \sin \theta_2 - \cos \alpha^{S5R} \cdot \cos \theta_1^{S5R} \cdot \cos \theta_2^{S5R}) \\ + \cos(2\alpha^{S5R}) \cdot \sin \theta_3^{S5R} \cdot (\cos \theta_2^{S5R} \cdot \sin \theta_1^{S5R} + \cos \alpha^{S5R} \cdot \cos \theta_1^{S5R} \cdot \sin \theta_2^{S5R}) \\ + \cos(2\alpha^{S5R}) \cdot \sin \alpha^{S5R} \cdot \cos \theta_1^{S5R} \cdot \cos \theta_3^{S5R}$$

$$Q_L^{S5R}(2,3) = \sin(2\alpha^{S5R}) \cdot \sin \theta_3^{S5R} \cdot (\cos \theta_2^{S5R} \cdot \sin \theta_1^{S5R} + \cos \alpha^{S5R} \cdot \cos \theta_1^{S5R} \cdot \sin \theta_2^{S5R}) \\ - \cos(2\alpha^{S5R}) \cdot (\sin \theta_1^{S5R} \cdot \sin \theta_2^{S5R} - \cos \alpha^{S5R} \cdot \cos \theta_1^{S5R} \cdot \cos \theta_2^{S5R}) \\ + \sin(2\alpha^{S5R}) \cdot \sin \alpha^{S5R} \cdot \cos \theta_1^{S5R} \cdot \cos \theta_3^{S5R}$$

$$Q_L^{S5R}(3,1) = \cos \alpha^{S5R} \cdot \sin \theta_3^{S5R} + \sin \alpha^{S5R} \cdot \cos \theta_3^{S5R} \cdot \sin \theta_2^{S5R}$$

$$Q_L^{S5R}(3,2) = \cos(2\alpha^{S5R}) \cdot \sin \alpha^{S5R} \cdot \sin \theta_2^{S5R} \cdot \sin \theta_3^{S5R} - \sin(2\alpha^{S5R}) \cdot \sin \alpha^{S5R} \cdot \cos \theta_2^{S5R} \\ - \cos(2\alpha^{S5R}) \cdot \cos \alpha^{S5R} \cdot \cos \theta_3^{S5R}$$

$$Q_L^{S5R}(3,3) = \cos(2\alpha^{S5R}) \cdot \sin \alpha^{S5R} \cdot \cos \theta_2^{S5R} - \sin(2\alpha^{S5R}) \cdot \cos \alpha^{S5R} \cdot \cos \theta_3^{S5R} \\ + \sin(2\alpha^{S5R}) \cdot \sin \alpha^{S5R} \cdot \sin \theta_2^{S5R} \cdot \sin \theta_3^{S5R}$$

$$Q_R^{S5R}(1,1) = \cos \theta_2^{S5R} \cdot \cos \theta_3^{S5R}$$

$$Q_R^{S5R}(1,2) = \cos \theta_2^{S5R} \cdot \sin \theta_3^{S5R}$$

$$Q_R^{S5R}(1,3) = \sin \theta_2^{S5R}$$

$$Q_R^{S5R}(2,1) = -\cos \alpha^{S5R} \cdot \cos \theta_3^{S5R} \cdot \sin \theta_2^{S5R} + \sin \alpha^{S5R} \cdot \sin \theta_3^{S5R}$$

$$Q_R^{S5R}(2,2) = -\sin \alpha^{S5R} \cdot \cos \theta_3^{S5R} - \cos \alpha^{S5R} \cdot \sin \theta_2^{S5R} \cdot \sin \theta_3^{S5R}$$

$$Q_R^{S5R}(2,3) = \cos \alpha^{S5R} \cdot \cos \theta_2^{S5R}$$

$$Q_R^{S5R}(3,1) = \cos \alpha^{S5R} \cdot \sin \theta_3^{S5R} + \sin \alpha^{S5R} \cdot \cos \theta_3^{S5R} \cdot \sin \theta_2^{S5R}$$

$$Q_R^{S5R}(3,2) = \sin \alpha^{S5R} \cdot \sin \theta_2^{S5R} \cdot \sin \theta_3^{S5R} - \cos \alpha^{S5R} \cdot \cos \theta_3^{S5R}$$

$$Q_R^{S5R}(3,3) = -\sin \alpha^{S5R} \cdot \cos \theta_2^{S5R}$$

The results the compatible equation of Spherical 6R linkage are

$$\begin{aligned} Q_L^{S6R}(1,1) &= \sin \theta_2^{S6R} \cdot (\cos(2\alpha^{S6R}) \cdot \cos \theta_1^{S6R} \cdot \sin \theta_2^{S6R} + \sin(2\alpha^{S6R}) \cdot \sin \alpha^{S6R} \cdot \sin \theta_1^{S6R}) \\ &+ \cos(2\alpha^{S6R}) \cdot \cos \alpha^{S6R} \cdot \cos \theta_2^{S6R} \cdot \sin \theta_1^{S6R} \\ &+ \cos \theta_2^{S6R} \cdot (\cos \theta_1^{S6R} \cdot \cos \theta_2^{S6R} - \cos \alpha^{S6R} \cdot \sin \theta_1^{S6R} \cdot \sin \theta_2^{S6R}) \end{aligned}$$

$$\begin{aligned} Q_L^{S6R}(1,2) &= -\cos^2 \alpha^{S6R} \cdot \sin \theta_1^{S6R} \cdot (\cos^2 \theta_2^{S6R} - 1) + \cos(2\alpha^{S6R}) \cdot \sin \theta_1^{S6R} \cdot (\cos^2 \alpha^{S6R} - 1) \\ &+ 2 \cdot \cos^3 \alpha^{S6R} \cdot \cos \theta_1^{S6R} \cdot \cos \theta_2^{S6R} \cdot \sin \theta_2^{S6R} - 2 \cdot \cos \alpha^{S6R} \cdot \cos \theta_1^{S6R} \cdot \sin \theta_2^{S6R} \cdot (\cos^2 \alpha^{S6R} - 1) \\ &- 2 \cdot \cos \alpha^{S6R} \cdot \cos \theta_1^{S6R} \cdot \cos \theta_2^{S6R} \cdot \sin \theta_2^{S6R} + \cos(2\alpha^{S6R}) \cdot \cos^2 \alpha^{S6R} \cdot \cos^2 \theta_2^{S6R} \cdot \sin \theta_1^{S6R} \\ &- 4 \cdot \cos^2 \alpha^{S6R} \cdot \cos \theta_2^{S6R} \cdot \sin \theta_1^{S6R} \cdot (\cos^2 \alpha^{S6R} - 1) \end{aligned}$$

$$\begin{aligned} Q_L^{S6R}(1,3) &= 2 \cdot \sin \alpha^{S6R} \cdot (\cos^2 \alpha^{S6R} + \cos \theta_2^{S6R} - \cos^2 \alpha^{S6R} \cdot \cos \theta_2^{S6R}) \\ &\cdot (-\cos \alpha^{S6R} \cdot \sin \theta_1^{S6R} + \cos \theta_1^{S6R} \cdot \sin \theta_2^{S6R} + \cos \alpha^{S6R} \cdot \cos \theta_2^{S6R} \cdot \sin \theta_1^{S6R}) \end{aligned}$$

$$\begin{aligned} Q_L^{S6R}(2,1) &= -\sin \theta_2^{S6R} \cdot (\sin(2\alpha^{S6R}) \cdot \sin \alpha^{S6R} \cdot \cos \theta_1^{S6R} - \cos(2\alpha^{S6R}) \cdot \sin \theta_1^{S6R} \cdot \sin \theta_2^{S6R}) \\ &+ \cos(2\alpha^{S6R}) \cdot \cos \alpha^{S6R} \cdot \cos \theta_1^{S6R} \cdot \cos \theta_2^{S6R} + \cos \theta_2^{S6R} \cdot (\cos \theta_2^{S6R} \cdot \sin \theta_1^{S6R} \\ &+ \cos \alpha^{S6R} \cdot \cos \theta_1^{S6R} \cdot \cos \theta_2^{S6R}) \end{aligned}$$

$$\begin{aligned} Q_L^{S6R}(2,2) &= -\cos(2\alpha^{S6R}) \cdot \cos \theta_1^{S6R} \cdot (\cos^2 \alpha^{S6R} - 1) + \cos^2 \alpha^{S6R} \cdot \cos \theta_1^{S6R} \cdot (\cos^2 \theta_2^{S6R} - 1) \\ &+ 2 \cdot \cos^3 \alpha^{S6R} \cdot \cos \theta_2^{S6R} \cdot \sin \theta_1^{S6R} \cdot \sin \theta_2^{S6R} - 2 \cdot \cos \alpha^{S6R} \cdot \sin \theta_1^{S6R} \cdot \sin \theta_2^{S6R} \cdot (\cos^2 \alpha^{S6R} - 1) \\ &- \cos(2\alpha^{S6R}) \cdot \cos^2 \alpha^{S6R} \cdot \cos \theta_1^{S6R} \cdot \cos^2 \theta_2^{S6R} + 4 \cdot \cos^2 \alpha^{S6R} \cdot \cos \theta_1^{S6R} \cdot \cos \theta_2^{S6R} \cdot (\cos^2 \alpha^{S6R} - 1) \\ &- 2 \cdot \cos \alpha^{S6R} \cdot \cos \theta_2^{S6R} \cdot \sin \theta_1^{S6R} \cdot \sin \theta_2^{S6R} \end{aligned}$$

$$\begin{aligned} Q_L^{S6R}(2,3) &= 2 \cdot \sin \alpha^{S6R} \cdot (\cos^2 \alpha^{S6R} + \cos \theta_2^{S6R} - \cos^2 \alpha^{S6R} \cdot \cos \theta_2^{S6R}) \\ &\cdot (\cos \alpha^{S6R} \cdot \cos \theta_1^{S6R} + \sin \theta_1^{S6R} \cdot \sin \theta_2^{S6R} - \cos \alpha^{S6R} \cdot \cos \theta_1^{S6R} \cdot \cos \theta_2^{S6R}) \end{aligned}$$

$$Q_L^{S6R}(3,1) = -2 \cdot \sin \alpha^{S6R} \cdot \sin \theta_2^{S6R} \cdot (2 \cdot \sin^2 \left(\frac{\theta_2^{S6R}}{2} \right) \cdot \sin^2 \alpha^{S6R} - 1)$$

$$\begin{aligned} Q_L^{S6R}(3,2) &= 2 \cos \alpha^{S6R} \cdot \sin \alpha^{S6R} \cdot (\cos \theta_2^{S6R} - 1) \\ &\cdot (\cos \theta_2^{S6R} + \cos^2 \alpha^{S6R} - \cos^2 \alpha^{S6R} \cdot \cos \theta_2^{S6R}) \end{aligned}$$

$$\begin{aligned} Q_L^{S6R}(3,3) &= 8 \cdot \sin^2 \alpha^{S6R} \cdot \sin^2 \frac{\theta_2^{S6R}}{2} - 8 \cdot \sin^2 \frac{\theta_2^{S6R}}{2} \cdot \sin^4 \alpha^{S6R} \\ &+ 2 \cdot \sin^4 \alpha^{S6R} \cdot \sin^2 \theta_2^{S6R} - 1 \end{aligned}$$

$$\begin{aligned} Q_R^{S6R}(1,1) &= \sin(2\alpha^{S6R}) \cdot \sin \alpha^{S6R} \cdot \sin \theta_1^{S6R} \cdot \sin \theta_2^{S6R} + \cos \theta_1^{S6R} \cdot (\cos^2 \theta_2^{S6R} \\ &+ \cos(2\alpha^{S6R}) \cdot \sin^2 \theta_2^{S6R}) + 2 \cdot \cos \alpha^{S6R} \cdot \cos \theta_2^{S6R} \cdot \sin \theta_1^{S6R} \cdot \sin \theta_2^{S6R} \cdot \sin^2 \alpha^{S6R} \end{aligned}$$

$$\begin{aligned} Q_R^{S6R}(1,2) &= -2 \cdot \cos \alpha^{S6R} \cdot \cos \theta_1^{S6R} \cdot \cos \theta_2^{S6R} \cdot \sin \theta_2^{S6R} \cdot \sin^2 \alpha^{S6R} - \sin(2\alpha^{S6R}) \cdot \sin \alpha^{S6R} \\ &\cdot \cos \theta_1^{S6R} \cdot \sin \theta_2^{S6R} + \sin \theta_1^{S6R} \cdot (\cos^2 \theta_2^{S6R} + \cos(2\alpha^{S6R}) \cdot \sin^2 \theta_2^{S6R}) \end{aligned}$$

$$Q_R^{S6R}(1,3) = 2 \cdot \sin \alpha^{S6R} \cdot \sin \theta_2^{S6R} \cdot (\cos^2 \alpha^{S6R} + \cos \theta_2^{S6R} - \cos^2 \alpha^{S6R} \cdot \cos \theta_2^{S6R})$$

$$\begin{aligned}
 Q_R^{S6R}(2,1) &= \sin(2\alpha^{S6R}) \cdot \sin \alpha^{S6R} \cdot \cos \theta_1^{S6R} \cdot \sin \theta_2^{S6R} + \cos^2 \alpha^{S6R} \cdot \sin \theta_1^{S6R} \cdot \sin^2 \theta_2^{S6R} \\
 &- \sin^2 \alpha^{S6R} \cdot \sin \theta_1^{S6R} \cdot \cos^2 \alpha^{S6R} - \cos \alpha^{S6R} \cdot \cos \theta_1^{S6R} \cdot \cos \theta_2^{S6R} \cdot \sin \theta_2^{S6R} \\
 &+ \cos(2\alpha^{S6R}) \cdot \cos^2 \alpha^{S6R} \cdot \cos^2 \theta_2^{S6R} \cdot \sin \theta_1^{S6R} + 4 \cos^2 \alpha^{S6R} \cdot \cos \theta_2^{S6R} \cdot \sin \theta_1^{S6R} \cdot \sin^2 \alpha^{S6R} \\
 &+ \cos(2\alpha^{S6R}) \cdot \cos \alpha^{S6R} \cdot \cos \theta_1^{S6R} \cdot \cos \theta_2^{S6R} \cdot \sin \theta_2^{S6R}
 \end{aligned}$$

$$\begin{aligned}
 Q_R^{S6R}(2,2) &= -\cos^2 \alpha^{S6R} \cdot \cos \theta_1^{S6R} \cdot \sin^2 \theta_2^{S6R} + \cos(2\alpha^{S6R}) \cdot \sin^2 \alpha^{S6R} \cdot \cos \theta_1^{S6R} \\
 &+ \sin(2\alpha^{S6R}) \cdot \sin \alpha^{S6R} \cdot \sin \theta_1^{S6R} \cdot \sin \theta_2^{S6R} - \cos(2\alpha^{S6R}) \cdot \cos^2 \alpha^{S6R} \cdot \cos \theta_1^{S6R} \cdot \cos^2 \theta_2^{S6R} \\
 &- 4 \cdot \cos^2 \alpha^{S6R} \cdot \cos \theta_1^{S6R} \cdot \theta_2^{S6R} \cdot \sin^2 \alpha^{S6R} - \cos \alpha^{S6R} \cdot \cos \theta_2^{S6R} \cdot \sin \theta_1^{S6R} \cdot \sin \theta_2^{S6R} \\
 &+ \cos(2\alpha^{S6R}) \cdot \cos \alpha^{S6R} \cdot \cos \theta_2^{S6R} \cdot \sin \theta_1^{S6R} \cdot \sin \theta_2^{S6R}
 \end{aligned}$$

$$\begin{aligned}
 Q_R^{S6R}(2,3) &= 2 \cdot \cos \alpha^{S6R} \cdot \sin \alpha^{S6R} \cdot (\cos \theta_2^{S6R} - 1) \cdot (\cos^2 \alpha^{S6R} + \cos \theta_2^{S6R}) \\
 &- \cos^2 \alpha^{S6R} \cdot \cos \theta_2^{S6R}
 \end{aligned}$$

$$\begin{aligned}
 Q_R^{S6R}(3,1) &= 2 \sin \alpha^{S6R} \cdot (\cos^2 \alpha^{S6R} + \cos \theta_2^{S6R} - \cos^2 \alpha^{S6R} \cdot \cos \theta_2^{S6R}) \\
 &\cdot (-\cos \alpha^{S6R} \cdot \sin \theta_1^{S6R} + \cos \theta_1^{S6R} \cdot \sin \theta_2^{S6R} + \cos \alpha^{S6R} \cdot \cos \theta_2^{S6R} \cdot \sin \theta_1^{S6R})
 \end{aligned}$$

$$\begin{aligned}
 Q_R^{S6R}(3,2) &= 2 \sin \alpha^{S6R} \cdot (\cos^2 \alpha^{S6R} + \cos \theta_2^{S6R} - \cos^2 \alpha^{S6R} \cdot \cos \theta_2^{S6R}) \\
 &\cdot (\cos \alpha^{S6R} \cdot \cos \theta_1^{S6R} + \sin \theta_1^{S6R} \cdot \sin \theta_2^{S6R} - \cos \alpha^{S6R} \cdot \cos \theta_1^{S6R} \cdot \cos \theta_2^{S6R})
 \end{aligned}$$

$$\begin{aligned}
 Q_R^{S6R}(3,3) &= -4 \cdot \cos^2 \alpha^{S6R} \cdot \cos \theta_2^{S6R} - 2 \cdot \cos^2 \theta_2^{S6R} - 2 \cdot \cos^4 \alpha^{S6R} + 4 \cdot \cos^4 \alpha^{S6R} \cdot \cos \theta_2^{S6R} \\
 &+ 4 \cdot \cos^2 \alpha^{S6R} \cdot \cos^2 \theta_2^{S6R} - 2 \cdot \cos^4 \alpha^{S6R} \cdot \cos^2 \theta_2^{S6R} + 1
 \end{aligned}$$

The results the compatible equation of plane-symmetric Bricard linkage are

$$\begin{aligned}
 T_L^{Br}(1,1) &= -\sin \theta_2^{Br} \cdot (\cos(2\alpha^{Br}) \cdot \cos \theta_1^{Br} \cdot \sin \theta_2^{Br} - \sin(2\alpha^{Br}) \cdot \sin \alpha^{Br} \cdot \sin \theta_1^{Br}) \\
 &+ \cos(2\alpha^{Br}) \cdot \cos \alpha^{Br} \cdot \cos \theta_2^{Br} \cdot \sin \theta_1^{Br} - \cos \theta_2^{Br} \cdot (\cos \theta_1^{Br} \cdot \cos \theta_2^{Br} \\
 &- \cos \alpha^{Br} \cdot \sin \theta_1^{Br} \cdot \sin \theta_2^{Br})
 \end{aligned}$$

$$\begin{aligned}
 T_L^{Br}(1,2) &= \cos^2 \alpha^{Br} \cdot \sin \theta_1^{Br} \cdot (\cos^2 \theta_2^{Br} - 1) - \cos(2\alpha^{Br}) \cdot \sin \theta_1^{Br} \cdot (\cos^2 \alpha^{Br} - 1) \\
 &- 2 \cdot \cos^3 \alpha^{Br} \cdot \cos \theta_1^{Br} \cdot \cos \theta_2^{Br} \cdot \sin \theta_2^{Br} - 2 \cdot \cos \alpha^{Br} \cdot \cos \theta_1^{Br} \cdot \sin \theta_2^{Br} \cdot (\cos^2 \alpha^{Br} - 1) \\
 &+ 2 \cdot \cos \alpha^{Br} \cdot \cos \theta_1^{Br} \cdot \cos \theta_2^{Br} \cdot \sin \theta_2^{Br} - \cos(2\alpha^{Br}) \cdot \cos^2 \alpha^{Br} \cdot \cos^2 \theta_2^{Br} \cdot \sin \theta_1^{Br} \\
 &- 4 \cdot \cos^2 \alpha^{Br} \cdot \cos \theta_2^{Br} \cdot \sin \theta_1^{Br} \cdot (\cos^2 \alpha^{Br} - 1)
 \end{aligned}$$

$$\begin{aligned}
 T_L^{Br}(1,3) &= 2 \cdot \sin \alpha^{Br} \cdot (\cos^2 \alpha^{Br} - \cos \theta_2^{Br} + \cos^2 \alpha^{Br} \cdot \cos \theta_2^{Br}) \cdot (\cos \alpha^{Br} \cdot \sin \theta_1^{Br} \\
 &+ \cos \theta_1^{Br} \cdot \sin \theta_2^{Br} + \cos \alpha^{Br} \cdot \cos \theta_2^{Br} \cdot \sin \theta_1^{Br})
 \end{aligned}$$

$$\begin{aligned}
 T_L^{Br}(1,4) &= l_1 \cdot \cos \theta_1^{Br} - \sin \theta_2^{Br} \cdot (l_1 + l_2) \cdot (\cos(2\alpha^{Br}) \cdot \cos \theta_1^{Br} \cdot \sin \theta_2^{Br} \\
 &- \sin(2\alpha^{Br}) \cdot \sin \alpha^{Br} \cdot \sin \theta_1^{Br} + \cos(2\alpha^{Br}) \cdot \cos \alpha^{Br} \cdot \cos \theta_2^{Br} \cdot \sin \theta_1^{Br}) \\
 &+ l_2 \cdot \cos \theta_1^{Br} \cdot \cos \theta_2^{Br} - \cos \theta_2^{Br} \cdot (l_1 + l_2) \cdot (\cos \theta_1^{Br} \cdot \cos \theta_2^{Br} \\
 &- \cos \alpha^{Br} \cdot \sin \theta_1^{Br} \cdot \sin \theta_2^{Br}) - l_2 \cdot \cos \alpha^{Br} \cdot \sin \theta_1^{Br} \cdot \sin \theta_2^{Br}
 \end{aligned}$$

$$\begin{aligned} T_L^{Br}(2,1) &= -\sin\theta_1^{Br} \cdot (\sin(2\alpha^{Br}) \cdot \sin\alpha^{Br} \cdot \cos\theta_1^{Br} + \cos(2\alpha^{Br}) \cdot \sin\theta_1^{Br} \cdot \sin\theta_2^{Br} \\ &\quad - \cos(2\alpha^{Br}) \cdot \cos\alpha^{Br} \cdot \cos\theta_1^{Br} \cdot \cos\theta_2^{Br}) - \cos\theta_2^{Br} \cdot (\cos\theta_2^{Br} \cdot \sin\theta_1^{Br} \\ &\quad + \cos\alpha^{Br} \cdot \cos\theta_1^{Br} \cdot \sin\theta_2^{Br}) \end{aligned}$$

$$\begin{aligned} T_L^{Br}(2,2) &= -\cos(2\alpha^{Br}) \cdot \cos\theta_1^{Br} \cdot \sin^2\alpha^{Br} + \cos^2\alpha^{Br} \cdot \cos\theta_1^{Br} \cdot \sin^2\theta_2^{Br} \\ &\quad - 2\cos^3\alpha^{Br} \cdot \cos\theta_2^{Br} \cdot \sin\theta_1^{Br} \cdot \sin\theta_2^{Br} + 2\cos\alpha^{Br} \cdot \sin\theta_1^{Br} \cdot \sin\theta_2^{Br} \cdot \sin^2\alpha^{Br} \\ &\quad + \cos(2\alpha^{Br}) \cdot \cos^2\alpha^{Br} \cdot \cos\theta_1^{Br} \cdot \cos^2\theta_2^{Br} - 4\cos^2\alpha^{Br} \cdot \cos\theta_1^{Br} \cdot \cos\theta_2^{Br} \cdot \sin^2\alpha^{Br} \\ &\quad + 2\cos\alpha^{Br} \cdot \cos\theta_2^{Br} \cdot \sin\theta_1^{Br} \cdot \sin\theta_2^{Br} \end{aligned}$$

$$\begin{aligned} T_L^{Br}(2,3) &= -2\sin\alpha^{Br} \cdot (\cos^2\alpha^{Br} - \cos\theta_2^{Br} + \cos^2\alpha^{Br} \cdot \cos\theta_2^{Br}) \cdot (\cos\alpha^{Br} \cdot \cos\theta_1^{Br} \\ &\quad - \sin\theta_1^{Br} \cdot \sin\theta_2^{Br} + \cos\alpha^{Br} \cdot \cos\theta_1^{Br} \cdot \cos\theta_2^{Br}) \end{aligned}$$

$$\begin{aligned} T_L^{Br}(2,4) &= l_1 \cdot \sin\theta_1^{Br} - \sin\theta_2^{Br} \cdot (l_1 + l_2) \cdot (\sin(2\alpha^{Br}) \cdot \sin\alpha^{Br} \cdot \cos\theta_1^{Br} \\ &\quad + \cos(2\alpha^{Br}) \cdot \sin\theta_1^{Br} \cdot \sin\theta_2^{Br} - \cos(2\alpha^{Br}) \cdot \cos\alpha^{Br} \cdot \cos\theta_1^{Br} \cdot \cos\theta_2^{Br}) \\ &\quad + l_2 \cdot \cos\theta_2^{Br} \cdot \sin\theta_1^{Br} - \cos\theta_2^{Br} \cdot (l_1 + l_2) \cdot (\cos\theta_2^{Br} \cdot \sin\theta_1^{Br} + \cos\alpha^{Br} \cdot \cos\theta_1^{Br} \cdot \sin\theta_2^{Br}) \\ &\quad + l_2 \cdot \cos\alpha^{Br} \cdot \cos\theta_1^{Br} \cdot \sin\theta_2^{Br} \end{aligned}$$

$$T_L^{Br}(3,1) = -2\sin\alpha^{Br} \cdot \sin\theta_2^{Br} \cdot (2\sin^2\frac{\theta_2^{Br}}{2} \cdot \sin^2\alpha^{Br} - 2\sin^2\alpha^{Br} + 1)$$

$$T_L^{Br}(3,2) = -2\sin(2\alpha^{Br}) \cdot \cos^2\frac{\theta_2^{Br}}{2} \cdot (2\sin^2\frac{\theta_2^{Br}}{2} \cdot \sin^2\alpha^{Br} - 2\sin^2\alpha^{Br} + 1)$$

$$\begin{aligned} T_L^{Br}(3,3) &= 8\sin^2\alpha^{Br} - 8\sin^4\alpha^{Br} - 8\sin^2\frac{\theta_2^{Br}}{2} \cdot \sin^2\alpha^{Br} + 8 \cdot \sin^2\frac{\theta_2^{Br}}{2} \cdot \sin^4\alpha^{Br} \\ &\quad + 2\sin^4\alpha^{Br} \cdot \sin^2\theta_2^{Br} - 1 \end{aligned}$$

$$\begin{aligned} T_L^{Br}(3,4) &= \sin\alpha^{Br} \cdot \cos\theta_2^{Br} \cdot \sin\theta_2^{Br} \cdot (l_1 + l_2) - l_2 \cdot \sin\alpha^{Br} \cdot \sin\theta_2^{Br} \\ &\quad - \sin\theta_2^{Br} \cdot (l_1 + l_2) \cdot (\sin(2\alpha^{Br}) \cdot \cos\alpha^{Br} + \cos(2\alpha^{Br}) \cdot \sin\alpha^{Br} \cdot \cos\theta_2^{Br}) \end{aligned}$$

$$T_L^{Br}(4,1) = 0$$

$$T_L^{Br}(4,2) = 0$$

$$T_L^{Br}(4,3) = 0$$

$$T_L^{Br}(4,4) = 1$$

$$\begin{aligned} T_R^{Br}(1,1) &= \sin(2\alpha^{Br}) \cdot \sin\alpha^{Br} \cdot \sin\theta_2^{Br} \cdot \sin\theta_4^{Br} - \cos\theta_4^{Br} \cdot (\cos^2\theta_2^{Br} + \cos(2\alpha^{Br}) \cdot \sin^2\theta_2^{Br}) \\ &\quad + 2 \cdot \cos\alpha^{Br} \cdot \cos\theta_2^{Br} \cdot \sin\theta_2^{Br} \cdot \sin\theta_4^{Br} \cdot \sin^2\alpha^{Br} \end{aligned}$$

$$\begin{aligned} T_R^{Br}(1,2) &= -2\cos\alpha^{Br} \cdot \cos\theta_2^{Br} \cdot \cos\theta_4^{Br} \cdot \sin\theta_2^{Br} \cdot \sin^2\alpha^{Br} - \sin(2\alpha^{Br}) \cdot \sin\alpha^{Br} \\ &\quad \cdot \cos\theta_4^{Br} \cdot \sin\theta_2^{Br} - \sin\theta_4^{Br} \cdot (\cos^2\theta_2^{Br} + \cos(2\alpha^{Br}) \cdot \sin^2\theta_2^{Br}) \end{aligned}$$

$$T_R^{Br}(1,3) = -2 \cdot \sin\alpha^{Br} \cdot \sin\theta_2^{Br} \cdot (\cos^2\alpha^{Br} - \cos\theta_2^{Br} + \cos^2\alpha^{Br} \cdot \cos\theta_2^{Br})$$

$$\begin{aligned}
 T_R^{Br}(1,4) &= (l_1 + l_2) \cdot (\cos^2 \theta_2^{Br} + \cos(2\alpha^{Br}) \cdot \sin^2 \theta_2^{Br}) - l_2 \cdot \cos \theta_2^{Br} - l_1 \\
 T_R^{Br}(2,1) &= \sin(2\alpha^{Br}) \cdot \sin \alpha^{Br} \cdot \cos \theta_4^{Br} \cdot \sin \theta_2^{Br} - \cos^2 \alpha^{Br} \cdot \sin^2 \theta_2^{Br} \cdot \sin \theta_4^{Br} \\
 &+ \sin^2 \alpha^{Br} \cdot \sin \theta_4^{Br} \cdot \cos^2 \alpha^{Br} + \cos \alpha^{Br} \cdot \cos \theta_2^{Br} \cdot \cos \theta_4^{Br} \cdot \sin \theta_2^{Br} - \cos(2\alpha^{Br}) \\
 &\cdot \cos^2 \alpha^{Br} \cdot \cos^2 \theta_2^{Br} \cdot \sin \theta_4^{Br} + 4 \cos^2 \alpha^{Br} \cdot \cos \theta_2^{Br} \cdot \sin \theta_4^{Br} \cdot \sin^2 \alpha^{Br} \\
 &- \cos(2\alpha^{Br}) \cdot \cos \alpha^{Br} \cdot \cos \theta_2^{Br} \cdot \cos \theta_4^{Br} \cdot \sin \theta_2^{Br} \\
 T_R^{Br}(2,2) &= \cos^2 \alpha^{Br} \cdot \cos \theta_4^{Br} \cdot \sin^2 \theta_2^{Br} - \cos(2\alpha^{Br}) \cdot \sin^2 \alpha^{Br} \cdot \cos \theta_4^{Br} + \sin(2\alpha^{Br}) \\
 &\cdot \sin \alpha^{Br} \cdot \sin \theta_2^{Br} \cdot \sin \theta_4^{Br} + \cos(2\alpha^{Br}) \cdot \cos^2 \alpha^{Br} \cdot \cos^2 \theta_2^{Br} \cdot \cos \theta_4^{Br} \\
 &- 4 \cos^2 \alpha^{Br} \cdot \cos \theta_2^{Br} \cdot \cos \theta_4^{Br} \cdot \sin^2 \alpha^{Br} + \cos \alpha^{Br} \cdot \cos \theta_2^{Br} \cdot \sin \theta_2^{Br} \cdot \sin \theta_4^{Br} \\
 &- \cos(2\alpha^{Br}) \cdot \cos \alpha^{Br} \cdot \cos \theta_2^{Br} \cdot \sin \theta_2^{Br} \cdot \sin \theta_4^{Br} \\
 T_R^{Br}(2,3) &= -2 \cos \alpha^{Br} \cdot \sin \alpha^{Br} \cdot (\cos \theta_2^{Br} + 1) \cdot (\cos^2 \alpha^{Br} - \cos \theta_2^{Br} + \cos^2 \alpha^{Br} \cdot \cos \theta_2^{Br}) \\
 T_R^{Br}(2,4) &= l_2 \cdot \cos \alpha^{Br} \cdot \sin \theta_2^{Br} - \cos \alpha^{Br} \cdot \sin \theta_2^{Br} \cdot (\cos \theta_2^{Br} + 1) \cdot \sin^2 \alpha^{Br} \cdot (l_1 + l_2) \\
 T_R^{Br}(3,1) &= 2 \sin \alpha^{Br} \cdot (\cos^2 \alpha^{Br} - \cos \theta_2^{Br} + \cos^2 \alpha^{Br} \cdot \cos \theta_2^{Br}) \cdot (\cos \alpha^{Br} \cdot \sin \theta_4^{Br} \\
 &+ \cos \theta_4^{Br} \cdot \sin \theta_2^{Br} + \cos \alpha^{Br} \cdot \cos \theta_2^{Br} \cdot \sin \theta_4^{Br}) \\
 T_R^{Br}(3,2) &= -2 \sin \alpha^{Br} \cdot (\cos^2 \alpha^{Br} - \cos \theta_2^{Br} + \cos^2 \alpha^{Br} \cdot \cos \theta_2^{Br}) \cdot (\cos \alpha^{Br} \cdot \cos \theta_4^{Br} \\
 &- \sin \theta_2^{Br} \cdot \sin \theta_4^{Br} + \cos \alpha^{Br} \cdot \cos \theta_2^{Br} \cdot \cos \theta_4^{Br}) \\
 T_R^{Br}(3,3) &= 4 \cdot \cos^2 \alpha^{Br} \cdot \cos \theta_2^{Br} - 2 \cos^2 \theta_2^{Br} - 2 \cos^4 \alpha^{Br} - 4 \cdot \cos^4 \alpha^{Br} \cdot \cos \theta_2^{Br} \\
 &+ 4 \cdot \cos^2 \alpha^{Br} \cdot \cos^2 \theta_2^{Br} - 2 \cdot \cos^4 \alpha^{Br} \cdot \cos^2 \theta_2^{Br} + 1 \\
 T_R^{Br}(3,4) &= -12 \cdot \sin \alpha^{Br} \cdot \sin \theta_2^{Br} - 2 \sin \alpha^{Br} \cdot \sin \theta_2^{Br} \cdot (l_1 + l_2) \cdot (\cos^2 \alpha^{Br} - \cos \theta_2^{Br} \\
 &+ \cos^2 \alpha^{Br} \cdot \cos \theta_2^{Br}) \\
 T_R^{Br}(4,1) &= 0 \\
 T_R^{Br}(4,2) &= 0 \\
 T_R^{Br}(4,3) &= 0 \\
 T_R^{Br}(4,4) &= 1
 \end{aligned}$$

中文大摘要

可展结构具有从一个小尺寸收拢状态展开为大尺寸工作状态的特性。其小尺寸的非工作状态给运输和存储提供了便利,大尺寸的工作状态又能保证该结构的功能不会缺失。航空航天技术中的伸展臂、太阳能帆板阵列、卫星的星载天线就是可展结构的典型使用范例。可展结构同时在吸能材料设计、可展建筑结构、微创手术器械等领域具有广泛的应用前景。

一些精巧且实用的机构发明出来后,工程师与科研人员将多个单一机构连接成网状,进而构造出具有大折展比的可展结构,比如由剪刀机构、Bennett 机构、Bricard 机构等构成的网状结构。这些结构都是基于平面机构和空间机构,而球面机构很少被使用。

球面机构是指构件间用轴线交于一点的转动副相连的机构,构件上各点的运动轨迹位于同心球面上。球面四杆机构是一种有四个旋转副的球面机构且该机构只有一个自由度。单个的球面四杆机构在制造业广泛使用,但是过约束特性使其很难构造出可动的机构网格。

随着航天技术的发展,卫星所搭载的可展结构需要更大的折展比和更加复杂的形状来实现更复杂的功能。同时,为了便于控制结构的展开过程,所使用的机构尽量只有一个自由度。现阶段对于可展结构的研究主要集中于利用平面机构来构造出所需的形态,但是平面机构很难完全实现上述需求。球面四杆机构和空间过约束机构均具有空间构型且单自由度的特性,在大折展比和复杂构型的可展结构设计领域具有很高的应用潜力。将多个球面机构和空间过约束机构连接起来构成大尺寸的可展结构是一项极具挑战性的工作。

艺术也可以给工程师带来灵感,进而被演变为一种新型的技术。折纸是一种将平面材料折叠成三维形状的传统艺术。现在科学家和工程师对这门艺术产生了浓厚的兴趣,并参照它开发出构建新型结构的技术。刚性折纸是折纸艺术的一个分支,这类折纸图案在折叠的过程中,纸面不变形,在折痕处有变形。因此,我们将纸片类比为刚性板件,折痕类比为旋转铰链,刚性折纸结构可以看作是旋转铰链连接的可展板状结构。根据刚性折纸的这种特性,我们可以将每一个刚性折纸顶点看作为一个球面机构。刚性折纸在工程领域具有很大的应用潜力。从太阳能帆板,太空反射镜,飞行器机翼到变形机器人,它们的构件都是由刚性材料制作的,整体结构基本上呈现板状构型,并且需要一定的可动性,刚性折纸技术均可以满足这些需要,在这些领域具有广泛的应用前景。

本文第二章主要是对单个球面四杆机构的运动学分析,探讨构建可动球面机构网格的方法。

为了能够将球面四杆机构用于构建可展结构,本文首先探讨了构建可动球面

四杆机构网络的可行性。在球面四杆机构上利用 DH 方法建立坐标系，然后利用闭环方程求出各个旋转副间的运动关系 θ_i v.s. θ_{i+1} 。

通过将球面四杆机构中几何参数 α_{ij} 更改为 α_{ij} 、 $\pi - \alpha_{ij}$ 、 $-\pi + \alpha_{ij}$ 、 $-\alpha_{ij}$ ，对于每一个球面四杆机构有 $256(=4 \times 4 \times 4 \times 4)$ 种组合形式。对于运动参数 θ_i ，我们只考虑四种基本变化形式 θ_i 、 $\pi - \theta_i$ 、 $-\pi + \theta_i$ 或者 $-\theta_i$ 。如果球面四杆机构中相邻两个铰链间的运动关系为 θ_i v.s. θ_{i+1} ，通过上述方式更改 α_{ij} ，可以获得 θ_i v.s. $(\pi - \theta_{i+1})$ 、 θ_i v.s. $(-\pi + \theta_{i+1})$ 、 θ_i v.s. $-\theta_{i+1}$ 等一共 16 种新的运动关系 R_i 。当已知某一种运动关系，比如 $(\pi - \theta_i)$ v.s. $(\pi - \theta_{i+1})$ ，我们也可以通过本文提供的表格可知如何更改几何参数 α_{ij} 来实现这种传递关系。

为了研究多个球面四杆机构间的连接方式，我们将四个相同的球面四杆机构连成一个封闭环路。对于相邻的两个球面四杆机构，遵循具有相同下标的铰链连接在一起的原则。例如，机构 A 的旋转副 a2 与机构 B 的旋转副 b2 相连，机构 B 的旋转副 b1 与机构 C 的旋转副 c1 相连，机构 C 的旋转副 c2 与机构 D 的旋转副 d2 相连，机构 D 的旋转副 d1 与机构 A 的旋转副 a1 相连，由此就构成一个封闭环路。本文提出了四种连接方式，其中有一种是重复的，剩下的三种分别命名为双重对称装配形式、对称装配形式、旋转对称装配形式。结合球面四杆机构运动学，分别归纳出这三种装配形式的协调条件，即三种闭环传递路径。

在四个具有相同几何参数的球面四杆机构组成的可动装配体的基础上，我们使用四个不同的球面四杆机构组建装配体。当球面四杆机构的几何参数改变时，运动学的输入输出特性会发生变化，装配体的传递路径也会发生相应的改变。基于对球面四杆机构的运动学分析，对由四个相同球面四杆机构组成的可动装配体进行调整，利用上文中的 16 种特殊的传递关系来更改调整这些装配体的协调条件，以此来保证装配体的传递路径最后是封闭的。在获得新的协调条件与传递路径后，对照球面四杆机构几何参数 α_{ij} 与 R_i 关系，选择更改原始 α_{ij} 来实现新的传递路径，从而可以构建由四个不同的球面四杆机构组成的可动装配体。

刚性折纸可以等效为一类特殊的球面机构网络，其中的纸片等效为杆件，折痕等效为铰链。基于刚性折纸和球面机构网络这种关联性，可以参照可动球面机构网络来设计新的刚性折纸图案，但是需要添加更多的几何条件来保证折纸图案中的纸片为平面。本文讨论了旋转对称的装配体，在添加纸片为平面的条件后，由四个相同球面四杆机构组成的装配体可以演变成为一种常见的刚性折纸图案。对于这个旋转对称的装配体，我们使用上文中的 16 种特殊的传递关系来更改调整该装配体的协调条件，获得新的由四个不同球面四杆机构组成的装配体。此时再引入纸片为平面的条件，可以获得一种新的刚性折纸图案。球面机构网络不仅可

以用来探索新的球面四杆机构，也可以分析给定的折纸图案的刚性可折叠性。折纸图案等效的球面四杆机构装配体如果满足运动协调条件，即若运动传递路径封闭，该折纸图案就是刚性折纸图案。

本文第三章主要分析了山谷线的排布形式对折纸图案刚性可折叠性的影响，并且用刚性折纸图案堆叠出具有负泊松比的超材料。

折纸图案中的折痕有两类形式，使纸面向上凸的山折痕和使纸面向下凹的谷折痕。除了几何设计参数，山谷折痕的排布方式也会影响折纸图案的刚性可折叠性。本文提出了一种运动学方法来分析刚性可折叠性，并阐明山谷线排布方式对刚性可折叠性的影响。因为 *double-corrugated* 折纸图案相比于 *Miura-ori*、*square-twist* 等折纸图案更为复杂，本文以 *double-corrugated* 图案为例重点介绍如何对折纸图案进行刚性可折叠性的判定，并探讨其刚性几何拓展形式。

Double-corrugated 折纸图案由两个基本单元组成：*P* 单元和 *Q* 单元。每个单元包含四个折纸顶点。*P* 单元中的折痕有 10 种山谷线排布形式，*Q* 单元中的折痕有 6 种山谷线排布形式。我们将折纸单元等效为球面机构网格后，根据上文中对球面四杆机构的运动学分析，可以获得折纸图案中相邻折痕间的运动关系曲线。我们将每个单元的铰链运动传递关系图直接以直线和圆弧标记在运动关系曲线上，如果能形成一个固定的环路，该单元就是刚性的。指定某条折痕为山线或者为谷线，就是指定了该折痕所对应铰链的旋转角度 θ_i 的取值范围。因此一个折纸单元的不同山谷线排布就会造成运动关系曲线图上的角度传递标记不同，有些角度传递标记可以形成闭环，有些则不能，所以不同的山谷线排布形式会使一个折纸图案具有不同的刚性可折叠性。在 *P* 单元中，*P1-P4* 这四种排布形式具有刚性可折叠性，*P5-P10* 这六种为非刚性的。在 *Q* 单元中，*Q1-Q4* 这四种排布形式具有刚性可折叠性，*Q5-Q6* 这两种为非刚性的。一个 *double-corrugated* 折纸图案是由多个 *P* 单元和 *Q* 单元排列组合而成，如果其包含的山谷线排布形式只属于 *P1-P4*、*Q1-Q4* 中的一种或多种，那么 *double-corrugated* 折纸图案整体都是刚性可折叠的。

在保证 *P* 单元和 *Q* 单元均是刚性可折叠的情况下，对于一个 *double-corrugated* 折纸图案，我们可以设计不同的刚性折叠方式。在不改变图案的几何参数设计的情况下，就可以获得不同的构型。通过这些刚性折纸图案多层叠加，可以获得相应的 3D 超材料。本文提出了四种 3D 超材料，它们具有不同的构型，折叠过程也不相同。但是它们均基于同一个 *double-corrugated* 图案，仅山谷线的排布形式不同。这些超材料都是基于刚性可折叠的折纸图案，因此当一个基本单元按照刚性运动进行折展时，能够引起整个超材料的刚性运动。从完全展开状态到完全折叠状态的过程中，面内方向上的尺寸一直减小，面外方向的尺寸先增大再减小。因此在折叠过程的后期阶段，面内与面外方向的泊松比均为负值。由于四种超材

料的折叠过程不同,因此具有不同的负泊松比特性。本文对这四种材料的泊松比都进行了计算,并进行了比较分析。

Square-twist 图案所具有的折痕排布形式共有四种,分别编号为 T1、T2、T3 和 T4。Square-twist 图案实际上是 Q 单元的特例,我们采用相同的方式对其所有的折痕排布形式进行分析,其中 T1 和 T2 具有刚性可折叠性,T3 和 T4 是非刚性。将 Square-twist 图案多层堆叠后,可以得到负泊松比的材料,本文对其泊松比也进行了计算分析。

本文第四章主要介绍了一种可以构建厚板折纸模型的新型机构综合方法,并将其与零厚度折纸模型的折叠运动进行了对比分析。

折纸图案通常被用于构造零厚度的薄板结构。但是在工程实际中,材料厚度不能忽略。目前已提出多种方法,主要通过调整板件的运动干涉区域来解决这类问题,所用的运动学模型仍然为球面机构。本文提出了一类全新且具有普适性的机构综合方法来解决厚板折纸问题。使用该方法构造的厚板折纸模型与零厚度折纸具有相同的运动路径。该方法能够有效地构造四折痕、五折痕、六折痕的单顶点和多顶点折纸图案的厚板模型,便于折纸技术在实际工程中应用。

迄今为止,刚性折纸的所有的运动学模型都不考虑纸片厚度,将厚度默认为零。在折纸图案的每个顶点处,所有的折痕相交于一点,因此等效为旋转铰链的轴线均相交于一点的球面机构。一个刚性折纸图案的运动学模型就是由许多这样的球面机构构建的网状结构。各种各样的使用非零厚度板件的刚性折纸技术,仍然使用这种球面机构网格作为其运动学模型。这些技术通过在零厚度模型的表面上添加适当的锥形材料,或者保持折痕位置不变,将折纸板件做一定的偏移。这些技术不能够实现将非零厚度折纸模型完全折叠为平面,或者保持板件的完整性。但是,这些非零厚度刚性折纸技术中有两个特例,Hoberman 做的 Miura-ori 折纸图案的板件模型和 De Temmerman 基于 diamond origami 折纸图案的板件模型,实现了结构的完全折叠且不出现运动干涉现象。这两个模型中,旋转铰链的中心线并没有交于一点,而是处于一种特殊的空间位置,这也说明它们的运动学模型并不是球面机构网格。根据这两个特例,我们首先寻找它们所等价的机构运动学模型,然后将这个运动学模型一般化后,应用到更多的厚板折纸模型中。

利用球面机构的运动学模型来构建刚性折纸的厚板模型,运动初始状态中所有铰链轴线位于同一平面,折展过程中会出现运动干涉问题,无法实现完全折叠,因此所有的折痕不能排布在同一个平面上。基于这个原因,我们将部分折痕排布在厚板的上方,另一部分折痕排布在下方,按此构建的装配体中的折痕不共面,并且相邻折痕不交于同一点。由球面机构网格构成的运动学模型最终被我们替换为铰链处于空间位置的运动学模型。新运动学模型的可动性基于两个条件:运动学模型中的每一个环路均为机构,该机构可以连续运动。

现在广泛使用的几种折纸图案 *miura-ori*、*square twist*、*diamond origami* 和 *waterbomb origami* 每个顶点处分别有四条、五条、六条折痕，对应于空间 $4R$ 、 $5R$ 和 $6R$ 机构，即 Bennett 机构，Myard 机构和 Bricard 机构。这些机构属于一类特殊的空间机构，根据 Kutzbach 准则，这类可动机构的自由度值小于 1，被称为过约束机构。这类机构必须满足特定的几何条件来保证其的可动性。在我们的研究过程中，首先发现四条、五条和六条折痕的单顶点折纸图案运动学等价的空间 $4R$ 、 $5R$ 和 $6R$ 空间机构所要满足的几何条件，然后扩展到多顶点的折纸模型，从而保证厚板模型与零厚度的折纸模型具有相同的折展运动。由于构建的厚板模型与零厚度模型具有相同的运动学特性，因此根据本文的方法可以直接参照现有的零厚度模型构建出厚板模型。

提出的这种使用空间过约束机构来构建刚性折纸厚板模型具有通用性，并且实现了厚板折纸模型与零厚度折纸模型的运动等价性，即所使用空间过约束机构能够匹配球面机构的运动。为了实现运动的匹配，空间过约束机构与球面机构的角度条件必须相同，通过三维模型和解析法可以完成证明。由于厚板模型与单自由度的空间过约束机构是一一对应的，可以表明厚板折纸模型都是单自由度的，具有方便控制结构折展状态的优点。而五条折痕和六条折痕的单顶点图案的零厚度模型分别具有 2 自由度和 3 自由度，它们所构成的多顶点模型自由度会更多更复杂，但是当构造出对应的厚板模型后，整个结构的自由度降为 1，使这类折纸结构更具实用性。

本文主要展示了我们在构建可动球面四杆机构网格和刚性折纸领域的工作，主要包括下面三个方面：

(1) 提出构建可动球面机构网格的方法。基于拓扑结构对称性，用四个完全相同的球面四杆机构构造出可动的球面机构网格，提出了三种装配形式，双重对称装配方式、对称装配方式和旋转对称装配方式。在球面四杆机构运动学分析的基础上，将上述装配方式进行拓展，使用几何参数不同的球面四杆机构来实现可动球面四杆机构网格。根据球面机构网格与刚性折纸间的关系，讨论刚性折纸，并提出了一种新的刚性折纸图案。

(2) 探讨山谷线排布对折纸图案的刚性可折叠性的影响，以及用刚性折纸图案构建负泊松比超材料。我们分析了 *double-corrugated* 折纸图案。将折纸图案的基本单元等效为球面四杆机构网格后，再利用机构运动学协调条件对折纸图案是否为刚性进行判定，指出山谷线排布对折纸图案的影响。然后对 *double-corrugated* 折纸图案采用不同的山谷线排布，得到不同的刚性折叠形式，再将 these 折纸图案多层堆叠后得到具有不同负泊松比的超材料。*Square-twist* 折纸图案是 *double-corrugated* 折纸图案的特例，因此也对其进行了分析。

(3) 提出新型厚板折纸理论。不同于传统理论使用球面机构来分析和利用刚

性折纸技术构建可展结构，我们用 Bennett 机构、Myard 机构、Bricard 机构等空间过约束机构来建立厚板折纸模型，解决了传统理论无法避免的板件干涉问题，使折纸技术更具实用价值。同时，我们也证明了利用新理论构建的厚板模型与传统模型具有运动学上的等价性，意味着只要符合完全可折叠的刚性折纸图案都可以使用新理论构造出厚板模型。

本文系统地研究了使用球面四杆机构网格和刚性折纸来构建可展结构的理论，并展示了如何用刚性折纸构建具有负泊松比的超材料。为了挺高可展结构的性能，本文未来的研究工作还可以通过下列方面进行探索：

(1) 去掉可动球面四杆机构网格的拓扑结构具有对称性这一预设条件，使用更加一般的方法来构建可动球面四杆机构网格，从而发现更多可行的装配形式。

(2) 利用本文提出的构造可动球面机构网格的方法和球面机构与刚性折纸间的联系，我们可以构造九宫格状的折纸图案。在以后的工作中，可以利用这些基础图案在多个方向上几何覆盖，从而得到更大尺寸的折纸图案。

(3) 对负泊松比超材料的力学特性进行分析，探索出更多的工程实际应用。

(4) 利用厚板理论设计出新型太阳能阵列、星载天线等其他太空应用领域所需的可展结构。

(5) 进行受力分析和优化设计参数，使基于刚性折纸技术的可展结构获得更高的性能，例如，更大的折展比、结构的展开更易驱动、展开和折叠过程具有更高的可控性等等。

Publications and Research Projects

Papers:

- [1] Chen Y, Peng R, You Z. Origami of thick panels [J]. Science, 2015, 349(6246):396-400.
- [2] Chen Y, Feng H, Ma J, Peng R, You Z. Symmetric waterbomb origami[J]. Proceedings of the Royal Society of London, 2016, 472(2190):20150846.

Patents:

- [1] 陈焱, 彭睿, 田沛霖, 李建民. 可折叠杆架结构, 授权号: ZL201310050611.2, 发明专利, 授权公告日: 2015.01.14.

Research Projects Participated in:

- [1] 国家自然科学基金优青项目: 机构运动学与可动结构(项目编号: 51422506), 主要参与者
- [2] 国家自然科学基金面上项目: 可重构机器人中折展结构基础设计理论研究(项目编号: 51275334), 主要参与者

Acknowledgements

First and foremost, I would like to express my sincere and warmest thanks to Prof. Chen Yan, for her guidance during my PhD period and pushing me to open the door to the world of science.

I would also like to give my thanks to the following professors: Prof. Zhong You, Prof. Li Jianmin, Prof. Kang Rongjie, Prof. Song Zhibing, Prof. Ma Jiayao, for their suggestions in my research fields.

My thanks also go to my fellow colleagues in the lab of No. 19 building, Mr. Xie Ruikang, Mr. Hou Degao, Mr. Liu Xiang and Dr. Lv Weilin. They have given me much help in making models and offer me an excellent scientific research atmosphere.

The kind and selfless help from Dr. Feng Huijuan and Dr. Yang Fufu really speed up my research process and let me have deep understanding of kinematics. I am also grateful to the colleagues Mr. Guo Yong, Mr. Gao Bingbing, Mr. Guo Xiaolei, Mr. Zhang Xiao, Mr. Gao Junjie, Mr. Song Jichao, Mr. Shang Zufeng.

Special deep appreciation and gratitude go to my roommates Mr. Li Zheng, Mr. Zou Yu, Mr. Wang Ziqian and my friend Mr. Liu Haiyang for their kind advice and warm words during the hard times, and tender care in the daily life.

Last but not least, I would like to express my sincerest thanks to my parents for their support and encouragement. Without their love, it is impossible for me to insist on finishing my research works.